Austrian Journal of Technical and Natural Sciences

2023, No 11 – 12

PREMIER Publishing

Vienna
2023

Austrian Journal of Technical and Natural Sciences

Scientific journal

№ 11–12 2023

ISSN 2310-5607

Proofreading Kristin Theissen
Cover design Andreas Vogel
Additional design Stephan Friedman
Editorial office Premier Publishing s.r.o.
Praha 8 – Karlín, Lyčkovo nám. 508/7, PSČ 18600
E-mail: pub@ppublishing.org
Homepage: ppublishing.org

Austrian Journal of Technical and Natural Sciences is an international, English language, peer-reviewed journal. The journal is published in electronic form.

The decisive criterion for accepting a manuscript for publication is scientific quality. All research articles published in this journal have undergone a rigorous peer review. Based on initial screening by the editors, each paper is anonymized and reviewed by at least two anonymous referees. Recommending the articles for publishing, the reviewers confirm that in their opinion the submitted article contains important or new scientific results.

Premier Publishing is not responsible for the stylistic content of the article. The responsibility for the stylistic content lies on an author of an article.

Instructions for authors

Full instructions for manuscript preparation and submission can be found through the Premier Publishing home page at: http://ppublishing.org.

Material disclaimer

The opinions expressed in the conference proceedings do not necessarily reflect those of the Premier Publishing, the editor, the editorial board, or the organization to which the authors are affiliated.

Premier Publishing is not responsible for the stylistic content of the article. The responsibility for the stylistic content lies on an author of an article.

Included to the open access repositories:

SJIF 2023 = 5.859 (Scientific Journal Impact Factor Value for 2023).

Included to the Uzbekistan OAK journals bulletin.

Typeset in Berling by Ziegler Buchdruckerei, Linz, Austria.
Printed by Premier Publishing, Vienna, Austria on acid-free paper.Printed by Premier Publishing, Vienna, Austria on acid-free paper.

The Austrian Journal of Technical and Natural Sciences, No 11–12
ISSN 2310-5607

PREMIER Publishing
ppublishing.org

Section 1. Chemistry

DOI:10.29013/AJT-23-11.12-3-8

RESEARCH AND IDENTIFICATION AND CLASSIFICATION METHODS OF VEGETABLE OILS

Azada Abdurakhmanova [1], Kurbonkul Karimkulov [2], Muzaffar Karimkulov [3]

[1] Tashkent State Technical University, Uzbekistan, Tashkent

[2] Customs Institute of the Customs Committee, Uzbekistan, Tashkent

[3] Synergy University Dubai, UAE

Cite: *Abdurakhmanova, A., Karimkulov, K., Karimkulov, M. (2023). Research and Identification and Classification Methods of Vegetable Oils. Austrian Journal of Technical and Natural Sciences 2023, No 11-12.* https://doi.org/10.29013/AJT-23-11.12-3-8

Abstract

The article presents methods and results for determining the quality of olive, sunflower and corn oil. Modern organoleptic and physicochemical methods for determining the quality of fatty acids have been developed.

Keywords: *olive, sunflower and corn oil, methods of analysis, commodity nomenclature of foreign economic activity, methods of examination, identification*

Introduction

One of the most pressing issues in international economic relations and customs practice is the correct determination of the code numbers of the Commodity Nomenclature of Foreign Economic Activity (CN FEA) of all export-import goods. As a result of the analysis of goods by HS code numbers through customs inspection, they are divided into important information about their chemical composition, structure, organoleptic, physico-chemical and other parameters, as well as the processes of production of goods. This, in turn, makes it possible to correctly name goods, prevent a number of crimes that may occur in economic relations, and, finally, protect the interests of consumers. Therefore, the classification of food products based on the Commodity Nomenclature of Foreign Economic Activity is one of the most pressing issues for participants in foreign economic activity. This depends on a number of factors: under what code the goods are classified on the basis of the Commodity Nomenclature of Foreign Economic Activity, it depends on the customs rate subject to payment of customs duties; – classification of goods according to a particular HS code requires special knowledge in the field of classification and additional knowledge related to determining the description of goods and their application according to the Harmonized System (Andreeva, E.I., 2016).

Selection and preparation of samples for analysis (obtaining methyl esters of fatty acids) – according to Interstate standard (GOST) 31665, section 5 or 6 (except 6.1.3 and 6.2.4), with the following addition:

A sample of the spread weighing from 40 to 50 g is melted in a beaker in a water bath or in an oven at (60 ± 5) °C, and kept at this temperature until complete separation. The fat layer is filtered through a pleated filter. If the filtered fat is transparent, then proceed to measurement. If there is turbidity in the fat, it is filtered again. A sample is taken from the separated fat for measurements.

Considering that the triglycerides of the fat phase of the spread, baked mixture, milk and dairy products contain low molecular weight acids (starting with butyric acid -C4: 0), when obtaining methyl esters, filtration is replaced by centrifugation. The resulting solution of fatty acid methyl esters should be used for analysis immediately after preparation.

Determination (analysis of methyl esters of fatty acids) – according to GOST 31663.

Note – Please note that methyl esters of fatty acids contain methyl esters of low molecular weight acids (starting with butyric acid – C4:0), therefore gas chromatographic analysis should be carried out with mandatory temperature programming, starting from a temperature of 60 to 100 °C (depending on from the stationary phase used), ensuring satisfactory separation of butyric acid methyl ester from the solvent.

Processing the results

B.6.1 Processing of the results of the analysis of methyl esters of fatty acids is carried out by the method of internal normalization based on the peak areas of the components, using chromatograph software or according to GOST 31663 (clause 7.2.2). When calculating the mass fraction of milk fat, the calculation of the mass fraction of butyric acid methyl ester is carried out accurate to the third decimal place, followed by rounding to the second decimal place. Calculation of the mass fraction of milk fat in the fat phase of the product under study. If the obtained value of the mass fraction of butyric acid methyl ester is equal to or more than 3.10%, it is considered that the mass fraction of milk fat in the product exceeds 85%, that is, it exceeds the upper limit of the measurement range using this method.

The mass fraction of milk fat in the analyzed sample X_1,%, is calculated using the formula

$$X_1 = \frac{X_i}{X_{mi}} * 100$$

where X_i is the mass fraction of butyric acid methyl ester,%;

X_{mi} is the average value of the mass fraction of butyric acid methyl ester in milk fat,%, equal to 3.1.

Agilent Technologies 7820A GC Gas Chromatograph

Flame ionization detector

Column: SP-2560100 m × 0.25mm × 0.2 µm

The methods used in the examination of the quality of identification of vegetable oils have been studied. Expertise of the quality of vegetable oil is determined by studying the content of free fatty acids in its composition. The examination is carried out using a GC–MS instrument,

There are different ways to assign a sample to it:

1) Sulfuric acid-methanol method

Place 1 g sample in an Erlenmeyer flask, add 60 ml sulfuric acid-toluene-methanol solution (Add 2 ml concentrated sulfuric acid to 230 ml toluene: methanol = 1:3 (v/v) mixed solution). Heat in a refrigerator and boil for 2.5 hours, then cool, transfer to a separating funnel and add 100 ml of water. Extract twice, using 50 ml of petroleum ether each time. The extracts were combined and washed each time with 20 ml of water. Washing was repeated until it's over. After dehydrating the petroleum ether solution with anhydrous sodium sulfate, the solvent is removed using a rotary evaporator."

2) BF3-methanol method

Place 0.5 g of sample in an Erlenmeyer flask with a regular stopper, add 50 ml of 1 N. KOH-ethanol solution to dissolve, add zeolite, attach a reflux condenser and heat in a boiling water bath for about 1 hour.

After heating, add about 50 ml of water and pour into a separatory funnel. After cooling the contents to room temperature, add 30 ml of petroleum ether each time and shake twice to separate the petroleum ether layer.

Add 1 N. hydrochloric acid to the aqueous layer to make it acidic, and then extract twice, using approximately 30 ml of petroleum ether each time. The extracts are combined, a small amount of anhydrous sodium sulfate is added to dehydrate, and about 20 ml of the mixture is transferred to an Erlenmeyer flask. To this add 10 ml of BF3-methanol solution (boron trifluoride diethyl ether complex: methanol = 1:2 (v/v)), add a reflux condenser and heat in a boiling water bath for about 10 minutes, then add about 50 ml. water, ml, transfer to a separatory funnel, add 20 ml of petroleum ether, shake vigorously and extract the organic layer. 10 ml of petroleum ether is again added to the aqueous layer, extracted in the same way, combined with the previous organic layer and the solvent is removed using a rotary evaporator.

Olive oil quality analysis using GC-MS

Figure 1. *Olive oil quality analysis*

Qualitative Analysis Report

Data File	Olivka yogi .D	**Sample Name**	
Sample Type		**Position**	1
Instrument Name	GC-MS	**User Name**	Nodir
Acq Method	Нодир ёгпар.m	**Acquired Time**	7/7/2023 5:38:35 PM
IRM Calibration Status	Not Applicable	**DA Method**	default.m
Comment			
Требуется штрихкод		**Количество пробы:**	
Объем двойного ввода		**TuneName**	ATUNE.U
TunePath	C:\MassHunter\GCMS\1\5977\	**MSFirmwareVersion**	6.00.25
OperatorName	Nodir	**RunCompletedFlag**	True
Acquisition SW Version	MassHunter GC/MS Acquisition B.07.03.2129 18-May-2015 Copyright © 1989-2014 Agilent Technologies, Inc.		

User Chromatograms

Fragmentor Voltage	Collision Energy	0	Ionization Mode	Unspecifie d

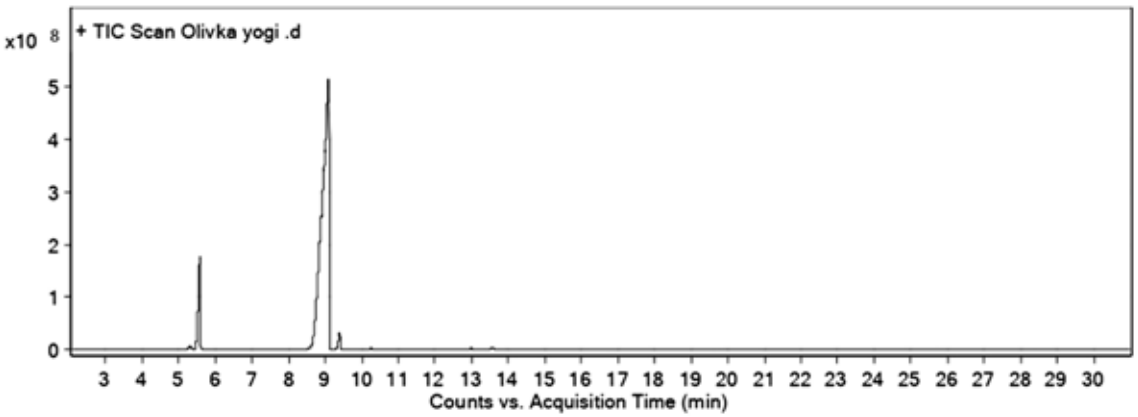

User Spectra

Fragmentor Voltage	Collision Energy	Ionization Mode
	0	Unspecified

Page 1 of 9 Printed at 6:22 PM on 7-Jul-2023

Agilent Technologies

3) BF3-methanol method (standard oil analysis method)

Take about 50 mg of sample into an Erlenmeyer flask, add 1 ml of 0.5 N. CON. -methanol solution Add. Turn on the cooler and heat in a water bath for 5–10 minutes. Add 1 ml of BF3-methanol solution from the top of the cooler. After boiling for 2 minutes, add 5 ml of

hexane from the top of the refrigerator and boil for another 1 minute. Remove the flask from the refrigerator and add saturated aqueous sodium chloride until the hexane layer reaches the neck of the flask. Transfer the hexane layer to a beaker and add anhydrous sodium sulfate."

Analysis of sunflower oil quality using a GC-MS device

Figure 2. *Analysis of sunflower oil quality*

Qualitative Analysis Report

Data File	kungaboqar yogi 2.D	**Sample Name**	
Sample Type		**Position**	1
Instrument Name	GC-MS	**User Name**	Nodir
Acq Method	Нодир ёғлар.m	**Acquired Time**	7/7/2023 7:03:10 PM
IRM Calibration Status	Not Applicable	**DA Method**	default.m
Comment			
Требуется штрихкод		**Количество пробы:**	
Объем двойного ввода		**TuneName**	ATUNE.U
TunePath	C:\MassHunter\GCMS\1\5977\	**MSFirmwareVersion**	6.00.25
OperatorName	Nodir	**RunCompletedFlag**	True
Acquisition SW Version	MassHunter GC/MS Acquisition B.07.03.2129 18-May-2015 Copyright © 1989-2014 Agilent Technologies, Inc.		

User Chromatograms

Fragmentor Voltage	Collision Energy	0	Ionization Mode	Unspecified

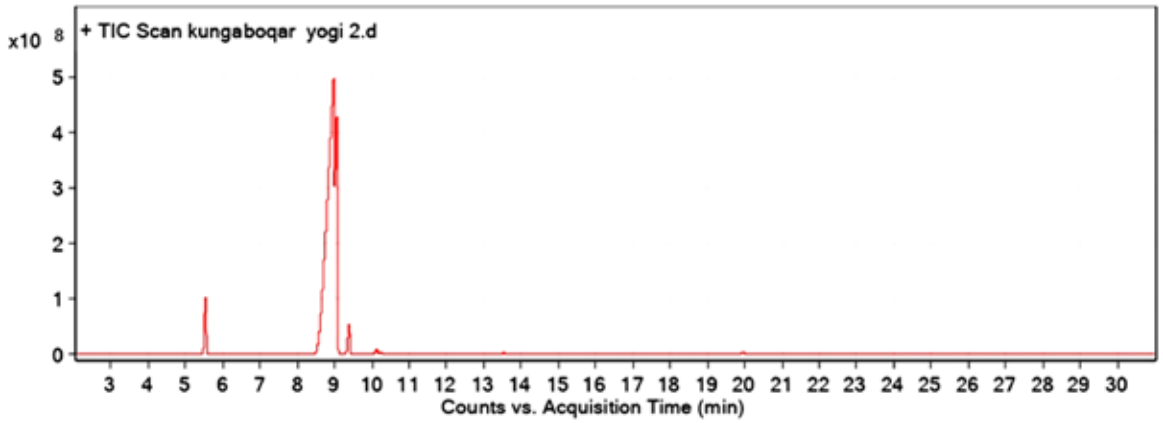

User Spectra

Fragmentor Voltage	Collision Energy	Ionization Mode
	0	Unspecified

Agilent Technologies

Page 1 of 13

Printed at 7:40 PM on 7-Jul-2023

4) m-TFPTAH method. "Melt the sample under heat and stir until homogenized. Transfer about 10 mg of sample to a vial, add 0.5 ml of toluene and stir. Add 0.2 ml m-TFPTA, cap tightly, mix well and leave at room temperature for 15 minutes."

5) KOH-methanol method.

Place approximately 100 mg of sample in an Erlenmeyer flask, add 2 ml of petroleum ether and toluene (1:1) and dissolve completely. Add 2 ml 0.4 N. KOH-methanol solution, mix well at room temperature and leave

for 5–10 minutes. After settling, distilled water is added until the organic layer reaches the neck of the flask. Add a few drops of ethanol if the organic layer is cloudy. Take the organic layer in a beaker and add anhydrous sodium sulfate."

In this work, sunflower, olive and corn oils were tested using the 5th method, the KOH-methanol method. The results of the analyzes are shown in Fig. 1–3.

Methods and results for determining the quality of corn, olive and sunflower oil were presented.

Corn oil quality analysis using GC–MS

Figure 3. *Corn oil quality analysis*

When the Customs Committee analyzed the database of customs cargo declarations, cases of oil-oil mixtures were found not in commodity heading 1517, but in other commodity headings (1512, 1515). In this case, in addition to inconsistencies in foreign trade statistics, as a result of wrong designation of the CN FEA codes of the goods, there is a situation of shifting the duty rates set for the goods to lower rate codes. If we look at

the tariff rates set according to the Decision No. 3818: vegetable oils – 5 percent; (Commodity position 1517) – 15, not less than 0.15 USD per kg.

An analysis of these rates shows that there are cases of illegal labeling of edible vegetable oil blends as disguised goods to pass customs clearance as single ingredient vegetable oil. At the same time, the prices of vegetable oils are different and are formed based on the method of extraction, time, quantity, demand and supply. In this case, taking into account that the mixtures are composed of different oils, their price (customs value) is determined based on the composition of oil-oil mixtures.

Recommended code for the product commodity nomenclature foreign economic activity of the Republic of Uzbekistan

1517 90910 1 – – – – mixture of olive oil

1517 90910 9 – – – – others

On the basis of the above scientific analysis, the need to correctly determine the CN FEA code of the fat-oil mixture suitable for consumption brings economic benefits in terms of statistics, tariff and customs value. The price of this oil is high due to the complexity of olive oil extraction and production technology. On this basis, it is natural that the price of mixtures of this oil and other vegetable oils is high. Based on the above situation, customs expertise methods were developed in order to introduce a separate CN FEA code to the mixtures of olive and other vegetable oils and to identify them.

Conclusion

Thus, methods and results for determining the quality of corn, olive and sunflower oil were presented. Modern organoleptic and physico-chemical methods for determining the quality of these goods have been developed and introduced into customs practice.

References

Andreeva, E. I. Development of methodology and improvement of the mechanism for managing the identification of goods for customs purposes: Monograph / E. I. Andreeva.– M.: RIO Russian Customs Academy, 2016.– 202 p.

Gail, L. Kramer, Clarence, W. Jensen, Douglas, D. Southgate Jr. Agricultural economics and agribusiness.– New York, 2001.– 519 p.

Gibilisko, S. Alternative energy without secrets / Stan Gibilisko; [transl. from English A. V. Solovyova].– M.: Eksmo, 2010.– 368 p.– (No secrets).

Shalygina, A. M., Kalinina, L. V. General technology of milk and dairy products.– Moscow: Colossus, 2006.– P. 180–182.

Dodaev, K. O., Absalyamov, F. M., Begmatov, A. B. Tuya sutuningshifobakhshlikhususiyati // “Kimevaozik-ovkat mҳsulotlarining sifati hamda havfsizligini taminlashda innovation technologylar”.

Mavzusidagi II Republic Ilmiy Amaliy-Technikaviy Conference Materiallari. – Tashkent, TKTI. (May 17, 2019).–P. 144–145.

Methods for determining toxic elements // State standards. Raw materials and food products.– Moscow: IPK publishing standards, 2002.– P. 50–70.

Ibragimov, U. K. Evaluation of antioxidants – food additives // STANDART, 2002.– No. 1.– P. 58–59.

Karimkulov, K. M., Uzohkov, I. E., Sarikulov, M. K. Studying The Classification and Quality of Food // The American Journal of Agriculture and Boimedical Engineering, 2021.– Vol. 03.– Issue 03–06.– P. 32–38.

submitted 02.12.2023;
accepted for publication 28.12.2023;
published 24.01.2024

Contact: abdurahmanovaazoda@gmail.com

The Austrian Journal of Technical and Natural Sciences, No 11–12
ISSN 2310-5607

PREMIER Publishing
ppublishing.org

DOI:10.29013/AJT-23-11.12-9-14

OBTAINING COLLAGEN-BASED FEED CONCENTRATES AND STUDYING THEIR EFFECT ON FISH PRODUCTIVITY

Radjabov O.I. [1]***, Buriev D.A.*** [1]***, Otajanov A. Yu.*** [1]***,***
Abdurahmanov J.A. [1]***, Turaev A.S.*** [1]

[1] Academy of Sciences of the Republic of Uzbekistan, Institute of Bioorganic Chemistry

Cite: *Radjabov, O.I., Buriev, D.A., Otajanov, A. Yu., Abdurahmanov, J.A., Turaev, A.S. (2023). Obtaining Collagen-Based Feed Concentrates and Studying Their Effect on Fish Productivity. Austrian Journal of Technical and Natural Sciences 2023, No 11-12.* https://doi.org/10.29013/AJT-23-11.12-9-14

Abstract

This paper examines the performance of feed concentrates based on bovine skin collagen and their effect on fish feeding efficiency. Because of research, it was possible to obtain a protein concentrate containing up to 50 and 70%. When these concentrates are added to fish feed for 10%, it was observed that they have a positive effect on the growth of fish, and it was found that the concentrates have no side effects on the parenchymatous organs of fish.

Keywords: *collagen; protein; concentrate; polysaccharide; fish*

Introduction

Feeds derived from animal raw materials play a key role in providing essential amino acids to maintain high animal productivity and improve meat quality. Finding new sources of food is very important in increasing the food supply. The daily increase in the demand for meat products requires additional protein-rich forages for feeding livestock, fish, and chickens (Soloveva A.A., Zinina O.V., Rebezov M.B., Lakeeva M.L., Gavrilova E.V., 2013; Lähteinen T., Rinttilä T., Koort J.M. K., Kant R., Levonen K., Viljanen M.J., Björkroth J., Palva A., 2015).

Currently, much attention is being paid to obtaining protein hydrolysates and their rational use in the production of feed additives from low-value products obtained from the slaughtering and processing of livestock (Radjabov O.I., Gulyamov T., Turaev A.S., 2011; Radjabov O.I., Turaev A.S., Gulmanov I.D., Otajanov A. Yu., Azimova L.B., 2022; Mora L., Reig M., Toldrá F. 2014; Martínez-Alvarez O., Chamorro S., Brenes A., 2015).

The most promising raw material as protein hydrolysates in the production of food additives is collagen storage waste. In many production enterprises, the ways of rational use of waste products of animal products have not yet been solved. As a result, in addition to material losses, it causes environmental pollution. Therefore, research aimed at the production of high-quality feed proteins from animal processing waste is one of the most urgent problems (Djekic I., Tomasevic I. 2016; Veeruraj A., Arumugam M., Ajithkumar T., Balasubramanian T., 2015).

The main goal of the work is to obtain protein-rich feed concentrates based on chemically processed collagen from collagen-preserving raw materials and to determine their effectiveness.

Materials and Methods

To obtain collagen splits from cattle hides are used as raw materials. The raw cut of cattle hides was washed with running water, and crushed into pieces of 1x1 cm. Then alkali-salt treatment was carried out to soften and swell. The treatment was carried out for 24 hours with stirring. After treatment, the alkali-salt mixture was neutralized with a solution of hydrochloric acid, the spent reaction mixture was drained, and the raw materials were washed with running water until the pH of the medium was 7 ± 0.5. The washed raw materials were homogenized until a homogeneous collagen mass was obtained. To obtain a high-protein concentrate, the aqueous mass of collagen was mixed with chaff and cotton meal in a 1:1 mass ratio. The resulting mixture was dried and crushed.

Experiments to determine the effect of protein concentrates on fish productivity were divided into 5 groups of 75 carp of different weights in closed ponds, and their total and average weights were determined.

Table 1. *Weight indicators of fish in each pond, g*

№	Pool number				
	Pool № 1	Pool № 2	Pool № 3	Pool № 4	Pool № 5
1.	350 g	337 g	418 g	421 g	359 g
2.	365 g	395 g	383 g	405 g	365 g
3.	380 g	363 g	393 g	373 g	371 g
4.	400 g	412 g	397 g	411 g	428 g
5.	420 g	410 g	368 g	409 g	417 g
6.	330 g	338 g	430 g	329 g	419 g
7.	380 g	339 g	480 g	398 g	383 g
8.	363 g	393 g	397 g	373 g	319 g
9.	412 g	418 g	362 g	421 g	422 g
10.	437 g	407 g	397 g	417 g	427 g
11.	396 g	387 g	426 g	436 g	391 g
12.	318 g	398 g	418 g	418 g	358 g
13.	369 g	379 g	409 g	379 g	379 g
14.	426 g	466 g	396 g	416 g	431 g
15.	431 g	451 g	381 g	429 g	398 g
Average	385.13 g	392.87 g	403.67 g	401.73 g	391.13 g

The fish in each pool were fed the following fixed diets for 30 days: № 1-OE-1, № 2-OE-2, № 3-OE-3, № 4-OE-4. For comparison, “ALLER CLASSIC” mixed feed for carp from “Aller Aqua Polska” was used. The quantitative composition of the feed is presented in Table 2.

The fish in each pool were fed three times a day and the water was completely recirculated.

Morphological study of parenchymal organs of fish. The material for histological examination was described macroscopically, pieces were cut out and placed in formalin fixative 10–15% for a day, then these pieces were washed in running water for several hours. Next, the pieces were passed through the battery with alcohol and chloroform; the battery consisted of 7 jars. The entire drum battery runs through within 24 hours. Then they were transferred to the “porridge”, which consists of chloroform + paraffin. We loaded it into a thermostat at 37 degrees for 1–2 hours, and then into a thermostat at 57 degrees for impregnation for 1 hour. Only after an hour, they were allowed to cool, and

harden, and then the paraffin block was cut out. The block was mounted on a wooden cube and cut into a thin layer using a microtome. The glasses were pre-prepared for cutting, smeared with protein, and pierced on an alcohol lamp, the cut materials were fixed on the glasses and stained with hematoxylin and eosin. After staining, they were fixed with balsam and covered with a coverslip. The finished histological preparations were viewed under a binocular microscope made in Germany LEIKA and photographed with a web camera of the NM-35 series.

Table 2. *Quantitative ratio of feed components, g,%*

№	Name	Content of products added to feed, g,%				
		OE-1	OE-2	OE-3	OE-4	OE-5
1.	Wheat	15	15	15	15	ALLER AQUA
2.	Wheat bran	9	9	9	9	POLSKA
3.	Soybean meal	15	15	15	–	
4.	Sunflower meal	15	15	15	15	“ALLER CLASSIC”
5.	Fish flour	–	–	10	–	
6.	Collagen-cotton meal	–	10	–	25	
7.	Collagen-chaff	10	–	–	–	
8.	Chicken meal	15	15	15	15	
9.	Bone flour	10	10	10	10	
10.	Corn	5	5	5	5	
11.	Sunflower oil	3	3	3	3	
12.	Tricalcium phosphate	2	2	2	2	
13.	Premix	1	1	1	1	
	Protein,%	28	30	33	38	30

Results and discussions

When chaff and cotton meal are introduced into the collagen mass, a homogeneous viscous-fluid composition is formed, where the collagen particles are destroyed to form a viscous continuous medium in which the components of the system are evenly distributed and no signs of physical incompatibility are observed. It should be noted here that polysaccharides affect the structure of collagen and as a result collagen dissolves, moreover, all this happens in an aqueous environment and during the dehydration process the mixture is released in the form of a powder. The indicators of collagen-based concentrates are presented in Table 3.

Table 3. *Nutrient concentrate based on collagen*

№	The composition of the concentrate				Moisture,%	Total protein content, g,%
	collagen aqueous mass, g	collagen, g	chaff, g	cotton meal, g		
1.	1200	160	160	–	12 ± 1	51 ± 2
2.	1200	160	–	160	11 ± 1	70 ± 2

Collagen is a protein substance obtained from animals. Collagen contains a common protein similar to fish meal. Currently, all intensive fish farms in our republic import fish-

meal from abroad. Taking this into account, the efficiency of feed concentrates developed based on collagen obtained by chemical treatment of cattle hides in the intensive cultivation of carp fish was studied.

Table 4 shows the changes in the mass of carp fish as a result of the 30-day experiment.

Table 4. *Mass changes in carp fish after 30 days*

№	Experimental pools and feed type (OE)				
	Pool № 1 OE-1	Pool № 2 OE-2	Pool № 3 OE-3	Pool № 4 OE-4	Pool № 5 OE-5
1.	557 g	631 g	678 g	463 g	572 g
2.	545 g	655 g	589 g	511 g	637 g
3.	680 g	573 g	693 g	424 g	563 g
4.	619 g	621 g	637 g	542 g	626 g
5.	628 g	617 g	588 g	492 g	587 g
6.	539 g	558 g	638 g	561 g	671 g
7.	587 g	579 g	690 g	523 g	602 g
8.	567 g	593 g	597 g	413 g	563 g
9.	652 g	658 g	662 g	543 g	631 g
10.	637 g	627 g	593 g	514 g	614 g
11.	594 g	587 g	723 g	458 g	636 g
12.	518 g	498 g	684 g	537 g	688 g
13.	467 g	579 g	657 g	484 g	579 g
14.	526 g	667 g	691 g	514 g	616 g
15.	611 g	689 g	675 g	423 g	624 g
Average	581.8 g	608.8 g	653 g	493.47 g	613.93 g

It was found that replacing collagen-chaff and collagen-cotton meal samples with a 10% equivalent amount of fishmeal in the feed did not cause negative changes in fish growth. However, when fishmeal and soybean meal were replaced by collagen-cotton meal (total 25%) in the feed, the total protein content increased and the fish growth slowed due to energy imbalance.

A comparative analysis of mass change in fish after 30 days of experiment is shown in Table 5.

Table 5. *Comparative analysis of changes in fish mass in experiments*

Indicators	Pool № 1 OE-1	Pool № 2 OE-2	Pool № 3 OE-3	Pool № 4 OE-4	Pool № 5 OE-5
Average mass before the experiment, g	385.13	392.87	403.67	401.73	391.13
Average mass after the experiment, g	581.8	608.8	653	493.47	613.9
Mass ratio	1.51	1.54	1.61	1.22	1.56
The amount of total protein in the feed,%	28	30	33	38	30

As can be seen from the results of the experiment presented in Table 5, the mass of the fish increased in all the conducted experiments for 30 days. The highest fish mass

was observed in experiment № 3, where 10% fishmeal was used in the feed, but the total protein content in this experiment was 33%. Experiments conducted with collagen-cotton meal in experiment № 2 and "ALLER AQUA POLSKA" feed in experiment № 5 showed almost the same indicator, fish productivity increased by 1.54 and 1.56 times, respectively. Also, based on physiological experiments in fish farming, it was found that good results can be achieved when collagen-based protein concentrates are included in the diet in an amount of up to 10%.

Histological examination of the parenchymal organs of fish from all groups revealed no significant changes. In the liver, slight fatty degeneration was observed in hepatocytes mainly in groups 1 and 3, hyperemia and vascular congestion in groups 4 and 5, the lobular structure and beam structure were preserved in all groups. In the spleen, hypoplasia of the white and in some areas of the red pulp was noted, as well as a sharp expansion of the lumen of blood vessels with congestion in one case. In the kidney, there are straight and convoluted tubules with clear contours, the basement membrane is preserved, the nuclei in the epithelium are arranged in a single row, the glomeruli are equal in size, and capillary loops are without signs of pathology. In the first group, a cystic-changed atrophic glomerulus was detected in the field of view. Heart – the fibrous structure of the muscle tissue is preserved, the transverse striation is determined, and the nuclei have a central location with clear contours. In isolated cases, slight fatty degeneration and congestion of the vessels of the intermuscular layers are noted.

According to the results of the histological study of the parenchymatous organs of fish, the structural and functional structure of the parenchymatous organs was preserved after using the nutrient concentrate, and no signs of pathological changes were detected. Some of the identified dystrophic changes and blockage of blood vessels have a common pathological feature, which does not depend on the use of protein concentrate, as it is present in all experimental groups.

Conclusion

High-protein concentrates based on collagen-chaff and collagen-cotton meal with a high content of total protein (50 and 70%) were obtained. Testing high-protein concentrates on fish showed that when using collagen-cotton meal concentrate, after 30 days of feeding, the weight of fish increases by 1.5 times and corresponds to imported feed. Histological studies of the parenchymal organs of fish after using the protein concentrate showed that the structural and functional structure of the parenchymal organs was preserved and no signs of pathological changes were identified.

References

Soloveva, A.A., Zinina, O.V., Rebezov, M.B., Lakeeva, M.L., Gavrilova, E.V. [Current Biotechnological Solutions for Meat Industry]. Molodoy uchenyy [Young Scientist]. 2013.– No. 5.– P. 105–107.

Lähteinen, T., Rinttilä, T., Koort, J.M. K., Kant, R., Levonen, K., Viljanen, M.J., Björkroth, J., Palva A. The effect of a multispecies lactobacillus.– Livestock Science, 2015.– 180.– P. 164–171.

Radjabov, O.I., Gulyamov, T., Turaev, A.S. Collagen medical, obtaining and research // Uzbek chemical journal. Special issue. 2011.– P. 94–97.

Radjabov, O.I., Turaev, A.S., Gulmanov, I.D., Otajanov, A. Yu., Azimova, L.B. Obtaining Collagen and Morphological Studies of Injection Solution on Its Basis. International Journal of Materials and Chemistry.– 12(3). 2022.– P. 39–43. DOI: 10.5923/j.ijmc.20221203.01.

Mora, L., Reig, M., Toldrá, F. Bioactive peptides generated from meat industry by-products. Food Research International. 2014.– 65.– P. 344–349.

Martínez-Alvarez, O., Chamorro, S., Brenes, A. Protein hydrolysates from animal processing by-products as a source of bioactive molecules with interest in animal feed. Food Research International, 2015.– 73.– P. 204–212.

Djekic, I., Tomasevic, I. Environmental impacts of the meat chain-Current status and future perspectives. Trends Food Sci. Technol. 2016.– 54.– P. 94–102.

Veeruraj, A., Arumugam M., Ajithkumar T., Balasubramanian T. Isolation and characterization of collagen from the outer skin of squid (Doryteuthis singhalensis). Food Hydrocolloids 2015.– 43.– P. 708–716.

submitted 15.12.2023;
accepted for publication 25.12.2023;
published 24.01.2024

Contact: abdurahmanovaazoda@gmail.com

The Austrian Journal of Technical and Natural Sciences, No 11–12
ISSN 2310-5607

PREMIER Publishing
ppublishing.org

DOI:10.29013/AJT-23-11.12-15-22

BIOSORBENT BASED ON RICE HUSK FOR REMOVING COPPER AND NICKEL IONS FROM WASTEWATER

Maksudova Aziza Abdukakharovna [1], Mutalov Shukhrat Akhmadzhonovich [1], Adilova Klara Muratdjanovna [1]

[1] Tashkent Institute of Chemical Technology, Republic of Uzbekistan

Cite: *Maksudova, A.A., Mutalov, Sh.A., Adilova, K.M. (2023). Biosorbent Based on Rice Husk for Removing Copper and Nickel Ions From Wastewater. Austrian Journal of Technical and Natural Sciences 2023, No 11-12*. https://doi.org/10.29013/AJT-23-11.12-15-22

Abstract

The adsorption of Cu (II) and Ni (II) ions from aqueous solutions by an adsorbent obtained by treating rice husks with an aqueous solution of monoethanolamine was studied. The structure of the adsorbent was studied using IR spectroscopy. It has been shown that adsorption reaches equilibrium within 60 minutes at an optimal pH value of 5–6. The adsorption process was found to correspond to the Freundlich model with high correlation coefficients. The resulting adsorbent can be used as an effective, inexpensive and environmentally friendly bioadsorbent for treating wastewater from heavy metal ions.

Keywords: *adsorption, rice husk, monoethanolamine, wastewater, modification, adsorption isotherm*

Introduction

One of the main pollutants of natural water bodies are heavy metals, which have toxic, mutagenic and carcinogenic properties. They tend to accumulate in living organisms, which leads to severe poisoning (Acharya J., Kumar U., & Rafi P.M., 2018). The main method of treating wastewater from heavy metal ions is reagent methods, which do not provide the required degree of water purification and lead to the formation of sludge that requires disposal. Recently, bioadsorbents based on agricultural waste, which are a cheap, annually renewable source of raw materials and do not pose a threat to the environment, are increasingly used to purify wastewater from heavy metal ions. Rice hulls, which are produced as a by-product of the rice milling process, can also be used as an adsorbent. The composition of rice husks includes cellulose (32%), hemicelluloses (21%), lignin (21%) and silicon oxide (20%), which gives the structure mechanical strength. Due to the presence of three hydroxyl groups in cellulose, it has adsorption properties towards heavy metal ions. However, untreated rice husks have low adsorption capacity because the hydroxyl groups are linked by intermolecular hydrogen bonds, which makes it difficult for metal ions to reach them when extracted from solution. To increase the adsorption capacity of rice husk, methods of treatment with alkali, tartaric acid, and epichlorohydrin have been proposed (Zhang Y., Zheng, R., Zhao J., Zhang, Y., Wong P.K., & Ma F., 2013;

Wong K. K., Lee C. K., Low K. S., & Haron M. J., 2003; Shrestha, B., Kour J., Homagai P. L., Pokhrel M. R., & Ghimire K. N., 2013).

In this work, an adsorbent was obtained by treating rice husks with an aqueous solution of monoethanolamine to purify wastewater from Cu (II) and Ni (II) ions. This treatment leads to the destruction of hydrogen bonds between hydroxyl groups, increasing their availability for binding metal ions, as well as the introduction of amino groups into the structure of the adsorbent. In this case, metal ions bind to the hydroxyl and amide groups of the adsorbent through the mechanisms of ion exchange and complex formation (Sud, D., Mahajan, G., & Kaur, M. P., 2008).

Materials and methods

Rice husk samples were treated with a solution of monoethanolamine in water according to the method (Maksudova A., Adilova K., 2022). Component ratio: rice husk (1g): modifier solution (100ml) = 1:100. The treatment was carried out for 24 hours with constant shaking. Next, the solution was filtered, the rice husks were washed with water and dried. IR spectroscopic studies of the original and modified rice husk were carried out using a Shimadzu "IRAffinity" IR-Fourier spectrometer (Japan). Wastewater solutions containing ions Cu (II) and Ni (II) with a concentration of 5–300 mg/l were prepared from the salts $CuSO_4 \times 5\ H_2O$ and $NiSO_4 \times 7\ H_2O$ by diluting the initial solution with distilled water.

Adsorption capacity studies were carried out in static mode. 100 ml of wastewater solution of a given concentration was poured into 250 ml flasks and 1 g of adsorbent was added. The flasks were kept for 60 minutes with constant shaking. Next, the solutions were filtered and the content of metal ions in water was determined using the atomic absorption method on an Agilent spectrophotometer Technologies 140 Series AA (France).

Results and discussion

IR spectra of the original and modified rice husk are shown in Figures 1 and 2.

Figure 1. *IR spectrum of original unprocessed rice husk*

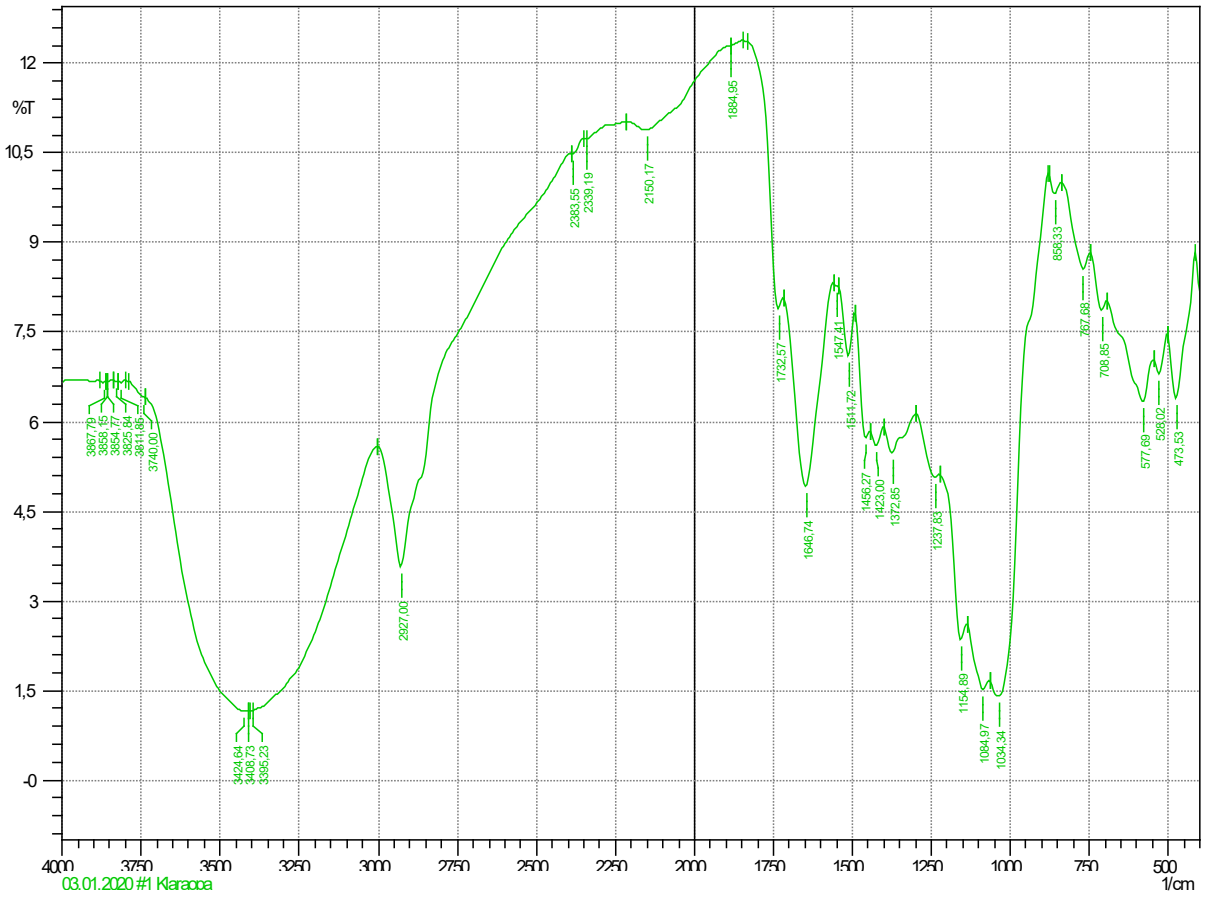

Figure 2. *IR spectrum of modified rice husk*

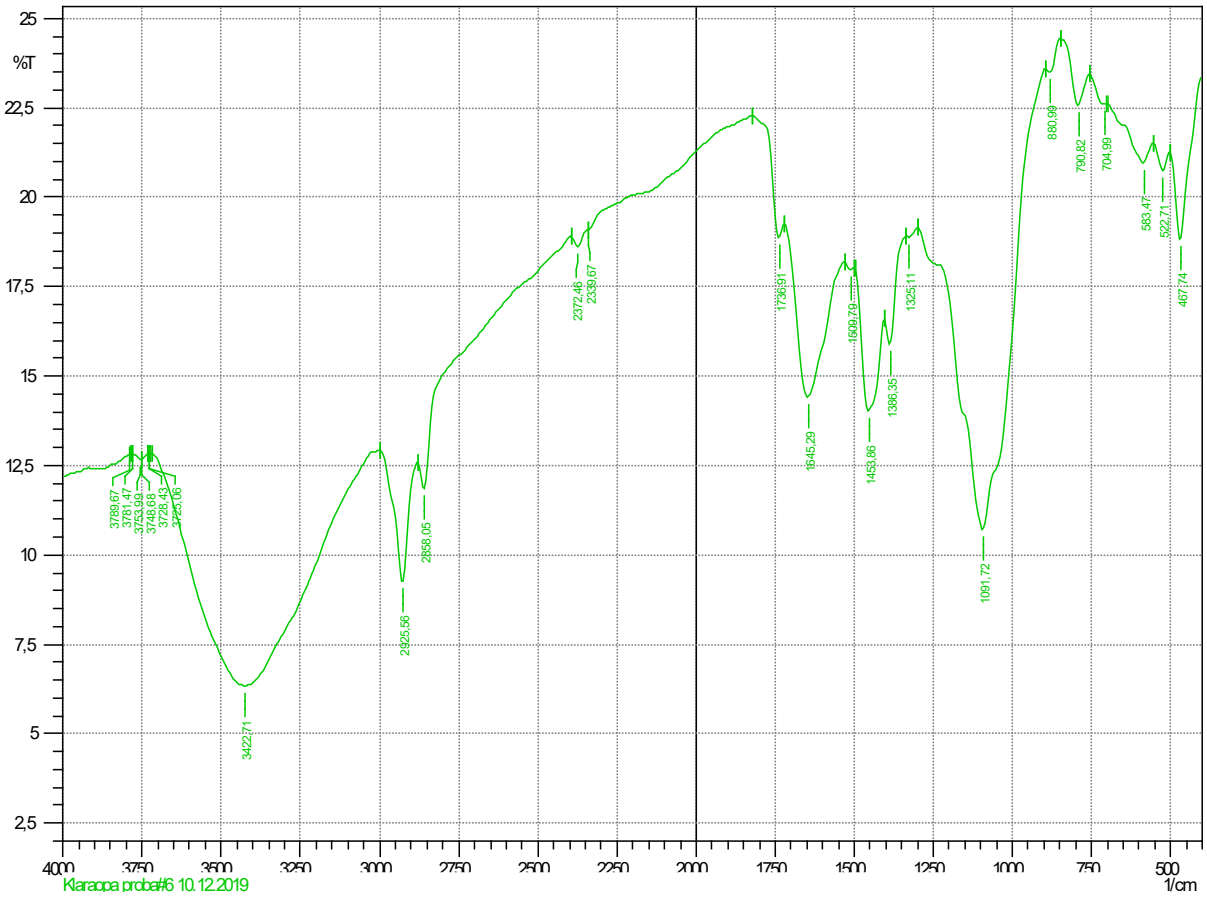

The IR spectra show that the band at 3395–3408 cm $^{-1}$, responsible for OH groups linked by hydrogen bonds, shifts to a value of 3422 cm $^{-1}$, which indicates the destruction of intermolecular hydrogen bonds. The absorption band in the region of 1732––1736 cm $^{-1}$ corresponds to vibrations of the carbonyl group C = O of lignin. After treatment with monoethanolamine, the intensity of this peak decreases, indicating a decrease in the number of C = O groups that enter into chemical interaction with monoethanolamine molecules. The appearance of a specific absorption band at 1091 cm $^{-1}$ in the IR spectra of the modified samples is associated with stretching of the C- N bond, which lies in the region of 1230–1030 cm $^{-1}$. This indicates the introduction of amino groups into the structure of the biosorbent.

When carrying out adsorption studies, the optimal pH values and adsorption time were determined at which the maximum absorption of metal ions was observed.

The adsorption value A (mg×g^{-1}) was determined using the formula (Bonilla- Petriciolet A., Mendoza-Castillo D.I., & Reynel -Ávila, H.E., 2017):

$$q_e = \frac{(C_0 - C_e)V}{m \times 1000}$$

V – volume of the test solution, ml;

C_0 and C_e – initial and equilibrium concentration of metals in water, mg × L^{-1};

m – mass of adsorbent, g.

A study of the effect of pH on adsorption showed that the optimal pH value is in the range of 5–6. At low pH, H $^{+}$ ions, which have high mobility, are predominantly adsorbed on the surface of the adsorbent. This leads to the formation of a positively charged adsorbent surface, which reduces the adsorption of metals. With increasing pH, the concentration of H $^{+}$ ions in the solution decreases and the adsorption of metal cations increases due to electrostatic attraction to the negatively charged surface.

The dependence of adsorption on time is shown in Figure 3.

Figure 3. *Dependence of adsorption of metal ions on contact time for ▲ – Cu^{2+} ions and ■ – Ni^{2+} ions*

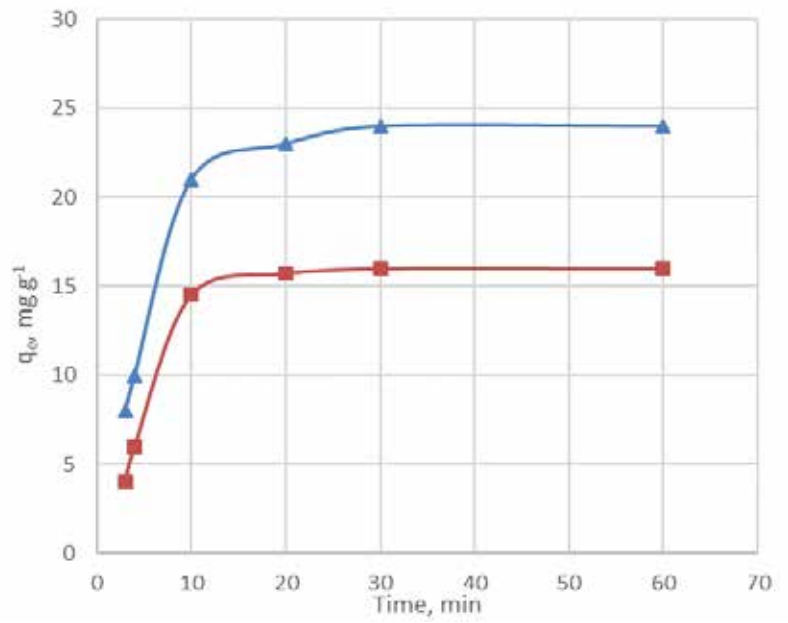

From Figure 3 it can be seen that at the beginning of the process, adsorption increases within 60 minutes balance is achieved. This is explained by the fact that at the beginning of the cleaning process there are enough active centers on the surface of the adsorbent capable of binding metal, after filling which the adsorption does not change. With an increase in the initial concentration of solutions, an increase in adsorption was observed due to an increase in the driving force necessary for metal ions to overcome the forces of resistance to mass transfer between the aqueous and solid phases. But at the same time, the degree of purification decreases, which is explained by the limited number of active centers on the surface of the adsorbent.

Figure 4. *Dependence of the degree of purification on the initial concentration of the solution: 1 – for Cu^{2+} ions, 2 – for Ni^{2+} ions*

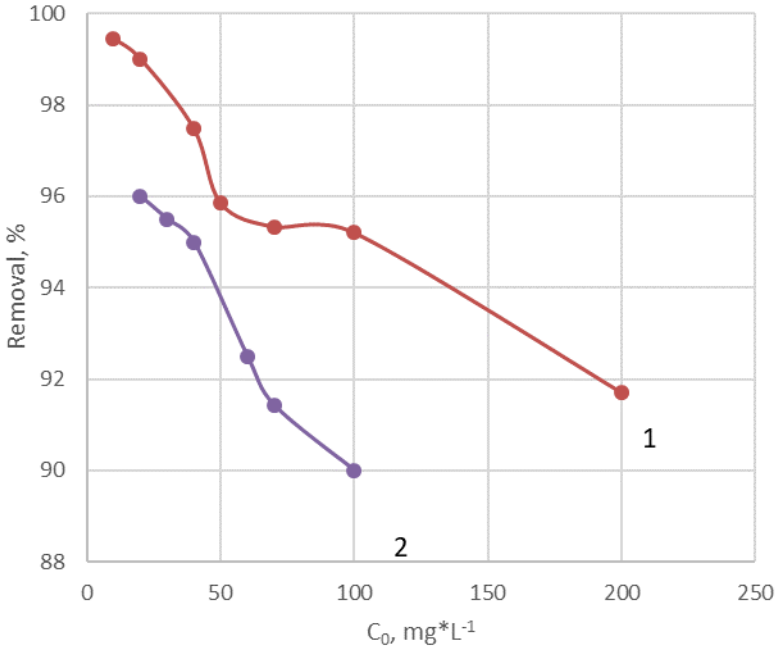

Figure 5. *Adsorption isotherms: 1,2 – modified rice husk for copper and nickel ions, respectively, 3,4 – untreated rice husk for copper and nickel ions, respectively*

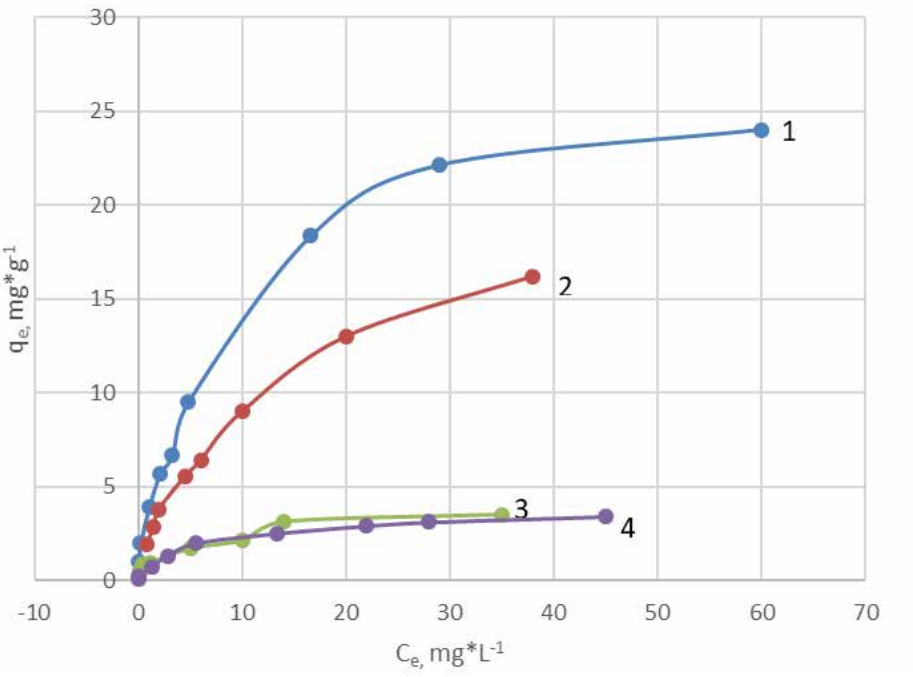

Figure 5 shows the adsorption isotherms of copper and nickel for the original and modified rice husks.

The linear form of the Langmuir equation (Langmuir I., 1916) is as follows:

$$\frac{C_e}{q_e} = \frac{1}{q_m \times K_L} + \frac{C_e}{q_m}$$

To determine the coefficients of the Langmuir equation, a graph of the dependence of C_e/q_e on C_e was plotted in linear form. The value of q_m and the Langmuir constant were found from the tangent of the slope of the straight line and the section cut off on the axis of values C_e/q_e.

Figure 6. *Graphs of the dependence of C_e/q_e on C_e: a – for copper ions, b – for nickel ions.*

a)

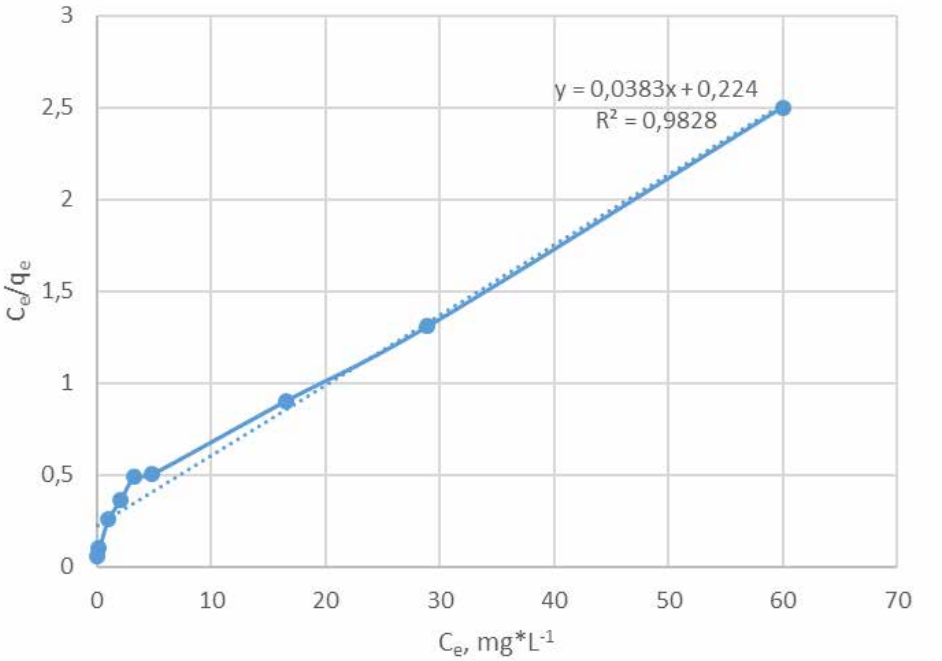

b)

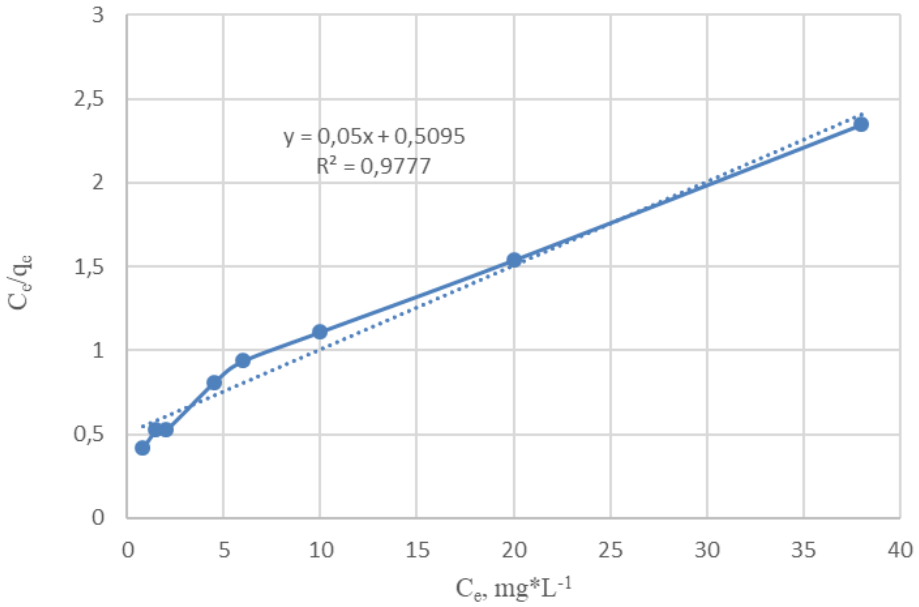

The Freundlich equation (Freundlich H. M. F., & Freundlich, H. M. F. (1906) in logarithmic form has the form:

$$lgq_e = lgK_F + \frac{1}{n} lgC_e$$

which allows you to graphically determine the constant parameters of the equation K_F and $1/n$.

Figure 7. *Graphs of dependence lgq_e/lgC_e in linear form: a – for copper ions, b – for nickel ions*

a)

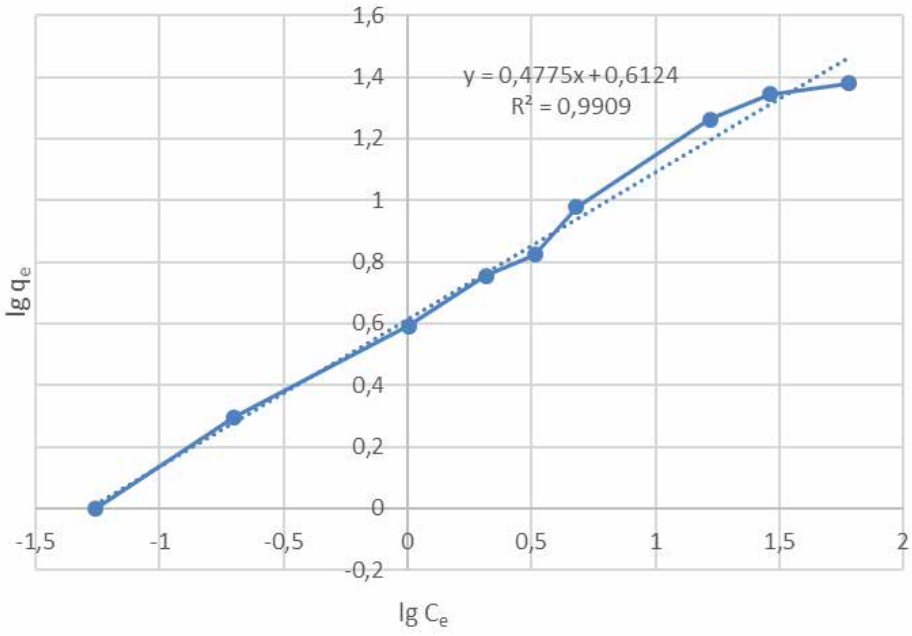

b)

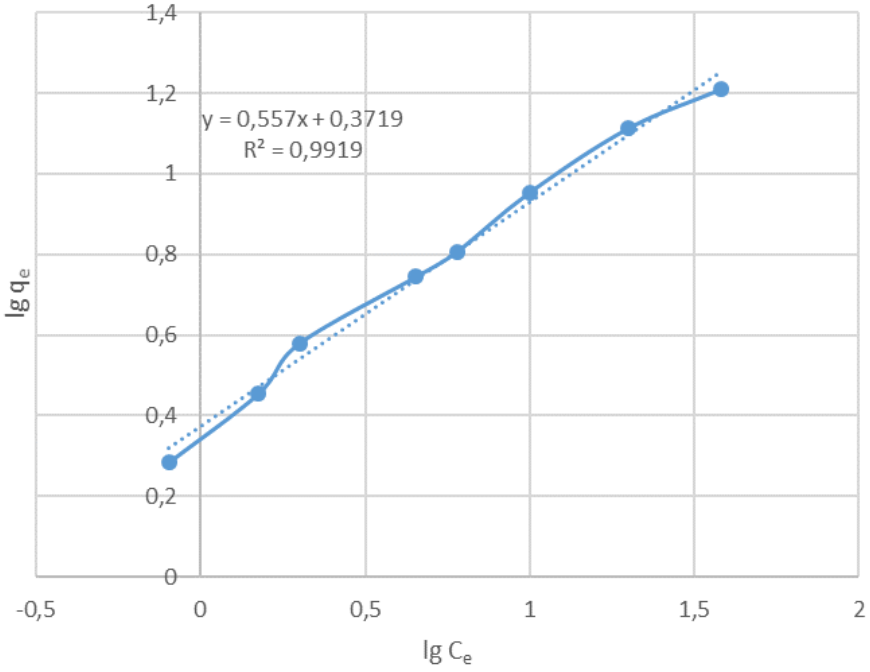

The correspondence of each model to the experimental data was determined by the standard deviations R^2.

The found adsorption parameters are given in Table 1.

Table 1. *Adsorption parameters of the Langmuir and Freundlich models and correlation coefficients*

Adsorbent	Freundlich model			Langmuir model		
	K_F	1/n	R^2	K_l (l×mg^{-1})	q_m(mg×g^{-1})	R^2
			Cu^{2+}			
Initial RH	0.957	0.3686	0.9759	0.392	3.604	0.963
Modified RH	4.096	0.4775	0.9909	0.171	26.109	0.9828
			Ni^{2+}			
Initial RH	0.716	0.4548	0.9893	0.273	3.5486	0.9854
Modified RH	2.355	0.557	0.9919	0.0981	20	0.9777

The correlation coefficients R^2 show that the adsorption process is better described by the Freundlich equation compared to the Langmuir equation. This suggests the participation of functional groups in the inner layers of the adsorbent in the binding of metal ions. Values n >1 indicate the spontaneous nature of adsorption.

Conclusion

The results of the study showed that adsorbents obtained by chemical treatment of rice husks with an aqueous solution of monoethanolamine can be used as effective, inexpensive and environmentally friendly bioadsorbents for treating wastewater from copper and nickel ions. The introduction of amide groups leads to an increase in the number of active sites for the binding of metal ions. Adsorption isotherms are better described by the Freundlich equation than by the Langmuir equation, which suggests the participation of functional groups of the internal layers of the adsorbent in the binding of metal ions.

References

Acharya, J., Kumar, U., & Rafi, P.M. (2018). Removal of Heavy Metal Ions from Wastewater by Chemically Modified Agricultural Waste Material as Potential Adsorbent-A Review. International Journal of Current Engineering and Technology, of. URL: https://doi.org/10.14741/ijcet/v.8.3.6

Zhang, Y., Zheng, R., Zhao, J., Zhang, Y., Wong, P.K., & Ma, F. (2013). Biosorption of zinc from aqueous solution using chemically treated rice husk. BioMed Research International, 2013. URL: https://doi.org/10.1155/2013/365163

Wong, K.K., Lee, C.K., Low, K.S., & Haron, M.J. (2003). Removal of Cu and Pb from electroplating wastewater using tartaric acid modified rice husk. Process Biochemistry,– 39(4).– P. 437–445. URL: https://doi.org/10.1016/S0032-9592(03)00094-3

Shrestha, B., Kour, J., Homagai, P.L., Pokhrel, M.R., & Ghimire, K.N. (2013). Surface Modification of the Biowaste for Purification of Wastewater Contaminated with Toxic Heavy Metals – Lead and Cadmium. Advances in Chemical Engineering and Science,– 03(03). URL: https://doi.org/10.4236/aces.2013.33022

Sud, D., Mahajan, G., & Kaur, M.P. (2008). Agricultural waste material as potential adsorbent for sequestering heavy metal ions from aqueous solutions – A review. In Bioresource Technology,– Vol. 99.– Issue 14. URL: https://doi.org/10.1016/j.biortech.2007.11.064

Maksudova, A., Adilova, K. (2022). Adsorbent based on rise husks. Patent No. 07247, Ministry of Justice of the Republic of Uzbekistan.

Bonilla-Petriciolet, A., Mendoza-Castillo, D.I., & Reynel -Ávila, H.E. (2017). Adsorption processes for water treatment and purification. In Adsorption Processes for Water Treatment and Purification. URL: https://doi.org/10.1007/978-3-319-58136-1

Langmuir I. (1916). The constitution and fundamental properties of solids and liquids. Part I. Solids. Journal of the American Chemical Society, 38 (eleven). URL: https://doi.org/10.1021/ja02268a002

Freundlich H.M. F., & Freundlich, H. M. F. (1906). About the adsorption in solution. Z. Phys. Chem., 57 (May).

submitted 12.12.2023;
accepted for publication 25.12.2023;
published 24.01.2024

Contact: klara.adilova57@gmail.com; aziza.maksudova2015@gmail.com

The Austrian Journal of Technical and Natural Sciences, No 11–12
ISSN 2310-5607

PREMIER Publishing
ppublishing.org

Section 2. Food processing industry

DOI:10.29013/AJT-23-11.12-23-28

TECHNOLOGY OF PRELIMINARY CLARIFICATION OF OILS FROM LOW-QUALITY COTTON SEEDS

Akhmedov Azimjon Normuminovich [1], ***Ishankulova Gavxar Norkulovna*** [2]

[1] Department of Food Technology of Products of the Karshi Engineering and Economic Institute, Karshi, Uzbekistan

[2] Department of Agricultural Product Storage and Preprocessing Technology of the Karshi Engineering and Economic Institute, Karshi, Uzbekistan

Cite: *Akhmedov A.N., Ishankulova G.N. (2023). Technology of Preliminary Clarification of Oils From Low-Quality Cotton Seeds. Austrian Journal of Technical and Natural Sciences 2023, No 11-12.* https://doi.org/10.29013/AJT-23-11.12-23-28

Abstract

This scientific article presents the results of pilot-production studies carried out at "Koson oil-extraction" JSC, in which the color of crude oil, its acid number, as a result of preliminary clarification of oils obtained from low-grade and non-standard cotton seeds using urea-modified soil adsorbents (UMSA) led to a decrease. At the same time, using crude oil UMSA-4, oil indicators, including color and soil consumption, decreased by approximately 2.0–2.2 times, and the acid number of oil decreased by 1.8–2 mg KOH. The technology of preliminary refining of crude oils obtained from these low-grade cotton seeds makes it possible to obtain oils that meet standard requirements.

Keywords: *food technology, cotton seeds, clarification of oils, urea-modified soil adsorbents, coloring of raw oils, acid numberoils oils*

Introduction

The difficulties of refining oils obtained from low-grade and non-standard cotton seeds require the development of more effective methods for their clarification. It is known that in cottonseed oil the color is determined by gossypol, chlorophyll and their derivatives, which react difficultly with alkali due to the presence of soap, phospholipids, etc. (Nadirov, N. K., 1973).

Various options have been proposed for reducing the color of "black" oils obtained from low-grade and non-standard cotton seeds (Mazhidov, K. Kh., Abdullaev, N. Sh., Salaev, S. 1986; Tarasov, V. E., 1985; Abullaev, N. Sh., 1989), which have not found their practical application. The reason is that they significantly reduce the oil yield, form new compounds that are difficult to remove, etc.

We consider the preliminary clarification of "black" cottonseed oils obtained from low-grade and non-standard seeds using activated adsorbents to be more economical and accessible for our enterprises.

The transfer of a certain amount of spent clay adsorbent into the cake composition is permissible because this is provided for by feed requirements (Katsitadze, B.V., Merabushvili, M.S., Aizikovich, L.E., Katsitadze, O.V., Bagishvili, M.G., 1979).

Cottonseed oils obtained from seeds III–IV and non-standard varieties of seeds, as well as as a result of deviations in technological conditions at the stage of extraction, extraction and especially distillation of miscella, belong to a number of oils called "hard to refine". These oils are characterized by a significant content of free fatty acids, phospholipids, unsaponifiable lipids and coloring substances: chlorophylls, gossypol and its modified and derivative forms, or a predominant content of coloring substances with moderate acidity of the oils.

In recent years, the number of low-grade seeds supplied to cotton processing enterprises amounted to 25–30% (Akhmedov, A.N., 2019). Therefore, the proportion of hard-to-refined oils, taking into account the quality of seeds and violations of technological conditions, increased to 40–50% of the total volume of processed unrefined cottonseed oils (Akhmedov, A.N., Abdurakhimov, S.A., 2018).

The presence of associated substances limits the use of cottonseed oils for various purposes, especially for food purposes. Therefore, they began to take measures to refine and refine them using the most accessible methods, including alkaline treatment of oils and miscellas (Abdurakhimov, S.A., Ergasheva, D.K., Nazirov, A.N., 1990; Guidance on research methods, 1967).

The intense dark color of cottonseed oil is given by the oxidation products of native gossypol, as well as melanoidin compounds, which are formed during self-heating and heat treatment of seeds. In addition, during the moisture-heat treatment of cotton mint at high temperatures, complex compounds of gossypol and chlorophyll derivatives are formed, which also change the color of the resulting crude oils.

The difficulty of refining cottonseed oils with high color lies in the use of alkaline solutions with high concentrations (more than 250 g/l) in large excess (more than 200%), which entails significant losses of valuable oil, alkali, etc. (Akhmedov, A.N., Abdurakhimov, S.A., 2018).

One of the ways to solve this problem is considered to be preliminary clarification of raw oils obtained from low-grade and non-standard cotton seeds using an effective adsorbent. An analysis of literary sources on the refining of cotton oils showed that it is necessary to improve the existing technology for refining oils obtained from low-grade and non-standard cotton seeds, since there are a number of disadvantages: large losses of raw materials, significant consumption of alkali, etc., low yield of the final product, which negatively affects the technical and economic indicators of oil and fat enterprises (Kopeikovsky, V.M., Danilguk, S.I., Garbuzova, G.I. and others. 1982).

Materials and methods

The article uses modern methods of chemical, physico-chemical and other analyzes with the processing of the results by statistical methods (Guidelines for research methods, 1964).

We have studied the content of chlorophyll and its derivatives in oils obtained from ordinary (grades I and II) and low-grade (grades III and IV) cotton seeds. Sampling was carried out during the normal operation of the JSC "Karshi yog-extraction" and JSC "Koson oil-extraction". The analyzes of these samples and the resulting oil were carried out according to the "Guidelines for research methods ..." (Guidelines for research methods, 1964; RST Uz 624–94. 1994).

Urea-modified clay adsorbent (UMCA) was obtained by impregnating the clay adsorbent with a 30% urea solution and drying it at a temperature of 95–100 °C to a residual moisture content of 7–8%. The finished UMCA is stored in a closed desiccator.

Experiments on preliminary clarification of raw dark cottonseed oil using UMCA and refining with a low-concentrated alkaline solution are carried out in a laboratory installation, the diagram of which is presented in Fig.1.

Figure 1. *Laboratory installation for preliminary clarification of raw dark cottonseed oils and their alkaline refining: 1 – stand; 2 – reactor; 3 – electric stove with oil bath; 4 – bath building; 5 – cover; 6 – stirrer; 7 – container with oil; 8 – engine; 9 – thermometer; 10 – LATR; 11 – rheostat*

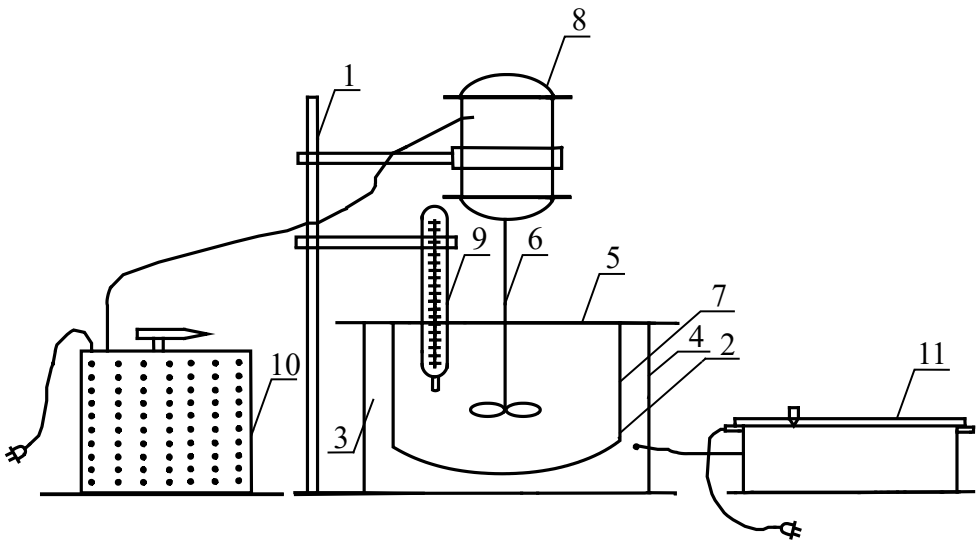

The acid number of oils was determined by potentiometric and indicator methods using a 1% alcohol solution of thymolphthalein as an indicator (Heftman, E. 1986):

– the color of cottonseed oil was determined using a Lovibond color meter (Akhmedov, A.N., 2012);

– quantitative determination of gossypol was carried out using high-performance liquid chromatography (Akhmedov, A.N., 2012);

Results

Modified adsorbents were used for pre-clarification of crude cottonseed oils obtained from low-grade and non-standard cotton seeds. The choice of the location of the UMCA input in the technological scheme determines the effectiveness of the proposed method for the preliminary clarification of raw oils obtained from low-grade and non-standard cotton seeds.

In agreement with the specialists of OA "Koson oil-extraction", a technological scheme was created for the preliminary clarification of raw cottonseed oil with a clay adsorbent modified with urea. A distinctive feature of this scheme from the known ones is that at the beginning of the line for collecting and supplying raw oils to a collection tank – a fusa-tank (thickness trap), a dosing hopper is installed, from which the UMCA is supplied to the raw oil (depending on the color of the original oil).

Figure 2 shows the proposed technological scheme for clarification of crude oils obtained from low-grade and non-standard cotton seeds using UMCA. This scheme functions as follows: through auger 1, moistened cotton mint enters the fryer 2, which is equipped with a motor and a stirrer 3. From the fryer, the pulp enters the press granulators 4, from where the pulp is sent through the auger 5 to the extraction shop. For preliminary clarification of raw oils obtained from low-grade and non-standard cotton seeds, a urea-modified clay adsorbent from Angre kaolin (UMCA –4) is fed from the collector 10 along line 11 into the raw oil collection screw 6 by a dispenser in an amount of 2–6% by weight of the oil. Next, the raw press oil is fed through line 6 into the fuso tank (thickening trap) 7, where it is cleaned of mechanical impurities and sludge. From the fuso tank 7, the return product (fuse) is sent via elevator 8 and line 9 to fryer 2, and the oil is supplied to the frame filter press 13 using pump 12 for polishing filtration. From filter press 13, the oil is sent to alkaline refining.

In table 1 shows the technological regimes for the preliminary clarification of crude oils obtained from low-grade and non-standard cotton seeds using UMCA.

Figure 2. *Technological scheme for preliminary clarification of raw cottonseed oil with a urea-modified clay adsorbent: 1 – screw; 2 – broiler; 3 – stirrer; 4 – press granulators; 5,6,9 and 14 – screw; 7 – fuso tank; 8 – noria; 10 – collection; 11 – valve; 12 – pump; 13 – filter press*

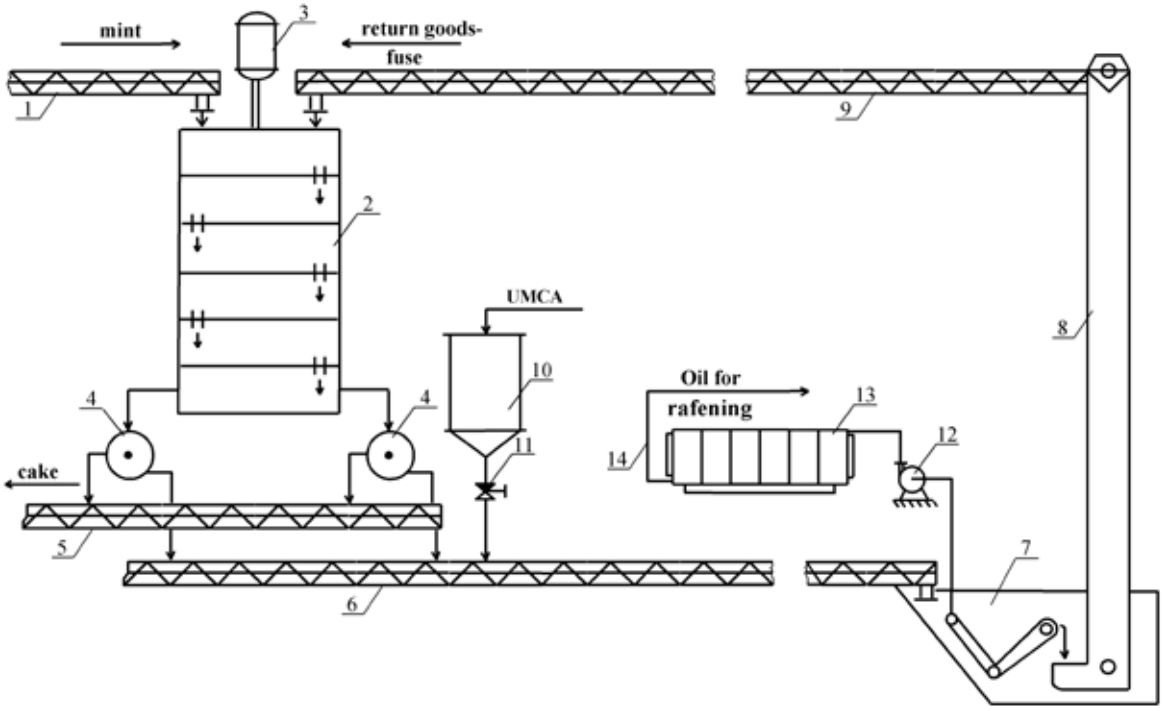

Table 1. *Standards for the technological regime of the process of preliminary clarification of crude oils using UMCA*

Name of processes and operations	Units	Values
I. Moisture and heat treatment of cotton mint:		
– huskiness of mint	%	15–17
– moisture content of mint	%	7–9
– quantity of return goods (fuza)	%	5–7
II. Pressing and granulating:		
– pulp temperature	°C	95–100
– pulp moisture	%	7.5–9.5
– dimensions of grates:		
– first	mm	1.0
– second	mm	0.75
– third	mm	0.45
– fourth	mm	0.35
– matrix size for granulation	mm	10–12
III. Pre-clarification of crude oils:		
– oil temperature	°C	80–90
– number of UMCA	%	2–6
– time	Hour	0.4–0.6
IV. Fusion separation:		
– oil temperature	°C	55–70
– speed of revolutions of the fuso tank	rev/min	50–60
V. Oil filtration:		
– oil temperature	°C	70–75
– press pressure	MPA	0.03–0.05

Table 2 presents the results of preliminary clarification of crude oils obtained from low-grade and non-standard cotton seeds using thermally activated modified adsorbents, for example UMCA-4.

From table 2 it can be seen that the preliminary clarification of crude oils obtained from low-grade and non-standard cotton seeds using 5% by weight of UMCA-4 oil made it possible to significantly reduce the color of the oils, their acid numbers and the sludge content in them. This is explained by the fact that the clay adsorbent modified with urea sorbs substances that color cottonseed oil and removes them when separating and filtering the oil.

It is known that urea is currently used in animal husbandry to enrich feed with non-protein nitrogen. Bentonites and kaolins are also used in the production of mixed feed for various purposes. Therefore, the choice of urea and natural clays when obtaining a modified adsorbent for preliminary clarification of raw oils obtained from low-grade and non-standard cotton seeds becomes justified.

Table 2. *Indicators of cottonseed oils purified in the usual way and pre-clarified using UMCA-4 in an amount of 5% of the total mass of raw materials*

Name of indicators of cottonseed oil	Oil obtained from:	
	low quality seeds	mixtures of low-grade and non-standard seeds
Crude oil, conventionally refined (control):		
Color, in 1 cm layer at 70 yellow units:	65.5	74.3
– only one red	3.7	6.5
– blue ones	5.3	6.1
Acid number, mg KOH/g	0.94	1.85
Sludge content,%		
Oil pre-clarified using UMCA:		
Color, in 1 cm layer at 70 yellow units:	36.7	42.4
– only one red	1.5	2.8
– blue ones	3.2	4.0
Acid number, mg KOH/g	0.73	0.98
Sludge content,%		

Discussion and Conclusion

Thus, pilot production studies conducted at Koson Yog-Extraction OJSC showed that the proposed technology for pre-clarification of raw oils obtained from low-grade and non-standard cotton seeds using UMCA gives positive results in reducing the color of raw oils, its acid number, content of unsaponifiable substances, moisture and volatile substances, etc. The use of UMCA-4 in the process of preliminary clarification of raw oils made it possible to reduce their color and sludge content by approximately 2.0–2.2 times. At the same time, their acid numbers also decrease (by 1.8–2 mg KOH). The developed technology for pre-clarification of raw oils obtained from low-grade cotton seeds makes it possible to obtain oils that meet the requirements of the standard. Therefore, this technology can be recommended for use when processing low-grade and non-standard cotton seeds at the plant.

References

Nadirov, N. K. Theoretical basis of activation and mechanism of action of natural sorbents in the process of clarification of vegetable oils.– M.: Food industry. 1973.– 352 p.
Mazhidov, K. Kh., Abdullaev, N. Sh., Salaev, S. Experience in complex processing of highly acidic oilseeds of cotton.– M.: INIITEI food industry, 1986.– Issue 1.– 16 p.
Tarasov, V. E. Improving the preparation of oilseed materials for oil extraction using surfactants. Abstract of Candidate of Technical Sciences. Krasnodar, KPI, 1985.– 26 p.
Abullaev, N. Sh. Development of a combined process of oil extraction and oil refining as applied to the processing of low-grade cotton seeds. Abstract of Candidate of Technical Sciences,– L.: All-Union Scientific Research Institute of Fats, 1989.– 19 p.
Katsitadze, B. V., Merabushvili, M. S., Aizikovich, L. E., Katsitadze, O. V., Bagishvili, M. G. Series: "Economics and organization of production in grain storage and processing enterprises." – M.: INIITEI Minzal, 1979.– 36 p.
Akhmedov, A. N. Investigation of indicators of cottonseed oil obtained by pre-pressing from low-grade cotton seeds // Universum: Technical Science.– Issue: 4(61). April, 2019.– Moscow 2019.– P. 23–26.
Akhmedov, A. N., Abdurakhimov, S. A. The study of the grinding process of rushanka from the nuclei of cotton seeds of different varieties. Journal chemistry and chemical engineering. 2018.– № 3.– P. 11–16.
Abdurakhimov, S. A., Ergasheva, D. K., Nazirov, A. N. Spectral evaluation of the qualitative composition of refined oils. Izvestiya vuzov. Food technology, 1990.– No. 6.– P. 77–78.
Guidance on research methods, techno chemical control and accounting of production in the oil and fat industry. // Under the general editorship of prof. Rzhekhin, V. P. and others – L.: All-Union Scientific Research Institute of Fats –1967.– I-585 p.
Kopeikovsky, V. M., Danilguk, S. I., Garbuzova, G. I. and others. Technology of production of vegetable oils.– M.: Light and food industry, 1982.– 416 p.
Guidelines for research methods, technical and chemical control and production accounting in the oil and fat industry / Ed. V. P. Rzhekhin, A. G. Sergeev-L.: VNIIZH, 1964.– T. 3.– 493 p.
RST Uz 624–94. Cottonseed oil. Color measurement method. – Tashkent. Gosstandart, 1994.– 7 p.
Heftman, E. Chromatography. Practical application of the method. In 2 parts. World.– M.: 1986.– 336 p.
Akhmedov, A. N. Improving the technology of complex refining of oils obtained from low-grade cotton seeds: Abstract of thesis. diss. ...cand. tech. Sci.– Tashkent, 2012.– 25 p.

submitted 28.11.2023;
accepted for publication 11.12.2023;
published 24.01.2024

Contact: a.ahmedov80@mail.ru

The Austrian Journal of Technical and Natural Sciences, No 11–12
ISSN 2310-5607

PREMIER Publishing
ppublishing.org

DOI:10.29013/AJT-23-11.12-29-32

STUDY OF PHYTOCHEMICAL COMPOSITION OF FROZEN APPLES AND THEIR HEALTH BENEFITS

Shakhlo Niyazova [1], Shermanov Beknazar [2], Shukhrat Khasanov [3]

[1] Shakhrisabz branch of Tashkent chemical-technological institute

[2] Alfraganus University

[3] Yu. Yunusov Institute of the Chemistry of Plant Substances

Cite: *Niyazova S., Shermanov B. Khasanov Sh. (2023). Study of Phytochemical Composition of Frozen Apples and Their Health Benefits. Austrian Journal of Technical and Natural Sciences 2023, No 11-12*. https://doi.org/10.29013/AJT-23-11.12-29-32

Abstract

Apples are widely consumed fruits known for their nutritional value and health benefits. Freezing is a common preservation method used for apples to extend their shelf life and maintain their quality. In recent years, there has been a growing interest in studying the phytochemical composition of frozen apples and understanding the potential health benefits they offer. In this article, we will explore the research conducted on the phytochemical composition of frozen apples and discuss the associated health benefits.

Keywords: *phytochemicals, phenolic, flavonoids, carotenoids, Golden spur*

Introduction

Freezing preservation of food has been used for thousands of years because of high product quality (Phoon, P.Y., Galindo, F.G., Vicente, A., Dejmek, P. 2008; Kutsakova, V.E., Frolov, S.V., Yakovleva, M.I., 1997). Generally speaking, the quality of frozen food is closely related to freezing and thawing processes. Biotechnological studies provide valuable information about the changes that occur in fruits when they are frozen. By analyzing the biochemical composition, nutritional content, and sensory attributes of frozen fruits, researchers can assess their quality and potential shelf life. These studies are essential for ensuring that exported fruits reach consumers in optimal condition, with minimal loss of nutritional value.

Apples are a widely consumed fruit and are known to be a rich source of phytochemicals. These phytochemicals, including phenolic, flavonoids, and carotenoids, have been associated with various health benefits and may play a key role in reducing the risk of chronic diseases such as cardiovascular disease and cancer (Jeanelle, Boyer, Rui Hai, Liu, 2004).

Health Benefits of Apples:

Reduced Risk of Chronic Diseases: Epidemiological studies have linked the consumption of apples with a reduced risk of certain cancers, cardiovascular disease, asthma, and diabetes. Antioxidant Activity: Apples have been found to have strong antioxidant activity, which helps protect the body against oxidative stress and damage caused by free radicals.

Inhibition of Cancer Cell Proliferation: Laboratory studies have shown that apples can inhibit the proliferation of cancer cells.

Decreased Lipid Oxidation: Apples have been found to decrease lipid oxidation, which is beneficial for cardiovascular health. Lowered Cholesterol: Consumption of apples has been associated with lower cholesterol levels.

Phytochemical Composition of Apples:

Apples contain a variety of phytochemicals, including quercetin, catechin, phloridzin, and chlorogenic acid, all of which are strong antioxidants. The phytochemical composition of apples can vary between different varieties and may also change during the maturation and ripening of the fruit. Storage has little to no effect on apple phytochemicals, but processing can greatly affect their composition (Jeanelle, Boyer, Rui Hai, Liu, 2004).

Based on the above, it is important to study the content of phytochemicals, including phenolics, flavonoids, and carotenoids in frozen apple fruit.

In this study, we investigated the antioxidant content of frozen apples (Golden spur) and analyzed their health benefits.

Materials and methods

The study used the following materials:

Frozen Apples, Laboratory Equipment: Various laboratory equipment was used to extract and analyze the phytochemicals present in the frozen apple samples. This equipment included a blender, centrifuge, analytical balance, spectrophotometer, and HPLC (high-performance liquid chromatography) system.

Chemicals and Reagents: Several chemicals and reagents were used during the analysis process. These included solvents like methanol, acetonitrile, and water, as well as standards of known phytochemical compounds for identification and quantification purposes.

The following methods were employed to analyze the phytochemical composition of frozen apples:

Sample Preparation: Frozen apple samples were thawed, and the cores were removed. The samples were then homogenized using a blender to obtain a uniform mixture for analysis.

Extraction of Phytochemicals: The extraction of phytochemicals from the frozen apple samples was carried out using a suitable solvent, such as methanol or a mixture of methanol and water. The extraction process involved shaking the samples for a specific duration to ensure efficient extraction of the targeted compounds.

Centrifugation: After the extraction process, the samples were centrifuged to separate the solid particles from the liquid extract. The supernatant obtained after centrifugation contained the phytochemicals of interest.

Quantification of Total Phenolic Content: The total phenolic content of the frozen apple samples was determined using a spectrophotometric method, such as the Folin-Ciocalteu assay. This method involves the reaction of phenolic compounds with Folin-Ciocalteu reagent, resulting in the formation of a blue-colored complex that can be quantified using a spectrophotometer.

Identification and Quantification of Individual Phytochemicals: High-performance liquid chromatography (HPLC) was used to identify and quantify individual phytochemical compounds present in the frozen apple samples. HPLC is a powerful analytical technique that allows for the separation, identification, and quantification of various compounds based on their chemical properties and retention times.

Results and discussion

Apples have gained special attention due to their chemical composition, especially for their antioxidant characteristics. Among different groups of natural antioxidants, phenolic compounds are the main constituents responsible for the antioxidant properties of apples (Arias, A., Feijoo, G., Moreira, M.T. 2022; Al Daccache, M., Koubaa, M., Maroun, R.G., Salameh, D., Louka, N., Vorobiev, E. 2020; Skinner, R.C., Gigliotti, J.C., Ku, K.M., Tou, J.C., 2004).

Apples contain high concentrations of flavonoids as well as other phytochemicals, and the concentration of these phytochemicals can depend on many factors, such as apple variety, apple picking and storage, and apple processing. Phytochemical concentrations also differ greatly between apple skin and apple flesh.

As a result of our research, the following antioxidant compounds were found in fro-

zen apples. quercetin-3-galactoside, quercetin-3-glucoside, quercetin-3-rhamnoside (https://pubchem.ncbi.nlm.nih.gov/compound/Quercetin), catechin (Kríz, Z., Koca, J., Imberty, A., Charlot, A., Auzély-Velty, R., (July 2003), chlorogenic acid (Clifford, M. N., (1999), gallic acid (Haslam, E., Cai, Y., (1994), and Phlorizin (Makarova, Elina; Górnaś, Paweł; Konrade, Ilze; Tirzite, Dace; Cirule, Helena; Gulbe, Anita; Pugajeva, Iveta; et al. (2015). (Figure 1). It was found that these substances have the following concentrations in 100 g of fruit: quercetin glycosides, 12.8 mg; vitamin C, 11.6 mg; procyanidin B, 7.23 mg; chlorogenic acid, 8.12 mg; epicatechin, 9.18 mg and phloretin glycosides, 6.21 mg.

In addition, a frozen apple sample was found to contain 120 mg of gallic acid equivalent (GAE) per 100 grams of fresh weight. It stands out as an important phenolic compound with antioxidant health benefits.

Figure 1. *Chemical structure of phytochemicals in frozen apples*

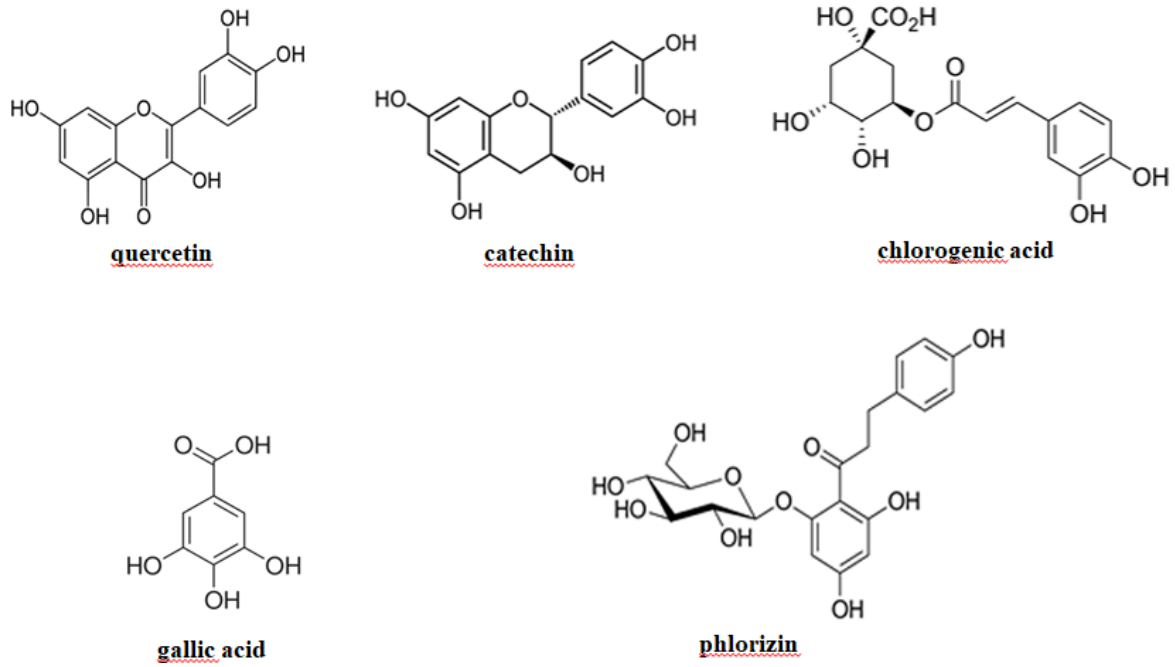

The results of this study highlight the nutritional value of frozen apples, particularly in terms of their phytochemical composition. The high total phenolic content indicates that frozen apples can be a rich source of antioxidants, which play a crucial role in protecting the body against oxidative stress and reducing the risk of chronic diseases.

The presence of flavonoids, such as quercetin and kaempferol, in frozen apples is noteworthy. These compounds have been extensively studied for their potential anti-inflammatory and anti-cancer effects. Quercetin, in particular, has been shown to have anti-allergic, anti-viral, and cardiovascular protective properties.

Hydroxycinnamic acids like caffeic acid and p-coumaric acid are also present in frozen apples. These compounds have been linked to various health benefits, including anti-inflammatory and anti-microbial activities. They may contribute to the overall antioxidant capacity of frozen apples.

It is important to note that the phytochemical composition of apples can vary depending on several factors, including the apple variety, ripeness, and storage conditions. Frozen apples, in particular, may undergo certain changes in their phytochemical profile due to the freezing and thawing process. However, this study provides valuable insights into the general composition of frozen apples and highlights their potential health benefits.

Conclusions

In conclusion, the research on the phytochemical composition of frozen apples demonstrates that they contain a significant amount of phenolic compounds, including flavonoids and hydroxycinnamic acids.

These compounds have been associated with various health benefits, including antioxidant, anti-inflammatory, and anti-cancer properties. Incorporating frozen apples into the diet can be a convenient and nutritious way to reap the benefits of these phytochemicals. However, further studies are needed to explore the impact of freezing and thawing on the phytochemical stability and bioavailability of apples.

References

Phoon, P.Y., Galindo, F.G., Vicente, A., Dejmek, P. Pulsed electric field in combination with vacuum impregnation with trehalose improves the freezing tolerance of spinach leaves. Journal of Food Engineering, 2008.– Vol. 88.– No. 1.– P. 144–148. DOI: 10.1016/j.jfoodeng.2007.12.016

Kutsakova, V.E., Frolov, S.V., Yakovleva, M.I. Mass transfer during freezing. Russian journal of applied chemistry. 1997.– Vol. 70.– No. 12.– P. 2061–2063.

Jeanelle, Boyer, Rui Hai Liu. Apple phytochemicals and their health benefits Nutr J. 2004; 3: 5. Published online 2004. May 12. Doi: 10.1186/1475–2891–3–5

Arias, A., Feijoo, G., Moreira, M.T. Exploring the Potential of Antioxidants from Fruits and Vegetables and Strategies for Their Recovery. Innov. Food Sci. Emerg. Technol. 2022; 77: 102974. Doi: 10.1016/j.ifset.2022.102974. [CrossRef] [Google Scholar]

Al Daccache, M., Koubaa, M., Maroun, R.G., Salameh, D., Louka, N., Vorobiev, E. Impact of the Physicochemical Composition and Microbial Diversity in Apple Juice Fermentation Process: A Review. Molecules. 2020; 25: 3698. Doi: 10.3390/molecules25163698. [PMC free article] [PubMed] [CrossRef] [Google Scholar]

Skinner, R.C., Gigliotti, J.C., Ku, K.M., Tou, J.C. A Comprehensive Analysis of the Composition, Health Benefits, and Safety of Apple Pomace. *Nutr. Rev.* 2018; 76: 893–909. Doi: 10.1093/nutrit/nuy033. [PubMed] [CrossRef] [Google Scholar]

URL: https://pubchem.ncbi.nlm.nih.gov/compound/Quercetin

Kríz, Z., Koca, J., Imberty, A., Charlot, A., Auzély-Velty, R. (July 2003). "Investigation of the complexation of (+)-catechin by beta-cyclodextrin by a combination of NMR, microcalorimetry and molecular modeling techniques". Organic & Biomolecular Chemistry.– 1 (14): 2590–2595. Doi:10.1039/B302935M. PMID12956082.

Clifford, M.N. (1999). "Chlorogenic acids and other cinnamates – nature, occurrence and dietary burden". *Journal of the Science of Food and Agriculture*.– 79 (3): 362–372. Doi:10.1002/(SICI)1097-0010(19990301)79:3<362: AID-JSFA256>3.0.CO;2-D

Haslam, E., Cai, Y. (1994). "Plant polyphenols (vegetable tannins): Gallic acid metabolism". Natural Product Reports.– 11 (1): 41–66. Doi:10.1039/NP9941100041. PMID15206456

Makarova, Elina, Górnaś, Paweł, Konrade, Ilze, Tirzite, Dace, Cirule, Helena, Gulbe, Anita; Pugajeva, Iveta, et al. (2015). "Acute anti-hyperglycaemic effects of an unripe apple preparation containing phlorizin in healthy volunteers: A preliminary study". *Journal of the Science of Food and Agriculture*.– 95 (3): 560–568. Doi:10.1002/jsfa.6779. PMID24917557.

submitted 29.11.2023;
accepted for publication 20.12.2023;
published 24.01.2024

Contact: shuhrat.hasanov.0305@gmail.com

The Austrian Journal of Technical and Natural Sciences, No 11–12
ISSN 2310-5607

PREMIER Publishing
ppublishing.org

Section 3. Physic

DOI:10.29013/AJT-23-11.12-33-38

POLARIZATION DEPENDENCE OF SINGLE-PHOTON INTERBAND LINEAR CIRCULAR DICROISM IN A_3B_5 SEMICONDUCTORS

Rasulov Rustam Yavkachovich [1], ***Kasimov Forrukh Kasimovich*** [2], ***Isomiddinova Umida Mamurjonova*** [3], ***Urinova Kamola Komoljonovna*** [3]

[1] Department Physics, Fergana State University, Uzbekistan

[2] Department Physics, Andijzn State University, Uzbekistan

[3] Department Physics, Kokand State Pedagogical Institute, Uzbekistan

Cite: *Rasulov, R.Y., Kasimov, F.K., Isomiddinova, U.M., Urinova, K.K. (2023). Polarization Dependence of Single-Photon Interband Linear Circular Dicroism in A_3B_5 Semiconductors. Austrian Journal of Technical and Natural Sciences 2023, No 11-12.* https://doi.org/10.29013/AJT-23-11.12-33-38

Abstract

The polarization, spectral, and temperature dependences of the single-photon absorption coefficient of polarized radiation are calculated, and its linear-circular dichroism in crystals of tetrahedral symmetry is studied. In this case, the contribution to the coefficients of one-photon absorption of light from the effect of coherent saturation of optical transitions is taken into account.

Keywords: *polarization, spectral, and temperature dependences of the single-photon light absorption coefficient, linear-circular dichroism, crystal of tetrahedral symmetry, coherent saturation effect*

Introduction

Nonlinear absorption of light in a semiconductor with a degenerate valence band, which is due to direct optical transitions between heavy and light hole subbands and depends on the state of radiation polarization, was studied in (Ivchenko, 1972; Rasulov, 1993; Ganichev, 1983; Parshin, 1987; Rasulov, 2017; Rasulov, 1996; Rasulov, 1988; Rasulov, 1993). In these papers, it is assumed that the nonlinearity in the intensity dependence of the single-photon absorption coefficient arises due to resonant absorption saturation. This saturation is due to the photoinduced change in the distribution functions of light and heavy holes in the region of momentum space near the surface corresponding $E_{hh}(\vec{k})-E_{hl}(\vec{k})-\hbar\omega=0$ to the resonance condition. Here, $E_{hh}(\vec{k})\left(E_{hl}(\vec{k})\right)$ is the energy spectrum of heavy (light) holes, and ω is the frequency of light.

In (Rasulov, 1993) multiphoton linear-circular dichroism (*LCD*) for *p-Ge* was studied in the regime of developed nonlinearity, when n-photon processes make a comparable contribution to absorption with $n=(1\div 5)$. In (Rasulov, 2016; Rasulov, 2015), four-photon processes in semiconductors due to optical transitions between subbands of the valence band were studied. However, interband single-photon linear-circular dichroism, as well as intraband two-photon linear-circular dichroism, where the intermediate states are in the conduction band or in the spin-orbit splitting zone in crystals of tetrahedral symmetry, taking into account the effect of coherent saturation, remained open, to which this article is devoted.

Here we consider one- or two-photon linear-circular dichroism of the absorption of polarized radiation, taking into account the effect of coherent saturation (Ganichev, 1983; Parshi, 1987) in direct-gap crystals, which is due to direct optical transitions between subbands of the valence band, where we take into account the fact that intermediate states of current carriers can be located not only in the light and heavy subbands, but also in both the conduction band and the spin-orbital splitting zone. When calculating intraband single-photon light absorption, we assume that the photon energy satisfies the conditions $\hbar\omega \geq E_g$, $E_g+\Delta_{SO}$, where E_g is the band gap, Δ_{SO} is the spin-orbit splitting of the valence band.

One-photon interband linear-circular dichroism

In case $\hbar\omega \geq E_g$, $E_g+\Delta_{SO}$ there are two variants of interband optical transitions, the first of which satisfies the condition $E_g \leq \hbar\omega \langle E_g+\Delta_{SO}$, and in the second case the condition $\hbar\omega \geq E_g+\Delta_{SO}$ is satisfied. Therefore, in the first case, optical transitions occur between the subbands of light and heavy holes in the valence band and the conduction band, and in the second case, optical transitions occur between the spin-orbit splitting and conduction bands, which we will analyze separately:

a) let the initial states be in the heavy hole subband of the valence band, then, in the Luttinger-Kohn and Kane approximation transition from $|V,\pm 3/2\rangle$ into the $|c,\pm 1/2\rangle$ conduction band, i.e. $M^{(1)}_{C,\pm 1/2;\pm V,3/2}$, which is schematically depicted as $|V,\pm 3/2\rangle \to |c,\pm 1/2\rangle$, is determined by the relations: $M^{(1)}_{C,+1/2;V+3/2}=\left(\frac{eA_0}{c\hbar}\right)pe'_+$, $M^{(1)}_{C,-1/2;V-,3/2}=$ $=-i\left(\frac{eA_0}{c\hbar}\right)pe'_-$, and an optical transition of the $|V,\pm 3/2\rangle \to |c,\mp 1/2\rangle$ type is forbidden, where $e'_\pm=e'_x\pm ie'_y$, e'_α $(\alpha=x,y,z)$-are the projections of the light polarization vector, relative to the coordinates the Oz axis of which is directed along the wave photoexcited current carriers ($\vec{k}$), A_0 – is the amplitude of the electromagnetic wave potential vector, p – is the Kane parameter (Ivchenko, 1989; Bir, 1972), the rest are well-known quantities. The law of conservation of energy of this transition is described by $\delta\left(E_c\left(\vec{k}\right)-E_{hh}\left(\vec{k}\right)-\hbar\omega\right)$ functions, where $E_c\left(\vec{k}\right)=\frac{\hbar^2k^2}{2m_c}+E_g$ is the energy spectrum of electrons in the conduction band, $E_L\left(\vec{k}\right)=\frac{\hbar^2k^2}{2m_L}$ is the energy spectrum of holes in the subband of light $(L=lh)$ and heavy $(L=hh)$ holes, $m_c(m_L)$ is the effective masses of current carriers in the conduction band and in the valence band, $L=lh\,(hh)$ is for subbands of light (heavy) holes.

Based on the last relations, one can obtain the polarization dependence of the probabilities of the considered optical transitions. Calculations show that for optical transitions of the $|V,\pm 3/2\rangle \to |C,\pm 1/2\rangle$ type, the polarization dependence of the probability of this transition, determined by the polarization dependence $\left|M^{(1)}_{C,\pm 1/2;V,\pm 3/2}\right|^2=\left(\frac{eA_0}{c\hbar}\right)^2 p^2\left|e'_\pm\right|^2$, for both linear and circular polarizations, this dependence has an oscillatory character with respect to the angle between the polarization vector and the wave vector of current carriers. We note that, without taking into account the Rabi effect (Parshin, 1987; Rasulov, 2017; Rasulov, 1996), in this case the coefficient of interband linear-circular dichroism, defined as the ratio of the probabilities of optical transitions for linear and circular polarization, is equal to unity, i.e. linear-circular dichroism is not observed;

b) if the initial states are in the light hole subband of the valence band, then the matrix element of the single-photon optical transition from the light hole subband $|V,m\rangle\,(m\pm1/2)$ to the conduction band $|c,m'\rangle\,(m'=\pm1/2)$, i.e. $M^{(1)}_{\mathrm{C,m';V,m}}$, which is schematically depicted as $|V,m\rangle\to|c,m'\rangle$ is defined as the ratios: $M^{(1)}_{c,+1/2;\mathrm{V},+1/2}=\left(\frac{eA_0}{c\hbar}\right)\frac{1}{\sqrt{3}}p_{cV}e'_-$, $M^{(1)}_{c,-1/2;\mathrm{V},-1/2}=$ $=\left(\frac{eA_0}{c\hbar}\right)\frac{-i}{\sqrt{3}}e'_+p_{cV}$, $M^{(1)}_{c,+1/2;V,-1/2}=\left(\frac{eA_0}{c\hbar}\right)\frac{1}{\sqrt{3}}e'_zp_{cV}$, $M^{(1)}_{c,+1/2;\mathrm{V},-1/2}=\left(\frac{eA_0}{c\hbar}\right)i\sqrt{\frac{2}{3}}e'_zp_{cV}$. Then the square of the modulus of the matrix elements of the considered optical transitions is expressed as: $\left|M^{(1)}_{c,\pm1/2;\mathrm{V},\pm1/2}\right|^2=\left(\frac{eA_0}{c\hbar}\right)^2\frac{1}{3}p^2_{cV}\left|e'_{\mp}\right|^2$, $\left|M^{(1)}_{c,\mp1/2;\mathrm{V},\pm1/2}\right|^2=$ $=\left(\frac{eA_0}{c\hbar}\right)^2\frac{2}{3}p^2_{cV}\left|e'_z\right|^2$. The energy conservation law of these transitions is described by the $\delta\left(E_c(\vec{k})-E_{lh}(\vec{k})-\hbar\omega\right)$ function.

Then the wave vector of photoexcited current carriers is determined by the relation: $k^{(1\omega)}_{c,lh}=\sqrt{\frac{2\mu^{(c,lh)}_+}{\hbar^2}\left(\hbar\omega-E_g\right)}$, where $\mu^{(c,lh)}_+=$ $=\frac{m_cm_{lh}}{m_c+m_{lh}}$ is the reduced effective mass relative to the effective masses of electrons and light holes.

Figure 1. *Polarization dependence and dependence on the Rabi parameter of probability of the optical transitions type* $|\mathrm{V},hh\rangle\to|\mathrm{C}\rangle$ *(a) for linear and (b) for circularly polarized light and the wave vector of the current carriers, the amplitude value of which is almost independent of the parameter of the coherent saturation effect*

a) b)

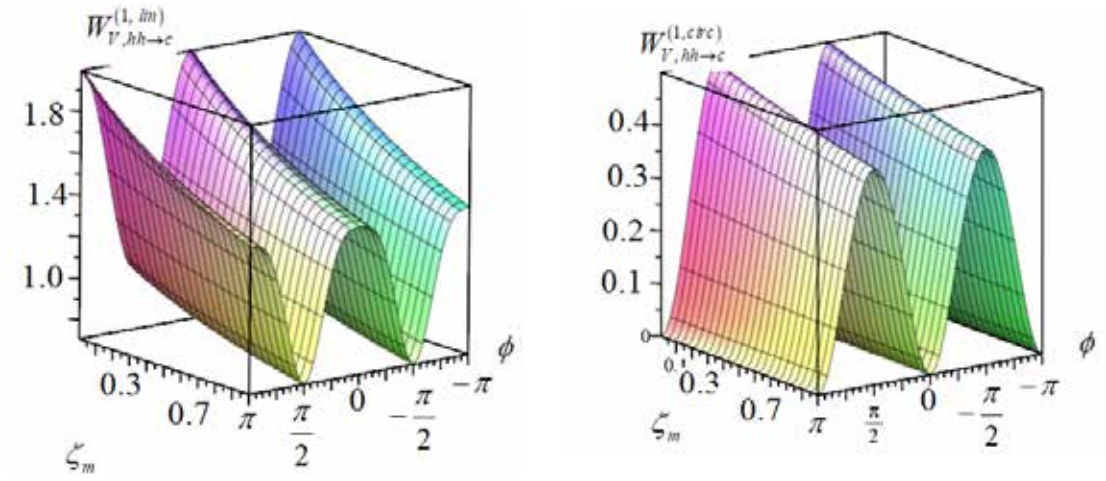

Taking into account the polarization dependence of matrix elements $M^{(1)}_{c,\pm1/2;\mathrm{V},\pm1/2}$ and $M^{(1)}_{c,\mp1/2;\mathrm{V},\pm1/2}$ for optical transitions of types $|\mathrm{V},\pm1/2\rangle\to|\mathrm{C},\pm1/2\rangle$ and $|\mathrm{V},\pm1/2\rangle\to$, $\to|\mathrm{C},\mp1/2\rangle$ it is possible to determine the polarization dependence of the probability of this transition, which is shown in (fig. 1 a). It can be seen from (fig. 1b) that the polarization dependence of the probability of the considered optical transition for both linear and circular polarizations have an oscillatory character with respect to the angle between the polarization vectors and the wave vector of the current carriers, but with an increase in the parameter of the coherent saturation effect $\zeta_\omega=4\frac{\alpha_\omega}{\hbar^2\omega^2}\left(\frac{eA_0}{c\hbar}\right)^2p^2_{cV}$, the amplitude of the oscillations decreases by 20% for linear, 15% for circular polarization.

Fig. 2 shows the polarization dependence of the single-photon linear-circular dichroism coefficient for type $|\mathrm{V},hh\rangle\to|\mathrm{C}\rangle$ optical transitions. It can be seen from (fig. 3) that the polarization dependence of the single-photon linear-circular dichroism coefficient for the considered optical transition also has an oscillatory character with respect to the angle between the polarization vectors

The probability of an optical transition upon absorption of linearly polarized light is

about five times greater than the probability of an optical transition upon absorption of circularly polarized light. The latter is explained by the dependence of the selection rule for the considered optical transition on the degree of light polarization;

c) if the initial states are in the spin-split band, then the matrix elements of single-photon optical transitions $M^{(1)}_{\mathrm{C},m';SO,m}$, which are schematically depicted as $|SO,m\rangle \to |c,m'\rangle$, are defined as the relations: $M^{(1)}_{\mathrm{C},+1/2;\mathrm{SO},+1/2} = \left(\frac{eA_0}{c\hbar}\right)\frac{1}{\sqrt{3}} p_{cV} e'_z$, $M^{(1)}_{\mathrm{C},-1/2;\mathrm{SO},+1/2} = \left(\frac{eA_0}{c\hbar}\right)\frac{1}{\sqrt{3}} p_{cV} e'_-$, $M^{(1)}_{\mathrm{c},+1/2;V,-1/2} = \left(\frac{eA_0}{c\hbar}\right)\frac{1}{\sqrt{3}} e'_z p_{cV}$, $= \left(\frac{eA_0}{c\hbar}\right)\frac{1}{\sqrt{3}} e'_z p_{cV}$, $M^{(1)}_{\mathrm{C},-1/2;\mathrm{SO},-1/2} = \left(\frac{eA_0}{c\hbar}\right)\frac{-i}{\sqrt{3}} p_{cV} e'_z$

The energy conservation law for these transitions is described by $\delta\left(E_c(\vec{k}) - E_{SO}(\vec{k}) - \hbar\omega\right)$ function, where $E_{SO}\left(\vec{k}\right) = \frac{\hbar^2 k^2}{2m_c} + \Delta_{SO}$ is the energy spectrum holes in the zone of spin orbital splitting, Δ_{SO} is the energy of spin orbital splitting.

Whence we have $\left|M^{(1)}_{\mathrm{C},\pm1/2;\mathrm{SO},\pm1/2}\right|^2 = \left(\frac{eA_0}{c\hbar}\right)^2 \frac{1}{3} p^2_{cV} e'^2_z$, $\left|M^{(1)}_{\mathrm{C},\mp1/2;\mathrm{SO},\pm1/2}\right|^2 = \left(\frac{eA_0}{c\hbar}\right)^2 \frac{1}{3} p^2_{cV} e'^2_\pm$. In this case, the wave vector of photoexcited current carriers is defined as $k^{(1\omega)}_{c,SO} = \sqrt{\frac{2\mu^{(c,SO)}_+}{\hbar^2}\left(\hbar\omega - E_g - \Delta_{SO}\right)}$, $\mu^{(c,SO)}_+$ – reduced effective mass with respect to current carriers in the conduction bands and the spin of the orbital splitting.

Figure 2. *Polarization dependence and dependence on the Rabi parameter of the coefficient of single-photon linear-circular dichroism for* $|\mathrm{V},hh\rangle \to |\mathrm{C}\rangle$ *type optical transitions.*

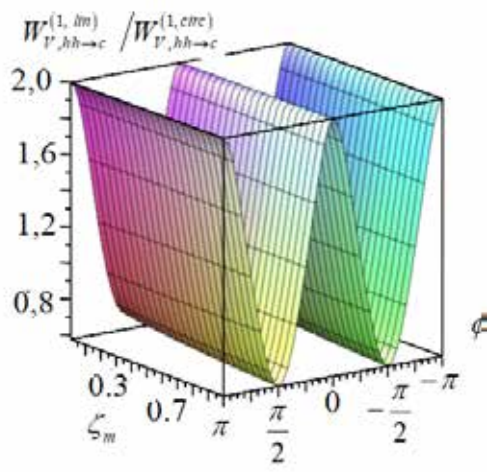

Taking into account the polarization dependences of the squares of the absolute value of matrix elements $\left|M^{(1)}_{\mathrm{C},\pm1/2;\mathrm{SO},\pm1/2}\right|^2$ and $\left|M^{(1)}_{\mathrm{C},\mp1/2;\mathrm{SO},\pm1/2}\right|^2$ for optical transitions of types $|\mathrm{V},\pm1/2\rangle \to |\mathrm{C},\pm1/2\rangle$ and $|\mathrm{V},\pm1/2\rangle \to |\mathrm{C},\mp1/2\rangle$, it is possible to determine the polarization dependence of the probability of this transition, taking into account the effect of coherent saturation (see fig. 3). It can be seen from (fig. 4) that the polarization dependences of the probabilities of optical transitions have an oscillatory character with respect to the angle between the polarization vector and the wave vector of current carriers, but the oscillation for linear polarization is approximately twice as large as for circular polarization. For both polarizations, the oscillation amplitude decreases with increasing coherent saturation effect parameter.

Fig. 3 shows the complex polarization dependence of the single-photon linear-circular dichroism coefficient for type $|SO\rangle \to |\mathrm{C}\rangle$ optical transitions. Such a non-monotonic polarization dependence is explained by the fact that the transition probability is determined not only by the distribution function of current carriers in the initial state, but also by the square of the

composite matrix element corresponding to the optical transition, which is under the radical (see, for example, (Ganichev, 1983; Parshin, 1987; Rasulov, 2017)).

Conclusion

Thus, we have defined the following:

1. The polarization dependence of the squared moduli of matrix elements for interband optical transitions for both linear and circular polarizations has an oscillatory character with respect to the angle between the polarization vector and the wave vector of current carriers.

Figure 3. *Polarization dependence and dependence on the Rabi parameter of the probability of optical transitions* $|SO\rangle \to |C\rangle$ *type (a) for linear and (b) for circular polarizations of light*

a) b)

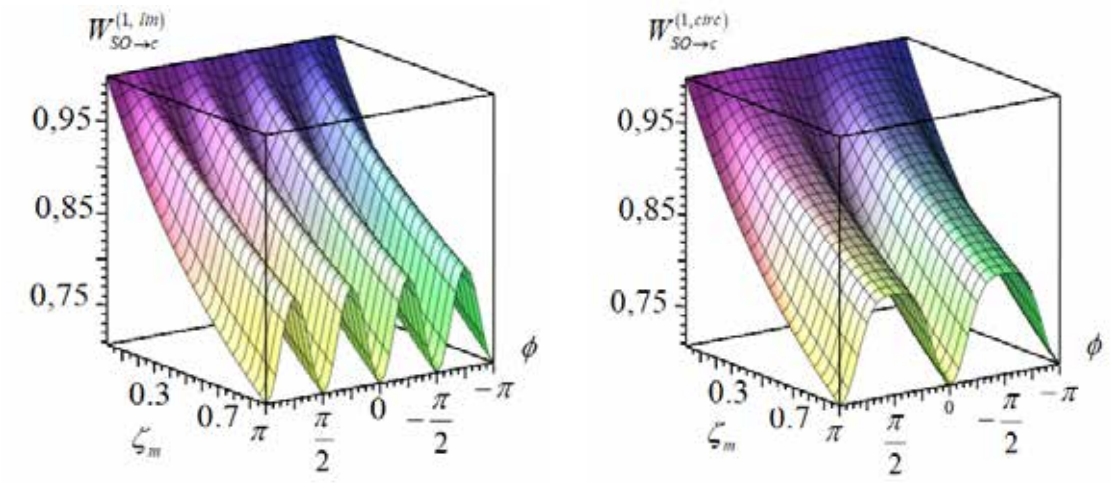

2. For a single-photon optical transition between the spin-orbit splitting zone and the conduction band, the oscillation for linear polarization is approximately twice as large as for circular polarization. For both polarizations, the oscillation amplitude decreases with increasing coherent saturation effect parameter.

References

Ivchenko, E. L. (1972). Two-photon absorption and optical orientation of free carriers in cubic crystals *Semiconductors*.– Vol. 14.– Issue 12.– P. 3489–3485. (In Russian).

Rasulov, R. Ya. (1993). Polarization optical and photovoltaic effects in semiconductors with linear and nonlinear absorption of light. Dissertation for thesis. of doctor's degree phys.-math. sciences.– St. Petersburg.– 206 p. (In Russian).

Ganichev, S. D., Ivchenko, E. L., Rasulov, R. Ya., Yaroshetskii, I. D. and Averbukh, B. Ya. (1983). Linear and circular dichroism of drag current due to nonlinear inter subband absorption of light in p-type Ge *Phys. Solidi State*.– Vol. 35.– No. 1.– P. 104–108.

Parshin, D. A., Shabaev, A. R. (1987). Theory of nonlinear absorption of infrared radiation in semiconductors with degenerate bands. *ZhETF*.– Vol. 92.– Issue. 4.– P. 1471–1484. (In Russian).

Rasulov, V. R. Rasulov, R. Ya., Eshboltaev, I. (2017). Linearly and circular dichroism in a semiconductor with a complex valence band with allowance for four-photon absorption of light *Physics of the Solid State*.– Vol. 59.– No. 3.– P. 463–468.

Rasulov, R. Ya., Khoshimov, G. Kh., Kholitdinov, Kh. (1996). Linear-circular dichroism of the nonlinear absorption of light in n-GaP. *FTP*.– Vol. 30.– No. 2.– P. 274–277. (In Russian).

Rasulov, R. Ya. (1988). Drag effect at three-photon absorption of light in semiconductors of the Ge type, *FTP*.– Vol. 22.– No. 11.– P. 2077–2080.

Rasulov, R. Ya. (1993). Linear circular dichroism in multiphoton interband absorption in semiconductors. *Semiconductors*.– Vol. 35.– No. 6.– P. 1674–1678. (in Russian).
Rasulov, R. Ya., Rasulov, V. R., Eshboltaev, I. (2016). The theory of the four photon of polarized radiation in a semiconductor with complex band structure. *American Scientific journal*.– No. 2.– P. 93–96.
Rasulov, V. R., Rasulov, R. Ya., Eshboltaev, I. (2015). Linear-Circular Dichroism of Four-Photon Absorption of Light in Semiconductors with a Complex Valence Band. *Russian Physics Journal*.– Vol. 58.– No. 12.– P. 1681–1686.
Ivchenko, E. L., Rasulov, R. Ya. (1989). Symmetry and real band structure of semiconductors.– Tashkent. Fan.– 126 p.
Bir, G. L., Pikus, G. E. (1972). Symmetry and strain effects in semiconductors.– M.: Science.– 584 p.

submitted 14.12.2023;
accepted for publication 26.12.2023;
published 24.01.2024

Contact: r_rasulov51@mail.ru

The Austrian Journal of Technical and Natural Sciences, No 11–12
ISSN 2310-5607

PREMIER Publishing
ppublishing.org

DOI:10.29013/AJT-23-11.12-39-44

INTERZONE ONE-PHOTON ABSORPTION OF POLARIZED LIGHT WITH ACCOUNT OF THE COHERENT SATURATION EFFECT IN A_3B_5 SEMICONDUCTORS

Rasulov Rustam Yavkachovich [1], ***Kasimov Forrukh Kasimovich*** [2], ***Isomiddinova Umida Mamurjonova*** [3], ***Urinova Kamola Komoljonovna*** [3]

[1] Department Physics, Fergana State University, Uzbekistan

[2] Department Physics, Andijan State University, Uzbekistan

[2] Department Physics, Kokand State Pedagogical Institute, Uzbekistan

Cite: *Rasulov R.Y., Kasimov, F.K., Isomiddinova, U.M., Urinova, K.K. (2023). Interzone One-Photon Absorption of Polarized Light With Account of the Coherent Saturation Effect in A_3B_5 Semiconductors. Austrian Journal of Technical and Natural Sciences 2023, No 11-12.* https://doi.org/10.29013/AJT-23-11.12-39-44

Abstract

The polarization, spectral, and temperature dependences of the one-photon absorption coefficient of polarized radiation are calculated, and its linear-circular dichroism in crystals of tetrahedral symmetry is studied. In this case, the contribution to the coefficients of one-photon absorption of light from the effect of coherent saturation of optical transitions is taken into account.

Keywords: *polarization, spectral, and temperature dependences of the one-photon light absorption coefficient, linear-circular dichroism, crystal of tetrahedral symmetry, coherent saturation effect*

Intraduction

Nonlinear absorption of light in a semiconductor with a degenerate valence band, which is due to direct optical transitions between heavy and light hole subbands and depends on the state of radiation polarization, was studied in (Ivchenko, 1972; Rasulov, 1993; Ganichev, 1983; Parshin D.A., 1987; Rasulov, 2017; Rasulov, 1996; Rasulov, 1988; Rasulov, 1993). In these papers, it is assumed that the nonlinearity in the intensity dependence of the one-photon absorption coefficient arises due to resonant absorption saturation. This saturation is due to the photoinduced change in the distribution functions of light and heavy holes in the region of momentum space near the surface corresponding $E_{hh}(\vec{k})-E_{hl}(\vec{k})-\hbar\omega=0$ to the resonance condition. Here, $E_{hh}(\vec{k})\left(E_{hl}(\vec{k})\right)$ is the energy spectrum of heavy (light) holes, and ω is the frequency of light.

Due to the smallness of the photon wave vector compared to the wave vector of the electron (hole) formed as a result of absorption, when calculating the light absorption

coefficient, we can assume $|\vec{q}| << |\vec{k}|$ and put $|\vec{q}| = 0$, where $\vec{q}(\vec{k})$ is the wave vector of the photon (holes).

In case $\hbar\omega \geq E_g$, $E_g + \Delta_{SO}$, there are two types of interband optical transitions, the first of which satisfies the condition $E_g \leq \hbar\omega \langle E_g + \Delta_{SO}$, and in the second case the condition $\hbar\omega \geq E_g + \Delta_{SO}$ is satisfied. Therefore, in the first case, optical transitions occur between the subbands of light and heavy holes in the valence band and the conduction band, and in the second case, optical transitions occur between the spin-orbit splitting and conduction bands, which we will analyze separately.

Interband one-photon absorption of polarized light with allowance for the effect of coherent saturation

Next, we investigate various variants of one-photon interband absorption of polarized light, where we take into account the contribution of the coherent saturation effect (Parshin, 1987; Rasulov, 2017; Rasulov, 1996) to the light absorption coefficient. Then the spectral – temperature dependence of the coefficient of one-photon absorption of light $K^{(1)}$ is determined by the formula (Parshin, 1987; Rasulov, 2017; (Rasulov, 1996)

$$K^{(1)}_{C,\pm1/2;V,\pm3/2} = \frac{2\pi}{\hbar}\hbar\omega\frac{1}{I}\rho(\hbar\omega)F(\beta,1,\omega)\times$$
$$\times\left(\left\langle\frac{\left|M^{(1)}_{C,\pm1/2;V,\pm3/2}(\vec{k})\right|^2}{\sqrt{1+4\frac{\alpha_\omega}{\hbar^2\omega^2}\left|M^{(1)}_{C,\pm1/2;V,\pm3/2}(\vec{k})\right|^2}}\right\rangle+\left\langle\frac{\left|M^{(1)}_{C,\pm1/2;V,\mp3/2}(\vec{k})\right|^2}{\sqrt{1+4\frac{\alpha_\omega}{\hbar^2\omega^2}\left|M^{(1)}_{C,M1/2;V,\mp3/2}(\vec{k})\right|^2}}\right\rangle\right), \quad (1)$$

where $I,(\omega)$ is the intensity (frequency) of light, $\rho(\hbar\omega)$ is the density of states of current carriers involved in optical transitions, where the energy conservation law is taken into account, $F(\beta,1,\omega)$ is the distribution function of current carriers in the initial state, $\beta^{-1} = k_B T$, k_B, – is Boltzmann's constant, T is the sample temperature: $F(\beta,1,\omega) = \left[1-\exp(1\beta\hbar\omega)\right]\exp\left[\beta\left(\mu - E_{L=hh}(k^{(\omega)}_{c,L=hh})\right)\right]$, $E_{L=hh}(k^{(\omega)}_{c,L=hh}) = \frac{m_c}{m_c+m_{hh}}\left(\hbar\omega - E_g\right)$, $\rho(\hbar\omega) = \mu^* k_\omega/(\pi^2\hbar^2)$, μ^* is the reduced effective mass of current carriers, the form of which depends on the type of optical transitions.

It can be seen from (1) that it is necessary to perform angular averaging of the squares of the composite matrix elements over the solid angles of the wave vector of the current carriers, i.e. we need to perform an integration of the type

$$\left\langle\frac{\left|M^{(1)}_{C,\pm1/2;V,\pm3/2}(\vec{k})\right|^2}{\sqrt{1+4\frac{\alpha_\omega}{\hbar^2\omega^2}\left|M^{(1)}_{C,\pm1/2;V,\pm3/2}(\vec{k})\right|^2}}\right\rangle = \quad (2)$$
$$= \left(\frac{eA_0}{c\hbar}\right)^2 p^2_{cV}\left[\Re_1(I)+\Re_2(I)\right],$$

where

$$\Re_1(I) = \left\langle\frac{|e'_\pm|^2}{\sqrt{1+\zeta_\omega|e'_\pm|^2}}\right\rangle, \qquad I = |\vec{S}| = \frac{n_\omega\omega^2A_0^2}{2\pi c}$$
$$\Re_2(I) = \left\langle\frac{|e'_z|^2}{\sqrt{1+\zeta_\omega|e'_z|^2}}\right\rangle,$$

is the light intensity, $\left\langle\left|M^{(N)}_{n'k',nk}\right|^2\right\rangle$ – is the square of the absolute value of the matrix element $M^{(N)}_{n'\vec{k}',n\vec{k}}$ averaged over the solid angles of the vector $\vec{k}$, $\zeta_\omega = 4\frac{\alpha_\omega}{\hbar^2\omega^2}\left(\frac{eA_0}{c\hbar}\right)^2 p^2_{cV}$, the wave vector k_ω is determined from the energy conservation law. In particular, for the optical transition considered above $k_\omega = k_{c,L} = \sqrt{\frac{2\mu^{(c,L)}_+}{\hbar^2}\left(\hbar\omega - E_g\right)}$, $\mu^{(c,L)}_+ = \frac{m_c m_L}{m_c+m_L}$.

The calculation of one-photon absorption of polarized light due to optical transitions from the subband of light and heavy holes to the conduction band is performed using the formula (Rasulov, 1996; Rasulov, 1988; Rasulov, 1993; Rasulov, 2016; Rasulov, 2015)

$$K^{(1)} = \frac{4\pi e^2}{c\omega m_0^2 n_\omega} \sum_{nn'\vec{k}} \left|\vec{e}\vec{p}_{nn'}\left(\vec{k}\right)\right|^2 \left(f_{n\vec{k}} - f_{n'\vec{k}}\right)\delta\left(E_{n'}\left(\vec{k}\right) - E_n\left(\vec{k}\right) - \hbar\omega\right), \quad (3)$$

whence, in the Luttinger-Kohn approximation and in the three-band Kane model (Ivchenko E. L., 1989; Bir G. L., 1972), the spectral-temperature dependence of the coefficient of interband one-photon absorption of light takes the form

$$K_{c,V}^{(1)} = \frac{1}{3} p_{cV}^2 \frac{e^2 p_{cV}^2}{c\hbar^3 n_\omega} \left\{ \left(f_{hh,k_{c,hh}^{(1\omega)}} - f_{c,k_{c,hh}^{(1\omega)}} \right) \mu_+^{(c,hh)} k_{c,hh}^{(1\omega)} + \left(f_{lh,k_{c,lh}^{(1\omega)}} - f_{c,k_{c,lh}^{(1\omega)}} \right) \mu_+^{(c,lh)} k_{c,lh}^{(1\omega)} \right\} \quad (4)$$

where the distribution functions of photoexcited light and heavy holes are defined as

$$f_{lh,k_{c,lh}^{(1\omega)}} = \exp\left[\frac{E_F}{k_B T}\right] \cdot \exp\left[-\frac{1}{k_B T} \frac{\mu_+^{(c,lh)}}{m_{lh}} \left(\hbar\omega - E_g\right)\right], \quad (6)$$

$$f_{hh,k_{c,hh}^{(1\omega)}} = \exp\left[\frac{E_F}{k_B T}\right] \exp\left[-\frac{E_{hh}\left(k_{c,hh}^{(1\omega)}\right)}{k_B T}\right] = \exp\left[\frac{E_F}{k_B T}\right] \cdot \exp\left[-\frac{1}{k_B T} \frac{\mu_+^{(c,hh)}}{m_{hh}} \left(\hbar\omega - E_g\right)\right], \quad (7)$$

and the Fermi energy is determined by the relation

$$e^{\frac{\mu}{k_B T}} = \frac{1}{2} p \left(\frac{k_B T}{2\pi\hbar^2}\right)^{-3/2} \left(m_{hh}^{3/2} + m_{lh}^{3/2}\right)^{-1}. \quad (8)$$

Figure 1 shows the spectral and temperature dependences of the coefficient of one-photon absorption of polarized light in *GaAs*, due to optical transitions between the subbands of light $\left(K_{c,lh}^{(1)}\right)$ and heavy $\left(K_{c,hh}^{(1)}\right)$ holes (fig. 1 a) and the conduction band, as well as the resulting one-photon absorption of light (fig. 116 b), where the contribution of the coherent saturation effect to the one-photon light absorption coefficient is not taken into account. In quantitative calculations, the maximum value of $K_{c,lh}^{(1)}$ is chosen as one.

Figure 1. *Spectral – temperature dependence of the coefficient of one-photon absorption of polarized light in GaAs, due to optical transitions between the subbands of light* $\left(K_{c,lh}^{(1)}\right)$ *and heavy* $\left(K_{c,hh}^{(1)}\right)$ *holes (a) and the conduction band and their sum (b)*

a) b)

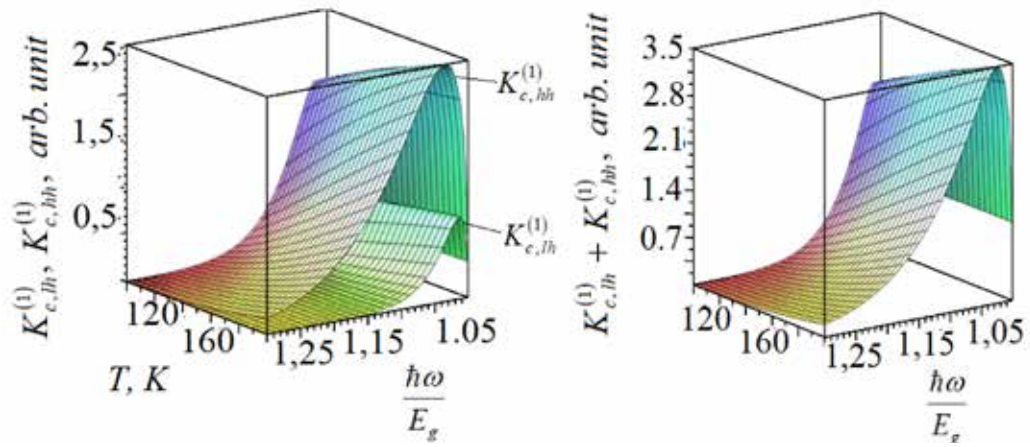

From fig. 2 a and 2 b, it can be seen that the spectral (temperature) dependence of the one-photon light absorption coefficient in GaAs, due to optical transitions between subbands of the valence band and the conduction band, first increases with increasing frequency (temperature) and, passing through a maximum, decreases. This is explained by the fact that the spectral dependence of the coefficient of one-photon absorption of light by the product of the density of states, with increasing frequency, which increases as a power function of frequency, and the distribution function of current carriers in the initial state, with increasing frequency, which decreases exponentially. The product of these quantities gives the graph shown in fig. 6. We note that here the temperature dependence

of the band gap is not taken into account, taking into account which will lead to a noticeable change in the spectral and temperature dependence of the one-photon absorption coefficient of polarized light, and it is shown in fig. 2 for *GaAs*. It can be seen from fig. 2 that, when the temperature dependence of the band gap is taken into account, the amplitude value of $K_{c,lh}^{(1)} + K_{c,hh}^{(1)}$ oscillates with increasing temperature in the region of low frequencies, while in the region of high frequencies, this value remains almost unchanged. In calculations, the temperature dependence of the band gap was chosen as: $E_g(T) = E_g(0) + \gamma_g T$, where $\gamma_g = 0{,}5405\ meV/K$ for *GaAs* (Vurgaftman, 2001).

Figure 2. *Spectral – temperature dependence of the coefficient of one-photon absorption of polarized light in GaAs, due to optical transitions between the subbands of light holes and the conduction band* $\left(K_{c,lh}^{(1)}\right)$ *without taking into account (a) and taking into account (b) the temperature dependence of the band gap on temperature*

a) b)

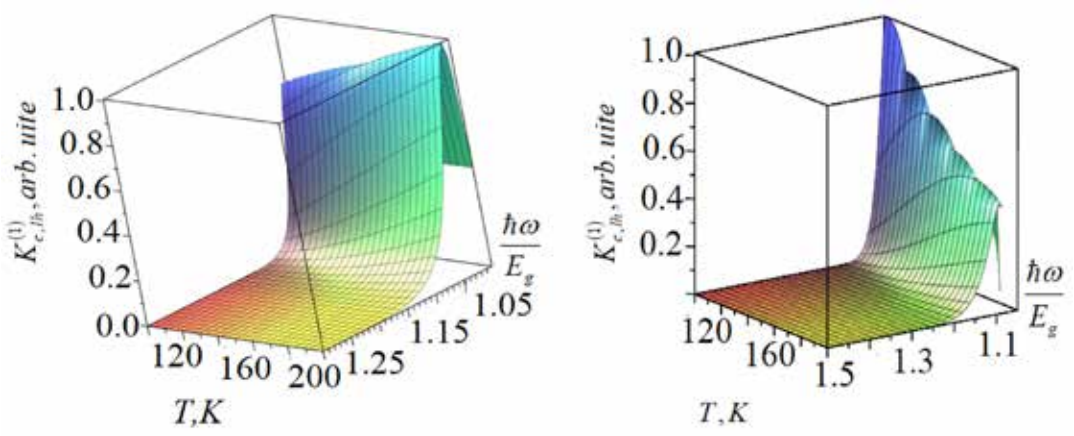

One-photon absorption of light between the spin-orbit splitting zone and the conduction band

The spectral-temperature dependence of the one-photon light absorption coefficient due to optical transitions between the spin-orbital splitting zone and the conduction band is defined as

$$K_{c,SO}^{(1)} = \frac{4\pi e^2}{c\hbar n_\omega}\frac{1}{3}p_{cV}^2 \iiint \left(|e_z'|^2 + |e_+'|^2\right)\left(f_{SO,\vec{k}} - f_{c,\vec{k}}\right)\delta\left(\frac{\hbar^2k^2}{2m_c} + E_g + \Delta_{SO} - \left(-\frac{\hbar^2k^2}{2m_{SO}}\right) - \hbar\omega\right)$$

or

$$K_{c,SO}^{(1)} = \frac{1}{3}\frac{e^2}{c\hbar n_\omega}\frac{p_{cV}^2}{\hbar^2}\mu_+^{(c,SO)}k_{c,SO}^{(1\omega)}f_{SO,k_{c,SO}^{(1\omega)}}\left\{1 - \exp\left[\frac{E_g}{k_BT}\left(x - 1 - \frac{E_{SO}}{E_g}\right)\right]\right\}, \quad (10)$$

where $\mu_+^{(c,SO)} = \frac{m_c m_{SO}}{m_c + m_{SO}}$ is the reduced effective mass, $k_{c,SO}^{(1\omega)} = \sqrt{\frac{2\mu_+^{(c,SO)}}{\hbar^2}\left(\hbar\omega - E_g\right)}$ is the wave vector of current carriers,

$$f_{SO,k_{c,SO}^{(1\omega)}} = \exp\left[\frac{E_F}{k_BT}\right]\cdot\exp\left[-\frac{1}{k_BT}\frac{\mu_+^{(c,SO)}}{m_{SO}}\left(\hbar\omega - E_g - E_{SO}\right)\right] \quad (11)$$

is the distribution function of current carriers in the spin-orbit splitting zone involved in optical transitions between the spin-orbit splitting zone and the conduction band.

Figure 3. *Spectral and temperature dependence of the coefficient of one-photon absorption of polarized light due to optical transitions between the spin-orbital splitting subband and the conduction band in InSb without (a) and with (b) the temperature dependence of the band gap and their ratio (c), where not the contribution of the coherent saturation effect to the one-photon light absorption coefficient is taken into account*

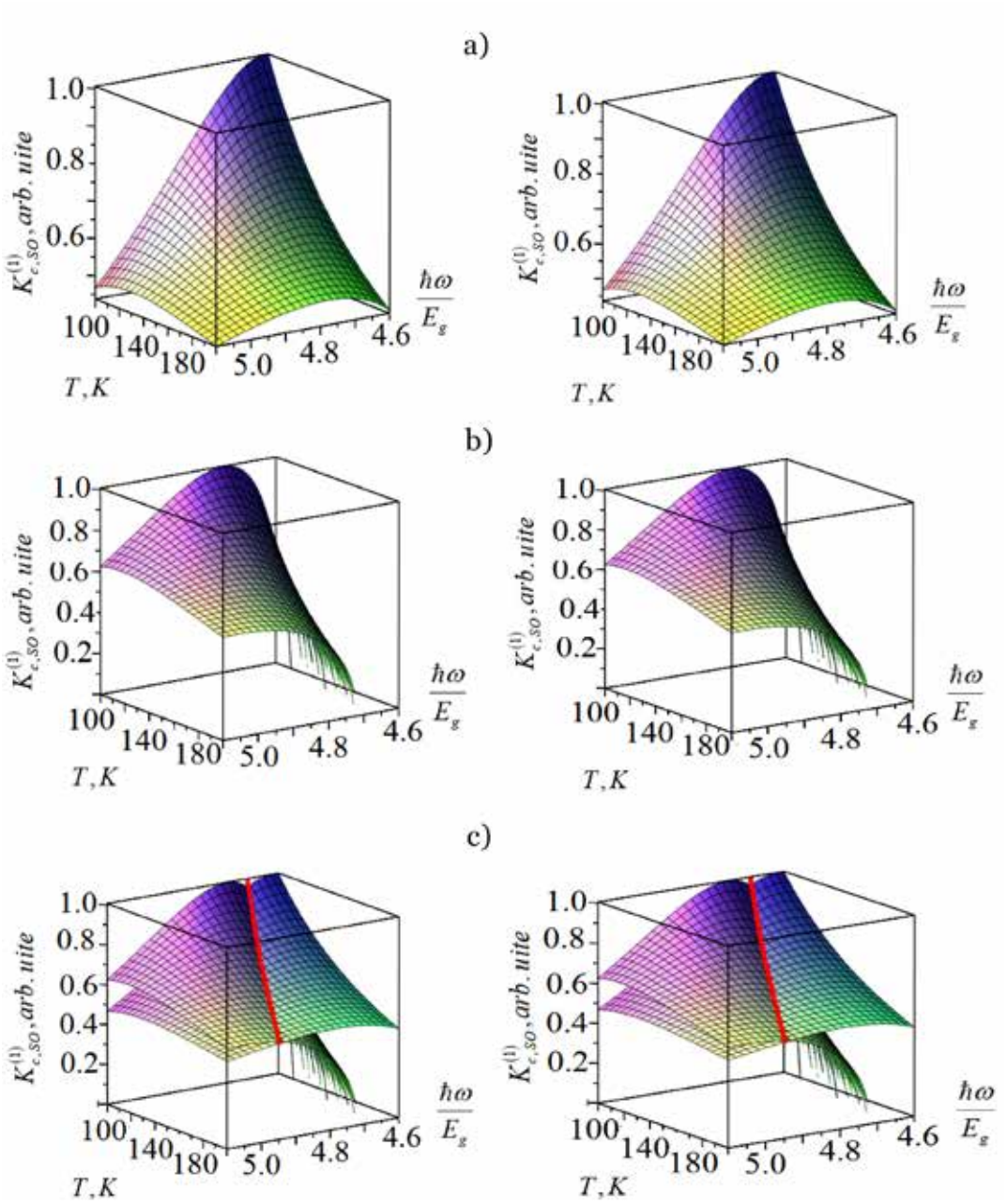

Figure 3 shows the spectral-temperature dependence of the one-photon absorption coefficient of polarized light, due to optical transitions between the spin-orbital splitting subband and the conduction band in *InSb* without taking into account (a) and taking into account (b) the temperature dependence of the band gap and their ratio (c), where not the contribution of the coherent saturation effect to the one-photon light absorption coefficient is taken into account. The red line marks the intersection of the spectral and temperature dependences of the one-photon absorption coefficient of polarized light, shown in figs. 3 a and 3 b. From fig. 3 it is seen that the spectral (temperature) dependence of the coefficient of one-photon interband absorption of light in *InSb*, both without taking into account and taking into account the temperature dependence of the band gap with increasing

frequency (temperature), first increases and reaches a maximum, and then decreases.

Conclusion

Thus, we have defined the following:

1. Spectral-temperature dependence of the one-photon absorption coefficient of polarized light in GaAs, caused by optical transitions between subbands of light holes and the conduction band, without and taking into account the temperature dependence of the band gap on temperature.

2. Spectral and temperature dependences of the one-photon absorption coefficient of polarized light, caused by optical transitions between the spin-orbital splitting subband and the conduction band in InSb without taking into account and taking into account the temperature dependence of the band gap and their ratio, where the contribution of the coherent saturation effect to the one-photon absorption coefficient is not taken into account.

References

Ivchenko E. L. (1972). Two-photon absorption and optical orientation of free carriers in cubic crystals *Semiconductors*.– Vol. 14.– Issue 12.– P. 3489–3485. (In Russian).

Rasulov R. Ya. (1993). Polarization optical and photovoltaic effects in semiconductors with linear and nonlinear absorption of light. Dissertation for thesis. of doctor's degree phys.-math. sciences.– St. Petersburg.– 206 p. (In Russian).

Ganichev S. D., Ivchenko E. L., Rasulov R. Ya., Yaroshetskii I. D. and Averbukh B. Ya. (1983). Linear and circular dichroism of drag current due to nonlinear inter subband absorption of light in p-type Ge *Phys. Solidi State*.– Vol. 35.– No. 1.– P. 104–108.

Parshin D. A., Shabaev A. R. (1987). Theory of nonlinear absorption of infrared radiation in semiconductors with degenerate bands. *ZhETF*.– Vol. 92.– Issue. 4.– P. 1471–1484. (In Russian).

Rasulov V. R. Rasulov R. Ya., Eshboltaev I. (2017). Linearly and circular dichroism in a semiconductor with a complex valence band with allowance for four-photon absorption of light *Physics of the Solid State*.– Vol. 59.– No. 3.– P. 463–468.

Rasulov R. Ya., Khoshimov G. Kh., Kholitdinov Kh. (1996). Linear-circular dichroism of the nonlinear absorption of light in n-GaP. *FTP*.– Vol. 30.– No. 2.– P. 274–277. (In Russian).

Rasulov, R. Ya. (1988). Drag effect at three-photon absorption of light in semiconductors of the Ge type, *FTP*.– Vol. 22.– No. 11.– P. 2077–2080.

Rasulov R. Ya. (1993). Linear circular dichroism in multiphoton interband absorption in semiconductors. *Semiconductors*.– Vol. 35.– No. 6.– P. 1674–1678. (in Russian).

Rasulov R. Ya., Rasulov V. R., Eshboltaev I. (2016). The theory of the four photon of polarized radiation in a semiconductor with complex band structure. *American Scientific journal*.– No. 2.– P. 93–96.

Rasulov V. R., Rasulov R. Ya., Eshboltaev I. (2015). Linear-Circular Dichroism of Four-Photon Absorption of Light in Semiconductors with a Complex Valence Band. *Russian Physics Journal*.– Vol. 58.– No. 12.– P. 1681–1686.

Ivchenko E. L., Rasulov R. Ya. (1989). Symmetry and real band structure of semiconductors. -Tashkent. Fan.– 126 p.

Bir G. L., Pikus G. E. (1972). Symmetry and strain effects in semiconductors.– M.: Science.– 584 p.

Vurgaftman I., Meyer J. R.M., Ram-Moha J.R. (2001). Band parameters for III–V compound semiconductors and their alloys. *J. Appl. Phys*.– Vol. 89.– P. 5815–5821.

submitted 20.12.2023;
accepted for publication 26.12.2023;
published 24.01.2024

Contact: r_rasulov51@mail.ru

The Austrian Journal of Technical and Natural Sciences, No 11–12
ISSN 2310-5607

PREMIER Publishing
ppublishing.org

Section 4. Technical science in general

DOI:10.29013/AJT-23-11.12-45-51

ASSESSMENT OF ABSORPTION-RADIATION CHARACTERISTICS OF AN IDEAL SELECTIVE SURFACE

Ergashev Sirojiddin Fayazovich [1], ***Tojiboev Abror Kahorovich*** [1], ***Tojiboeva Muhayo Djamoldinovna*** [1]

[1] Fergana Polytechnical Institute, Fergana, Uzbekistan

Cite: *Ergashev S.F., Tojiboev A.K., Tojiboeva M.D. (2023). Assessment of Absorption-Radiation Characteristics of an Ideal Selective Surface. Austrian Journal of Technical and Natural Sciences 2023, No 11-12.* https://doi.org/10.29013/AJT-23-11.12-45-51

Abstract

In this article, the absorption-radiative characteristics of an ideal selective surface are studied, in particular, the possibility of obtaining high heating temperatures due to solar radiation is analyzed, a model is developed and a threshold wavelength is selected, and the effective values of absorption and emissivity for a selective surface are determined. The question of the possibility and feasibility of using spectral-selective surfaces for high-temperature heating due to solar radiation has been studied, the indicators of real selective surfaces have been determined, the average effective values of absorption-emissivity and the magnitude of the characteristics of the selective surface have been given, and the corresponding conclusions have been presented.

Keywords: *concentration, collector, solar energy, selectivity, radiated energy, absorption, receiver, black body*

Introduction

The possibility of obtaining high heating temperatures due to solar radiation is associated with such a special property of the radiant energy of the Sun as the possibility of concentrating it to very high densities, as well as with the use of spectrally selective absorption beams as special receiving surfaces. In addition, a solar concentrator should be considered not only as a means of compressing a rather rarefied flux of radiation coming from the Sun, but also as its collector-catcher and transporter. As a transporter of captured solar energy to the place of use (conversion), a solar concentrator seems, in principle, to be a structure of extreme lightness, since its surface can perform only one simple function – to reflect the sun's rays. The selectivity property of the receiver allows, in turn, to reduce the required concentration values, reduce the requirements for the accuracy of the shape of the mirror surface and its tracking of the Sun, and reduce the weight of its structure and orientation system, which is especially important for reducing the cost of the power plant.

The question of the possibility and feasibility of using spectral-selective surfaces for high-temperature heating due to solar radiation is currently attracting much attention from researchers, both abroad and in our country. The issue has not yet been sufficiently considered, and not always from a fundamentally correct position. Even the basic concepts – about the ideal selective surface, about the maximum possible heating temperature, and the application of the second law of thermodynamics and Kirchhoff's law – need clarification. Explicitly or implicitly, it is usually concluded that the selectivity property degenerates with increasing temperature, and it is unclear, at least, whether the use of the selectivity effect in high-temperature installations will be useful (Abdurakhmanov, A.A., Turaeva, U.F., Klychev, Sh.I., 2008; Avezov, R.R. 1990; Renewable energy sources. 2001).

Materials and methods

Determination of the ideal selective surface (ISS). Selecting the threshold wavelength. Solar radiation, with a good approximation, can be represented as radiation from an absolute black body (ABB) with a temperature T_s = 5800 K, for which the highest intensities occur in the spectral range λ = 0.1 + + 2.5 m cm, where 97% of all emitted energy is concentrated. If a body absorbs maximum in this range, and has minimal emissivity in the range of its own radiation, then a significant effect is obtained (note, for example, that at heating temperature levels of 1000–1500 °K often used in power systems, the interval $\lambda = 2 + \infty$ mcm accounts for 83–73% of emitted energy) (Zahidov, R.A. 2008).

Based on the above, a suitable definition of an ideal selective surface (ISS) for the purpose of heating is its previously proposed (Zahidov, R.A., Saidov, M.S. 2009; Use of solar energy in space research, 1964) definition as a surface having $a_{s\lambda} = \mathcal{E}_\lambda = I$ in the wavelength region $\lambda < \lambda_{lim}$ and $a_{s\lambda} = \mathcal{E}_\lambda = 0$ in the region $\lambda \geq \lambda_{por}$, however, with the addition that the value of λ_{lim} is selected each time as optimal (depending on the density of the incident solar radiation flux and the operating temperature of the surface), providing the maximum temperature effect.

When the radiation receiver (concentrator-receiver system) operates in a vacuum, the calculated expression for $\lambda_{lim.opt}$ can be found from the condition of obtaining the extremum (maximum) of the expression:

$$P_c = \frac{\int_0^{\lambda\,\lim} r(\lambda T_s)d\lambda}{n} - \int_0^{\lambda\,\lim} r(\lambda T_n)d\lambda \qquad (1)$$

The maximum value of useful energy P_c will be when:

$$\frac{dP}{d\lambda\,\lim} = 0 \, that\ is, \text{ when}$$

$$\frac{r(\lambda_{\lim} T_s)}{n} - r(\lambda_{\lim} T_n) = 0 \qquad (2)$$

After performing the transformations, we get:

$$n = \frac{e^{c_2/(\lambda_{\lim})opt * T_n} - 1}{e^{c_2/(\lambda_{\lim})opt * T_s} - 1} \qquad (3)$$

In these expressions T_n – temperature of the surface receiving radiation; T_c – average temperature of the solar surface; C_2 – quantities included in the Planck formula; $r(\lambda T_s)r(\lambda T_n)$ n is the coefficient of attenuation of the solar radiation density at a given point in space compared to that directly at the surface of the Sun.

Relationship (3) can also be presented as:

$$T_n = \frac{C_2}{(\lambda_{\lim})_{opt} \ln\{n[e^{c_2/(\lambda_{\lim})_{opt} * T_s} - 1] + 1} \qquad (4)$$

Equations (3) and (4) give a relationship between three quantities: $n, (\lambda_{\lim})_{opt}$ and – temperature of the surface receiving radiation. Both Equations are relatively transcendental and do not allow one to accurately represent them explicitly as a function of magnitudes and n. It is possible to write an iterative type explicitly:

$$T_n (\lambda_{\lim})_{opt}\ n, (\lambda_{\lim})_{opt}\ T_n$$

$$(\lambda_{\lim})_{opt} = C_2 \left(\frac{1}{T_n} - \frac{1}{T_s}\right) \ln \frac{n}{e^{\frac{n-1}{C_2/\lambda_1 T_n}} + 1} \qquad (5)$$

where $\lambda_1 = C_2 \left(\frac{1}{T_n} - \frac{1}{T_s}\right) / \ln n$

Equations (3) and (4) can be obtained not only from an expression for the maximum received energy of type (2), but also in a simpler (algebraic) way, which allows for a better (simpler, more visual) representation of the expected result.

Figure 1. *Towards the representation of an ideal selective surface and determination of the value of the optimal threshold wavelength* $(\lambda_2 = \lambda_{\lim.opt})$

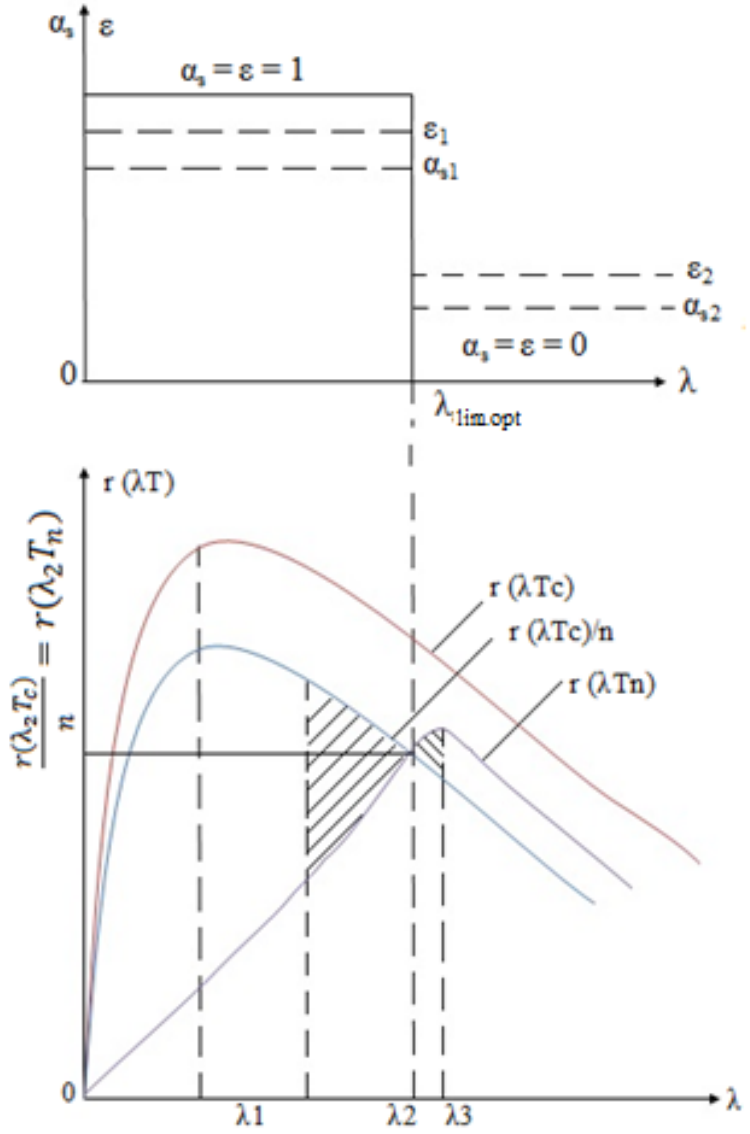

A simple graphical analysis of (Fig. 1) leads to the answer: $(\lambda_{\lim})_{opt}$ can be defined as the abscissa of the intersection point of curves 2 and 3 (i.e.). In fact, if we assume that it corresponds to a certain λ1, in this case, although the own radiation decreases, the reception of the incident energy deteriorates. Similarly, if we assume that it is equal to some $\lambda 3(\lambda_{\lim})_{opt} = \lambda_2 (\lambda_{\lim})_{opt} (\lambda_{\lim})_{opt}$, then there is a loss of energy due to radiation from the absorption capacity of the receiver. Writing the equations for curves (2) and (3) according to Planck and solving them together, we obtain:

$$\frac{r(\lambda_{\lim} T_s)}{n} = r(\lambda_2 T_n)$$

Finally, i.e. expression coinciding with (3) values calculated using Equations (3) and (4) for various quantities $n = \frac{e^{c_2/(\lambda_2 T_n)} - 1}{e^{c_2/(\lambda_{2T_s})} - 1} (\lambda_{\lim})_{opt}$ T_n and n are presented in the graph in (Fig. 2). The same graph shows the values $(\lambda_{\lim})_{opt}$, calculated using the approximate formula proposed in (Klychev, Sh.I. 2004; Beckman, W., Klein, S., Duffy, J., 1982). As can be seen, in a number of practically interesting

combinations of parameters, the error in the approximate determination of the value can be significant. The use of an approximate formula also complicates the general analysis of heating capabilities when using a selective receiving surface. The general pattern noticeable from the graph in (Fig. 2): a decrease in value with an increase $(\lambda_{\lim})_{opt}$ $(\lambda_{\lim})_{opt}$ Tn and a decrease in the radiation concentration.

Figure 2. *Values of the optimal threshold wavelength according to the exact formula (3) and the approximate one (Avezov, R.R. 1990; Renewable energy sources. 2001); 1 – exact value* $(\lambda_{\lim})_{opt}$ *; 2 – suitable area of application of selective surface*

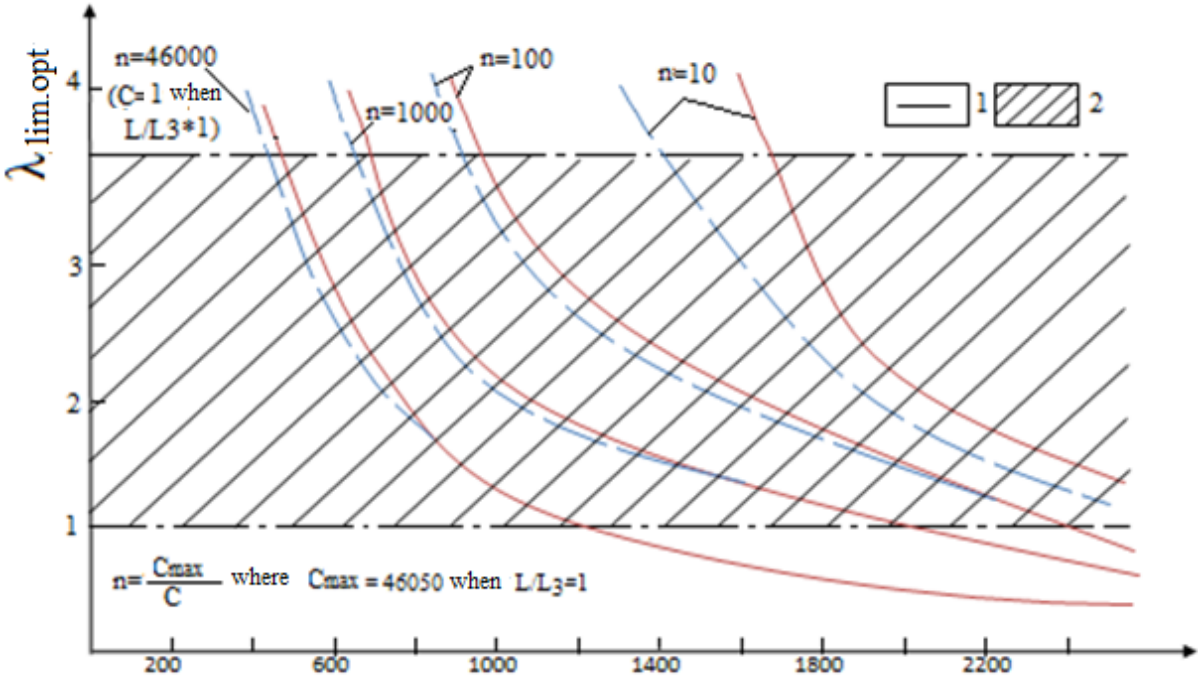

Results and discussion

Turning to the (Fig. 1) in detailed: 1-curve of radiation intensity distribution over wavelengths of the solar spectrum (approximately – the radiation curve of the black body at T_s = 5800K), 2-this is the same curve with ordinates reduced by times; 3- radiation curve of the black body (on the surface of the receiver) at the temperature of the receiving surface T_n.

$$\frac{r(\lambda_{\lim} T_s)}{n} = r(\lambda_2 T_n) \qquad (6)$$

From Equations (3) and (4) a somewhat unexpected conclusion is revealed about the presence of minimum temperatures, below which the effect of radiation absorption selectivity does not appear.

Believing $(\lambda_{\lim})_{opt} \to \infty$ from expression (4) one can find that the quantityTn tends to a certain limit

$$\lim T_n = \lim \frac{C_2}{(\lambda_{\lim})_{opt} \ln[n(e^{c_2/(\lambda_{\lim})_{opt} * T_s} - 1) + 1]} = \lim \frac{n e^{c_2/(\lambda_{\lim})opt * T_s} - 1}{n e^{c_2/(\lambda_{\lim})opt * T_n} - \frac{1}{T_s}} = -\lim \left[T_s \left(1 - \frac{1}{e^{c_2/(\lambda_{\lim})optT_s}} + \frac{1}{n e^{c_2/(\lambda_{\lim})optT_s}} \right) \right] = \frac{T_s}{n} \qquad (7)$$

Expression (7) determines the lower limit of the heating temperature, starting from which the property of selective radiation absorption can manifest itself. For example, to the levels of the Earth's orbit ($C_{\max} \approx$ $\approx$ 46000) at C = 4600 (n =10)^x the beginning of the selectivity effect corresponds to $(T_n)_{\min}$ = = 580 °K.

Figure 3. *Effective values of absorption-emitting characteristics for ISS*

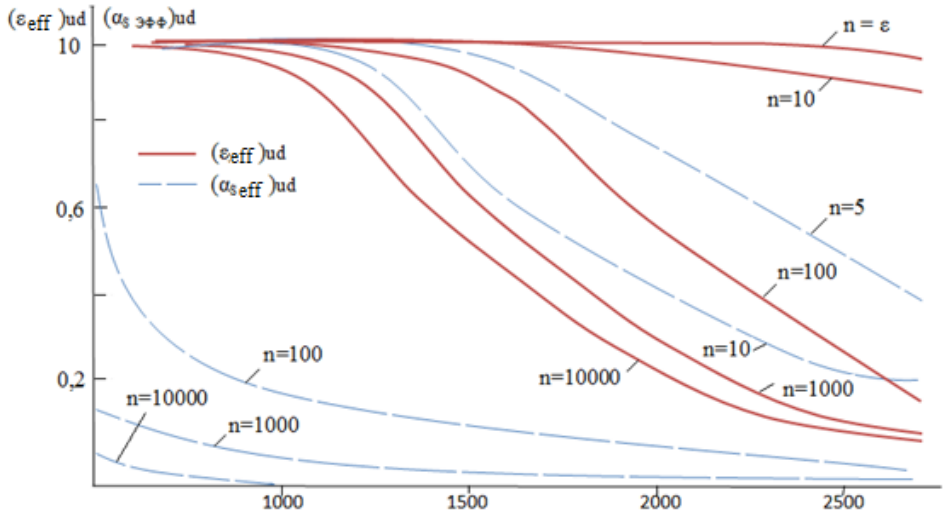

Determination of effective values of absorption and emissivity for a selective surface

To determine the integral (i.e., effective) values of the absorption-emitting abilities of an ideal selective surface, we can write

$$(a_{s\ эфф})_{ud} = \frac{\int_0^{(\lambda_{\lim})_{opt}} r(\lambda T_s)d\lambda}{\int_0^{\infty} r(\lambda T_s)d\lambda};$$

$$(\varepsilon_{эфф})_{ud} = \frac{\int_0^{(\lambda_{\lim})_{opt}} r(\lambda T_n)d\lambda}{\int_0^{\infty} r(\lambda T_n)d\lambda} \quad (8)$$

Real selective surfaces may have characteristics of change and $\mathcal{E}$ as a function of λ that are qualitatively similar to those for an ideal selective surface (ISS): in the region of a rather narrow interval of λ there may be a sharp drop in these values, which can be approximately represented as a "threshold" (Kuchkarov, A.A., Muminov, Sh.A. 2020; Yu. Yu. Pochekailov, A.V. Shashev, V.I. Yakovlev, N.A. Yakovlev, 2015). The values themselves $\alpha s1$ and $\mathcal{E}1$ (up to the threshold) turn out to be, although close to unity, but less than unity. The quantities $\alpha s2$ and $\mathcal{E}2\alpha_s$(after the threshold), turning out to be quite small, are still noticeably not equal to zero (see Fig. 1, a, b).

For such real selective surfaces, the average effective (over the spectrum) values of absorption-emissivity can be determined using the Equations:

$$(a_{s\ эфф})_p = (a_{s1} - a_{s2})\frac{\int_0^{\lambda_{\lim}} r(\lambda T_s)d\lambda}{\int_0^{\infty} r(\lambda T_s)d\lambda} + a_{s2} \quad (9)$$

and

$$(\varepsilon_{эфф})_p = (\varepsilon_1 - \varepsilon_2)\frac{\int_0^{\lambda_{\lim}} r(\lambda T_n)d\lambda}{\int_0^{\infty} r(\lambda T_n)d\lambda} + \varepsilon_2 \quad (10)$$

These numbers are quite realistic. The values Cav=4000+8000 can be obtained, in particular, for projector-type glass mirrors.

For the real selective surface (RSS) represented in this way, as well as for the ISP, the value of the optimal threshold wavelength is determined by relations (3), (4).

Figure (4) shows the calculated values of the effective absorption-emissive abilities of the ISS depending on the heating temperature at different values of the incident radiation density. With increasing heating temperature values $(\alpha s\ eff)_{ud}$ and $(\mathcal{E}\ \text{eff})_{ud}$ decreases and tends to zero at $T_n \to T_s$ (in accordance with Kirchhoff's law. An important characteristic of the selective surface is the value. Let's call it the selectivity parameter.

$\Pi_c = \frac{a_{s\ эфф}}{\varepsilon_{эфф}}$ For an ideal selective surface

$$(\Pi_c)_{ud} = \frac{\int_a^{(\lambda_{\lim})_{opt}} r(\lambda T_s)d\lambda}{\int_a^{(\lambda_{\lim})_{opt}} r(\lambda T_n)d\lambda}\left(\frac{T_n}{T_s}\right)^4 \quad (11)$$

Figure 4. *The value of the selectivity parameter* $(P_s)_{id} = \frac{(a_{s\,eff})_{u\partial}}{(\varepsilon_{eff})_{u\partial}}$ *for an ideally selective surface at different concentration values and different receiver temperatures*

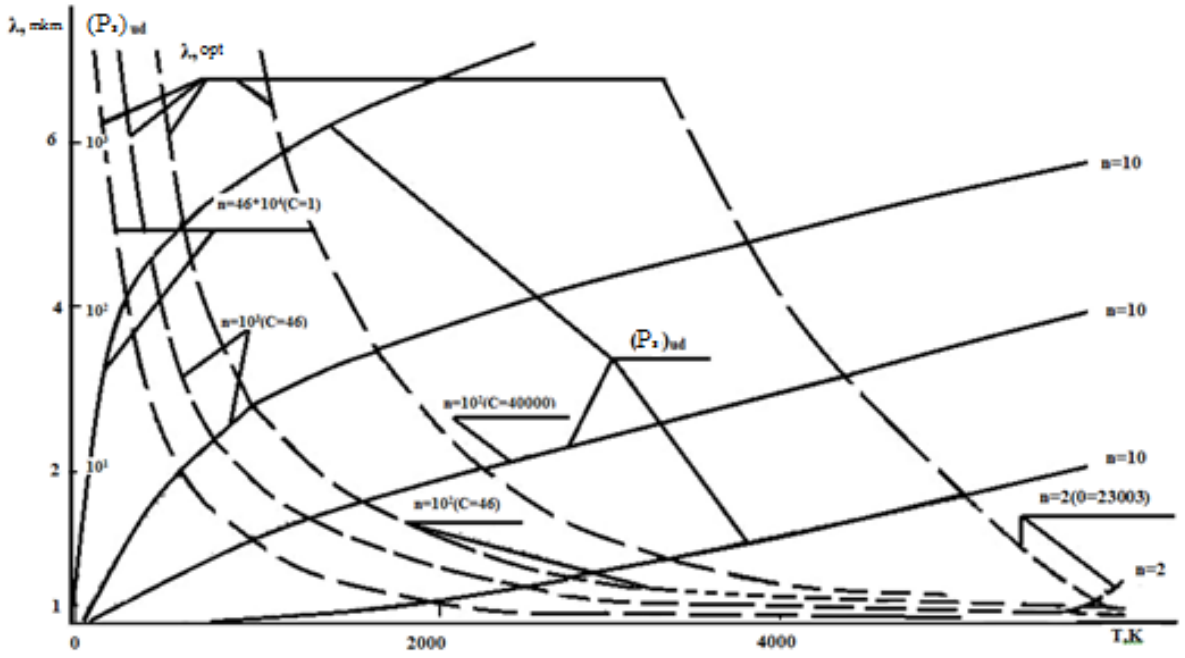

Figure 5. *Possible efficiency values concentrator-receiver systems in the case of an ideal spectral-selective surface* $\eta_R = 1$, *1-ISS; 2- ABB* ($\alpha_s = \mathcal{E} = 1$)

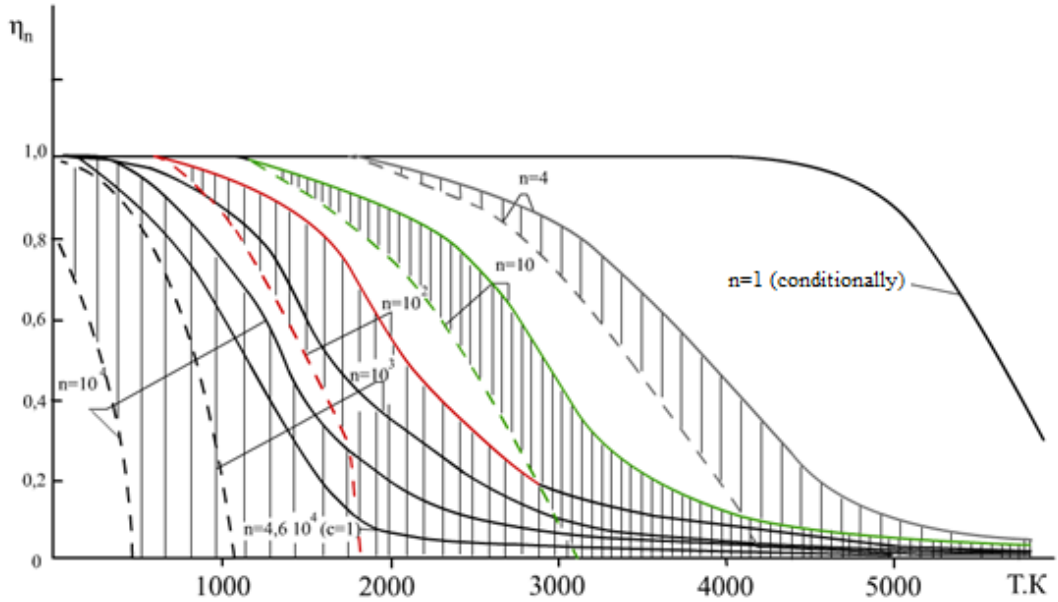

Let us find out for ISS the nature of the change in P_s depending on temperature. As established above, the lower level of heating temperature, where the properties of the ISS are still preserved, corresponds to $(T_n)_{\min} = \frac{T_n}{n}$ and $P_s = 1$. With increasing temperature, as the results of calculations show, Fig. (5), the possible values of the parameter Π_c for the ISS increase, reaching the highest values in the absence of radiation concentration and when $T_n \to T_s$ tends. The course of the curves on the graph in (Fig. (5)) predicts that, apparently, the limiting value of P_s for ISS at $T_n = T_s$ has the value $P = n$. This is shown quite strictly below.

Our term, referred to as the general criterion, determines the properties of the selective surface.

Conclusions

The results of studies on the absorption-emissivity characteristics of an ideal selective surface show that correctly designed thermal insulating material, threshold wavelength and effective valuesof absorption and emissivity sensitively affect the efficiency of solar energy installations.

References

Abdurakhmanov, A.A., Turaeva, U.F., Klychev, Sh.I. Methodology for determining the integral selectivity of real bodies. Solar engineering.– Tashkent, 2008.– No. 4.– P. 50–53.

Avezov, R.R. Increasing the efficiency of using low-potential solar heaters in heat supply systems. Dis. Doctor of Technical Sciences – Tashkent: 1990.– 447 p.

Renewable energy sources. In the book. The first national communication of the Republic of Uzbekistan under the UN Framework Convention on Climate Change. Phase 2. Main Directorate for Hydrometeology under the Cabinet of Ministers of the Republic of Uzbekistan.– Tashkent, 2001.– P. 34–36.

Zahidov, R.A. Increasing the role of alternative and renewable energy sources in the US energy strategy // Solar engineering, 2008.– No. 1.– P. 89–96.

Zahidov, R.A., Saidov, M.S. Renewable energy at the beginning of the 21st century and prospects for the development of solar technology in Uzbekistan // Solar engineering, 2009.– No. 1.– P. 3–12.

Use of solar energy in space research // Sat. translations under ed. V.I. Bauma. Introductory article.– Moscow, 1964.– P. 5–9.

Klychev, Sh.I. Modeling of receiving and concentrating devices of solar thermal power plants.: Dis. Doctor of Technical Sciences – T.: Physicotechnical Institute. 2004.– 268 p.

Beckman, W., Klein, S., Duffy, J. Calculation of solar heating systems. Per. from English – M Energoizdat, 1982.

Kuchkarov, A.A., Muminov, Sh.A. Modeling and creation of a flat Fresnel linear mirror solar concentrator // Universum: technical sciences. 2020.– No. 3–2 (72) / [Electronic resource].– Access mode: URL: http://7universum.com/ru/tech/arch.

Selective basalt detonation coatings for solar collector absorber / Yu. Yu. Pochekailov, A.V. Shashev, V.I. Yakovlev, N.A. Yakovleva // International Journal of Applied and Fundamental Research. 2015.– No. 4 – P. 35–39.

submitted 07.12.2023;
accepted for publication 20.12.2023;
published 24.01.2024

Contact: abrortak78@mail.ru

The Austrian Journal of Technical and Natural Sciences, No 11–12
ISSN 2310-5607

PREMIER Publishing
ppublishing.org

DOI:10.29013/AJT-23-11.12-52-55

STUDY OF THE PROTECTIVE EFFECT OF NAOH ON THE CORROSION RESISTANCE OF CARBON STEEL AND GRAY CAST IRON IN THE OIL AND GAS INDUSTRY

Makhmudov Mukhtor Jamolovich [1], ***Smanov Bakitjan Alkabayevich*** [2]

[1] Bukhara Engineering and Technology Institute

[2] Institute of the General and Inorganic chemistry Academy of Sciences of the Republic of Uzbekistan

Cite: *Makhmudov, M.J., Smanov, B.A. (2023). Study of the Protective Effect of Naoh on the Corrosion Resistance of Carbon Steel and Gray Cast Iron in the Oil and Gas Industry. Austrian Journal of Technical and Natural Sciences 2023, No 11-12.* https://doi.org/10.29013/AJT-23-11.12-52-55

Abstract

The article presents the results of a study of the protective effect of NAOH on the corrosion resistance of carbon steel and gray cast iron. Modern methods of corrosion research and their results applied in aqueous media of the main inhibitors of atmospheric corrosion, film inhibitors, in the presence of aggressive mixtures of hydrogen sulfide and concentrated acids are presented.

Keywords: *corrosion inhibitors, secondary amine salts, quaternary ammonium compounds, corrosion rate*

Introduction

One of the most important factors influencing metal corrosion is the pH of the solution: the possibility of using a particular metal in practice is often determined by those pH limits within which the metal is satisfactorily resistant (Hammood, S. Ali, lieth Mahdi Haider, 2012). As a rule, the pH of circulating water is maintained within 6...8 (Kumar Chiranjib, Gupta, 2003).

Caustic soda enters the circulating system of barometric condensers from evaporators, which can change the pH of the circulating water within a wide range. To maintain the required pH values, it is neutralized with hydrochloric acid, which leads to an increase in the chloride content in the circulating water and an increase in its corrosiveness. The rate of iron corrosion at alkaline pH values slows down (Lunarska, E. 1996). However, do these data relate to non-mineralized solutions, or did the studies use a universal buffer mixture containing an inhibitory component such as to maintain pH P_4^{3-}. Therefore, it is of interest to study the protective effect of sodium hydroxide on the structural materials of the circulating system of barometric capacitors when operating on mineralized water.

There was an assumption about using a reagent for protection against corrosion, which is actually a waste product and spontaneously enters the circulating water, instead of scarce and often toxic corrosion inhibitors. An additional criterion in favor of this premise was the fact that sodium hydroxide has a bactericidal effect (Espinoza, Vázquez, Figueroa, I.A., Sánchez, D. Molina, Rodríguez-Gómez, F.J., Angeles Beltrán, D. 2021). It was possible to use the same reagent for both corrosion protection and biofouling suppression.

Naturally, the increase in pH associated with the addition of NaOH can lead to increased scale deposition. However, in a circulating system of barometric condensers, when operating on water of high salinity, barometric condensate is sufficient to replenish the system, i.e. water that does not contain hardness salts.

Other circulating cycles at modern chlorine plants are fed not with river water, but with highly purified water, containing up to 2 g/l NaCl and having a total hardness of up to 1.5...2 mg-eq/l. Thus, in production conditions, replenishing the system with water containing a minimum amount of hardness salts will avoid the problem of scale deposits even at alkaline pH values of the circulating water.

The assumption of using NaOH to suppress corrosion in circulation cycles required laboratory testing in order to determine specific pH values, NaCl concentration and temperature at which the corrosion rate of equipment in the recycling water supply system would correspond to acceptable values (up to 0.1 g/m^{3}h) (Espinoza Vázquez, Figueroa I.A., Sánchez D. Molina, Rodríguez-Gómez F.J., Angeles Beltrán D. 2021). The studies were carried out using gravimetric and electrochemical methods.

The results of the influence of pH on the corrosion rate of carbon steel and gray cast iron in circulating water with a mineralization of 0.02 mol/l NaCI are given in table 1. Test duration is 1560 hours, temperature – 22 °C.

As you can see, with an increase in the pH of the solution to 13, the corrosion rate of metals decreases significantly, especially in the waterline zone (by 5...8 times). Obviously, this is due to the formation of insoluble protective films at alkaline pH values, which directly inhibit the electrochemical anodic stage of dissolution.

Table 1. *Effect of pH on the corrosion rate of carbon steel and gray cast iron in circulating water with a concentration of 0.02 mol/l NaCI*

Material	pH	Test site	Corrosion rate, g/m^{2}h	Nature of corrosion
Steel St.3	8	In the volume of electrolyte	0.0278	Spots
	10		0.0160	Spots
	11		0.0101	Spots
	13		0.0088	Spots
	8	In the waterline area	0.1045	Uneven
	10		0.0657	Uneven
	11		0.0560	Uneven
	13		0.0170	Spots
Cast iron SCh 18–36	8	In the volume of electrolyte	0.0425	Spots
	10		0.0248	Spots
	11		0.0177	Spots
	13		0.0128	Spots
	8	In the waterline area	0.1545	Uneven
	10		0.1133	Uneven
	11		0.0960	Spots
	13		0.0225	Spots

The observed dependencies are complemented by electrochemical studies on gray cast iron (Fig. 1). Similar curves were obtained for carbon steel.

Figure 1. *Effect of pH on the anodic polarization curves of gray cast iron in circulating water with a concentration of 0.02 mol/l NaCI. pH of mineralized water: 1–7.0; 2–10.0; 3–11.5; 4–12.5*

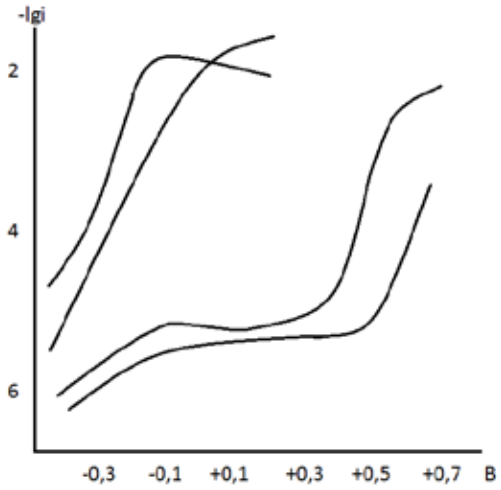

The main characteristics of anodic processes on cast iron depending on pH in circulating water containing 0.02 mol/l NaCl are summarized in table 2.

Table 2. *Influence of pH on the main electrochemical characteristics of anodic processes on cast iron*

pH	Stationary potential, V	Pitting potential, V	Passive state area, V
7.0	–0.44	–0.44	Absent
8.5	–0.40	–0.40	Absent
9.0	–0.40	–0.40	Absent
10.0	–0.45	–0.35	0.1
11.5	–0.35	0.78	0.9
12.5	–0.14	0.83	1.1

Analysis of the table 2 shows that the effective influence of pH on the characteristics of anodic processes under the conditions under study occurs at pH ≥ 11.5. At these pH values, the stationary potential of the metal improves, which indicates inhibition of the anodic process itself. At pH ≥ 11.5, the pitting potential shifts significantly to the positive side: the healing process pitting occurs faster than their formation. This increases the region of the passive state on the anodic polarization curve, and at pH 12.5 this region is equal to 1.2 V.

Thus, by changing the pH of the solution to the alkaline region, it is possible to effectively slow down the rate of corrosion of ferrous metals in circulating water, especially in the waterline area.

References

Hammood, S. Ali, lieth Mahdi, Haider. “Development Artificial Neural Network Model to Study the Influence of Oxidation Process and Zinc-Electroplating on Fatigue Life of Gray Cast Iron”, International Journal of Mechanical & Mechatronics Engineering IJMME-IJENS, 2012.– Vol. 12.– No. 5.– P. 74–78.

Kumar Chiranjib, Gupta. “Chemical Metallurgy”, International Journal of Mechanical & Mechatronics Engineering IJMME-IJENS, 20, Wiley -VCH Verlag GmbH & Co. KGaA, Weinheim, 2003.

Lunarska, E. “Effect of graphite shape on the Corrosion of Gray Cast Iron in phosphoric acid”. Journal of Materials and Corrosion, October, 1996.– Vol. 47.– Issue 10.– P. 539–544.
Zhang, H., L. Zhao, D. Liu, J. Wang, X. Zhang, C. Chen. Early period corrosion and scaling characteristics of ductile iron pipe for ground water supply with sodium hypochlorite disinfection. Water Res. 2020.– 176 p.
Espinoza, Vázquez, Figueroa, I.A., Sánchez, D. Molina, Rodríguez-Gómez F.J. Angeles Beltrán D. Effects of corrosion inhibition with xanthines in gray cast iron protection with Paraloid B-72 in a saline medium Prog. Org. Coat., 2021.– 154. (2020).

submitted 13.11.2023;
accepted for publication 01.12.2023;
published 24.01.2024

Contact: general-Saatova-nsoatova@bk.ru

The Austrian Journal of Technical and Natural Sciences, No 11–12
ISSN 2310-5607

PREMIER Publishing
ppublishing.org

DOI:10.29013/AJT-23-11.12-56-62

CALCULATION METHOD FOR DETERMINING THE REMAINING RESOURCE

Saatova Nodira Ziyayevna [1]

[1] Tashkent State Transport University, "Artificial structures on highways", Uzbekistan

Cite: *Saatova, N.Z. (2023). Calculation Method for Determining the Remaining Resource. Austrian Journal of Technical and Natural Sciences 2023, No 11-12.* https://doi.org/10.29013/AJT-23-11.12-56-62

Abstract

The paper presents calculated method for determining the measure of damage to concrete and reinforcement, based on the basic provisions of the linear theory of damage accumulation. The proposed dependences of the damage measure are convenient for using them in predicting the resource of superstructure structures.

Practical method for calculating the residual resource of the operated superstructures has been developed. It is shown that parameters determined during technical diagnostics are the main initial data for calculating the residual resource. It is established that the residual resource of superstructures subject to salt corrosion is up to 3 times less than the residual resource of the same structures under normal operating conditions.

Keywords and expressions: *operated bridge structures, damage, resource forecasting, critical values, damage measures*

Introduction

Currently operated bridge structures in the Republic of Uzbekistan operate under different force loads with simultaneous unfavorable environmental impact.

Therefore, it is practically impossible to develop a calculation method of bearing capacity and durability of bridge spans with simultaneous consideration of all influencing factors. In the presented work, the authors have limited themselves to the investigation of the part of this problem – prediction of service life of reinforced concrete bridge superstructures in accordance with slab durability. The main attention here is paid to probabilistic calculations of determined resource using modern methods of probability theory and calculations.

Improvement of questions devoted to the problems of increasing durability of bridge structures under conditions of corrosion of their concrete and reinforcement is closely connected with researches in the field of reliability of building structures (Bolotin, V.V., Iosilevskiy, L.I., Chirkov, V.P., Osipov, V.O., Potapkin, A.A., Ashrabov, A.A. and others), prognostication of service life of reinforced concrete bridge spans, (Antonov, E.A., Gordon S.S., Iosilevskiy L.I., Chirkov, V.P., Mamazhanov, R.K., Mukumov, T., Nizamutdinova, R.Z., Urmanov, I.A., Shesterikov, V.I.), corrosion processes in concrete and reinforce-

ment of reinforced concrete spans (Alekseyev, S.N., Moskvin, V.M., Kildeyeva, O.I.). However, based on the results of these data it is difficult to quantify the carrying capacity of operational bridge spans and to predict the residual life for planning the time between repairs. Thus, the research aimed at the development of effective ways to take into account the influence of concrete and reinforcement corrosion in bridge superstructures calculations is an actual problem, which has an important national economic importance. The results of this work will be used to improve the regulatory documents for the calculation of bridge structures in the regional conditions of the Republic of Uzbekistan.

Researching method

When predicting the service life of stressed elements of machines and structures (Bolotin, V.V., 1990; Iosilevsky, L.I., Shcherbakov, E.N., Mamajanov, R.T., 1989) as well as metal bridge spans, the main provisions of the linear theory of damage accumulation are currently used (Chirkov, V.P. 1990).

In this case, the damage caused by external action at a given moment of time does not depend on the loading history, and it can be summed up with the previous damage. The magnitude of the damage is evaluated by the value $0 \le \Psi \le 1$at the beginning of loading $\Psi = 0$; at the moment of exhaustion of the load-carrying capacity of the structure $\Psi = 1$. The accumulation of damage over time is described by the expression

$$\sum_{t=v}^{T} \frac{t_i}{T_i} \qquad (1)$$

For constructions subjected to cyclic loads,

$$\sum_{t=1}^{K} \frac{n_i}{N_i} = 1 \qquad (2)$$

Where n_i – is the number of cycles under uniform loading; Ni is the number of cycles before failure.

Damage measure by any point in time

$$\Psi_i = \sum_{t=0}^{T} \frac{t_i}{T_i} \qquad (3)$$

In the case of non-linear voltage loading σ

$$\Psi_i = \int_0^T \frac{dt}{T(\sigma)} \qquad (4)$$

Based on (3) in (Osipov, V.O. 1999), dependences for determining the resource of metal bridge elements have been proposed.

V.P. Chirkov has proposed mathematical models to predict the service life of reinforced concrete bridge spans on the basis of the above-mentioned provisions. A change in the transverse strain factor V was taken as a measure of concrete damage under repeated loading and dependences for determining the life of spans were obtained with this in mind.

In R. Mamajanov's work the main parameter of fracture mechanics – stress intensity coefficient K – was used to describe the process of degradation and development of cracking in concrete of compressed zone of span structures. Dependences for description of K in time under repeated loading have been proposed.

In the above-mentioned works the loading history, characteristics of loads and their statistical scatterings have been taken into account.

However, it should be noted that the use of these dependences to estimate the damage measure for practical calculations is difficult and large statistical data are required.

Results and the analyze of them

Based on the analysis of the above studies, it can be concluded that it is more promising to take the actual values of concrete strength, reinforcement corrosion degree as a damage measure. Knowing actual values of the mentioned parameters, it is possible to determine values of damage measure and to determine service life of span structures by concrete strength at salt corrosion and reinforcement corrosion.

Considering the above, the concrete damage measure is assumed to be

$$\Psi = \frac{R_b - R_{t\exp}}{R_b - R_{cr}} \qquad (5)$$

Where R_b – is the design value of the concrete strength;

R_{texp} – meaning of concrete strength at the time of technical diagnosis;

R_{cr} – is the maximum permissible value of reduction of concrete strength during salt corrosion.

For (5) the prerequisites fulfilled:

$$R_b = R_{texp}; \quad \Psi=0; \tag{6}$$

$$R_{texp} = R_{cr}; \quad \Psi=1 \tag{7}$$

Thus, Ψ = 0 corresponds to the case where there is no salt corrosion and strength is not reduced, and Ψ = 1 corresponds to the time when the limit state is reached.

From (5) we have

$$\Psi_b = a - bR_{t\exp}; \tag{8}$$

$$a = \frac{R_b}{R_b - R_{cr}} \tag{9}$$

$$b = \frac{1}{R_b - R_{cr}} \tag{10}$$

By substituting $R_{bt} = 0,9R_b e^{-0,01t}$ into (8), we obtain

$$\Psi_b = a - 0,9bR_b e^{-0,01t} \tag{11}$$

According to (11) it is possible to determine the value of the concrete damage measure at any time t of the technical diagnosis from actual measurements of the concrete strength.

Similarly, the reduction of the cross-sectional area of the reinforcement can also be expressed in terms of the damage measure

$$\Psi_s = a_s - b_s A_{st} \tag{12}$$

$$a_s = \frac{A_s}{A_s - A_{cr}} \tag{13}$$

$$b_s = \frac{1}{A_s - A_{cr}} \tag{14}$$

Where A_S – is the cross-sectional area of the reinforcement as designed;

A_{st} – sectional area of the reinforcement after corrosion;

A_{cr} – maximum permissible value of reduction of reinforcement cross-sectional area

Given A_{st}=*A_s0 e^0,015t*, expression (12) is written as

$$\Psi_s = a_s - 0,7b_s A_{so} e^{-0,015t} \tag{15}$$

The obtained dependences for description of damage measure in time allow determining residual life of span structures according to the results of technical diagnostics.

Differential equation for damage accumulation measure according to (Chirkov, V. P. 1998, Osipov, V. O. 1999) with regard to (13) is written as

$$\frac{d}{dt} = ce^{-\alpha t}; \tag{17}$$

Where $c = 0,9R_b \times b$.

The dependence obtained describes the rate of deterioration of concrete strength over time under salt corrosion conditions.

From (17) dividing the variables is can be written

$$\int_0^{\Psi} d\Psi = c\int_0^t e^{-at} dt \tag{18}$$

The accumulated damage measure Ψ_1 at time *t* is determined by integrating the equation

$$\int_0^{\Psi_1} d\Psi c\int_0^{t1} e^{-at} dt \tag{19}$$

$$\Psi_1 = -c \times e^{-\alpha tI} \tag{20}$$

The resource T_{res} of the span when the load-bearing capacity Ψ = 1 is exhausted is determined from the equation

$$\int_0^1 d\Psi = -c\int_0^{T_{res}} e^{-\alpha T} dt \tag{21}$$

From here, by integration we get

$$e^{-T_{res}} = 1/c \tag{22}$$

$$T_{res} = {}_h \frac{en\,1/c}{\alpha} \tag{23}$$

Suppose that by the time of technical diagnosis *t1* the damage accumulation is $\Psi = \Psi_1$. The permissible value of the damage measure is taken as $\Psi = \Psi_{cr}$. then to determine the time for damage to reach critical values Ψ_{cr} (20) is written as

$$\int_{\Psi_1}^{\Psi_{cr}} d\Psi = c\int_{T_1}^{T_{res}} e^{-\alpha t} dt \tag{24}$$

Integration gives

$$\Delta T_{resb} = \frac{\ln\left[\frac{\Psi_{cr} - \Psi_{1b}}{c}\right]}{\alpha} \tag{25}$$

Where $\Delta T_{res} = T_{res} - t_1$ – residual life – estimated service life since technical diagnosis;

T_{res} – the design life of the span.

The corrosion life of the span is determined using a similar methodology

$$\frac{d_3}{dt} = c_3 e^{-\beta t}; \tag{26}$$

$$\int_0^1 d_3 = c_3 \int_0^{T_{res}} e^{-\beta t} dt \quad (27)$$

$$T_{res} = \frac{\ln 1/c_3}{\beta} \quad (28)$$

Residual life by valve corrosion

$$\int_{\Psi_1}^{\Psi cr} d\Psi = c_3 \int_{t_1}^{T_{res}} e^{-\beta t} dt \quad (29)$$

$$\Delta T_{ress} = \frac{\ln\left[\frac{\Psi_{c3} - \Psi_{is}}{c_3}\right]}{\beta} \quad (30)$$

Thus, it is possible to determine the residual life of the reinforced concrete superstructures subject to salt spray corrosion using the obtained dependencies. The main input data are the results of technical diagnostics.

It should be noted that an important point in determining the residual life is the correct assignment of the limit values of the damage measure $\Psi_{cr.}$

Research on the assignment of Ψ_{cr} in practical tasks has been devoted to (Tynkov, I.B., Nizamutdinova, R.Z., 1990).

From the analysis of these works, it is clear that the normalized value Ψ_{cr} is a random variable, and its precise determination is a difficult task and presents mathematical difficulties. Therefore, (Osipov, V.O., 1999) provides evidence for the practical use of simple mathematical models to assign Ψ_{cr} when justifying assumptions.

In the works of V.O. Osipov, the value of $\Psi_{cr.}$ is substantiated for predicting the residual life of metal spans.

In works (Tynkov, I.B., Nizamutdinova, R.Z. 1990) the normalized value $\Psi_{cr.}$ is set separately for different types of span resource exhaustion – by endurance of concrete and reinforcement, by deflection and other attributes. The probability of non-destruction at any value of accumulated damage measure is given as

$$P(\Psi) = 1 - \frac{1}{\sigma\sqrt{2\tau}} \int_0^{cr} exp\left[-\frac{\left(-\overline{\Psi}\right)^2}{2\sigma^2}\right] d \quad (31)$$

Or

$$P(\Psi) = 1 - \left[\frac{\overline{\Psi} - \Psi_{cr}}{\sigma}\right] \quad (32)$$

Table 1 records the values Yc_r calculated according to (32) from the results of the repeated loading tests of the test specimens.

Table 1. – *Changing the meaning of a* Ψ_{cr}

Meaning of the Ψ_{cr}	0.35	0.4	0.45	0.5	0.55	0.6	0.65
Probability of non-destruction	0.999	0.996	0.989	0.971	0.934	0.864	0.722

As it can be seen from table 1, the probability of non-destruction decreases with increasing tolerance values Ψ_{cr}. Here, one of the main tasks is to establish the level of non-destruction $P(\Psi)$ – the level of reliability of the span structure operation according to the characteristic under consideration.

In works (Nizamutdinova, R.Z., 1994) for reinforced concrete structures with failure due to brittle failure, loss of stability it is proposed to take $P(\Psi) = 0.999$, and with failure without loss of load-bearing capacity $P(\Psi) = 0.99$.

In recommendations (Recommendation on Evaluation and Reliability of Transport Structures 1989) reliability level of $P(\Psi)$ is proposed to be assigned depending on the category of road on which the bridge structures are located.

As can be seen, there are currently no sufficiently well-founded suggestions for assigning $P(\Psi)$. Therefore, following the results of studies (Shesterikov, V.I. 1991), (Kildeeva, O.I., 1998) ($P(\Psi) = 0.95$ can be taken with some caution for resource calculations).

Example of calculating the residual lifetime of a reinforced concrete structure subject to salt spray corrosion

Input data. The 16.76 m long reinforced concrete span of the overpass. The year of construction of the overpass is 1967. The

girder design was developed for H30 and NK80 load.

The overpass was repeatedly examined by bridge departments of TashIIT and TADI.

The scheme of the span is shown in Figure 2.1. The main beam is reinforced with periodic profile reinforcement ø 14 mm of A-II class. The carriageway slab is reinforced with A-II class reinforcement ø 12 mm with 10 cm spacing. The distance between the main beams is 56 cm. The design class of concrete is B25 (M300).

The survey found that salt corrosion had reduced the original diameter of the reinforcement to 5.9 mm. The depth of salt penetration determined by the method specified in clause 2.3 is up to 12–17 mm. The actual strength of the concrete layer of the corroded slab is Rb = 12.0 MPa.

It is required to determine the residual life of the span in terms of slab strength.

Calculation of the slab load-bearing capacity at the time of the technical diagnosis.

Calculation diagram of the external cantilever slab

h1 – height of compression zone not subject to salt corrosion.

Figure 1.

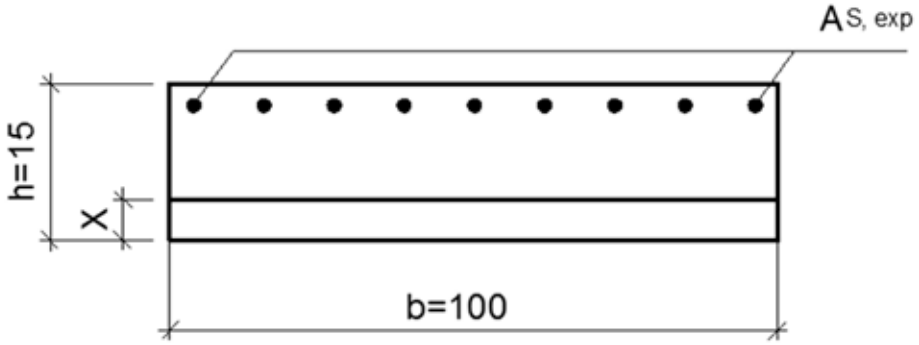

The height of the concrete compression zone, taking into account the actual condition of the slab, is determined according to the following expression

$$x = \frac{R_s A_{Sexp}}{R_{bexp}} = \frac{240 \cdot 5{,}9}{12 \cdot 100} = 2{,}36\ sm$$

Where A_{sexp} – actual cross-sectional area of the reinforcement;

R_{bexp} – actual design resistance of concrete.

Checking the load-bearing capacity of the section

$$R_{b\exp} bx\left[h_0 - \frac{x}{2}\right] = 12 \cdot 100 \cdot 2{,}36\left[12 - \frac{2{,}36}{2}\right] = 15{,}3\ кНм > M = 14{,}1\ kNm$$

Where M – the calculated bending moment in the considered cross-section, at the moment of diagnostics the bearing capacity of the cross-section is provided with a small reserve. Exhaustion of the resource can take place at reduction of concrete strength up to R_{crb} = 8.0 MPa and reduction of actual reinforcement area up to A_{scr} = 5.5 cm².

Determine the measure of damage accumulation in concrete and reinforcement by the time of technical diagnostics by formulas

$$\Psi_{1b} = \frac{R_b - R_{bexp}}{R_b - R_{cr}} = \frac{35-12}{35-8} = 0{,}85$$

$$\Delta T_{resb} = \frac{\ln\left[\frac{\Psi_{cr} - \Psi_{1b}}{c}\right]}{\alpha} = \frac{\ln\left[\frac{1{,}92-0{,}85}{1{,}18}\right]}{0{,}01} = 9{,}8\ years$$

$$C = 0{,}9\,Rbb = 0{,}9\frac{35}{35-8{,}5} = 1{,}18$$

$$\Psi_{cr} = \frac{1}{\left[\Psi_{cr}\right]} = \frac{1}{0{,}52} = 1{,}92$$

Where $\left[\Psi_{cr}\right]$ =0,5 for reliability level 0,95 by table 1.

$$\Psi_{1s} = \frac{A_S - A_{Sexp}}{A_S - A_{cr}} = \frac{11,3-5,9}{11,3-5,5} = 0,93$$

$$\Delta T_{ress} = \frac{\ln\left[\frac{\Psi_{c3} - \Psi_{1s}}{c_3}\right]}{\beta} =$$

$$= \frac{\ln\left[\frac{1,923-0,93}{1,42}\right]}{0,015} = 25,2 \text{ years}$$

$$\Delta T_{ress} = \frac{\ln\left[\frac{\Psi_{c3} - \Psi_{1s}}{c_3}\right]}{\beta} =$$

$$= \frac{\ln\left[\frac{1,923-0,95}{1,42}\right]}{0,015} = 25,2 \text{ years}$$

$$C_3 = 0,7 b_S A_{S0} = 0,7 \frac{1}{11,3-5,5} 11,3 = 1,42$$

Thus, the residual life of the span slab is $\Delta T_{res} = 9,8 \approx 10$ years on the basis of the bearing capacity of concrete corrosion.

Summary

The calculated method of determination of damage degree of concrete and reinforcement of bridge structures based on main provisions of linear theory of damage accumulation with regard for regional conditions of the Republic of Uzbekistan has been proposed. The proposed damage measure dependencies are convenient for their use in forecasting the service life of bridge superstructures.

The practical way of calculation estimation of residual resource of operating bridge spans has been developed. It is shown that the main initial data for residual resource calculation are the parameters, which are defined at technical diagnostics. It is established that the residual life of the spans that are exposed to salt corrosion is up to 3 times less than the residual life of the same structures which are under normal operation conditions.

References

Bolotin, V.V. (1990). Resource of machines and structures.– Moscow: Mashinostroenie.

Iosilevsky, L.I., Shcherbakov, E.N., Mamajanov, R.T. (1989). “Prediction of Service Life of Elements Subjected to Regime Loadings”, Report of the Academy of Sciences of UzSSR.– № 12.– P. 18–20.

Mamajanov, R.T.T. (1993). Probabilistic prediction of lifetime of Reinforced Concrete Bridge spans.– Tashkent: Fan.– 156 p.

Ryazanov, Y.S. (2003). About estimation of technical state of bridges // Way and track facilities, 2003.– № 7.– P. 26–27.

Tynkov, I.B., Nizamutdinova, R.Z.T. (1990). The causes of damage in reinforced concrete spans operated in conditions of Central Asia // Operational reliability of engineering structures under complex loads and influences of external environment.– Tashkent, 1990.– 40 p.

Chirkov, V.P. (1990). Fundamentals of Theory of Calculation of Reinforced Concrete Structure Life //Concrete and Reinforced Concrete, 1990.– № 10.– P. 35–36.

Osipov, V.O. (1982). Durability of metal spans of railway bridges. Transport. 1982.– 287 p.

Osipov, V.O. (1999). Reserves of metal bridges load-carrying capacity // Railway transport. 1999.– № 8.– P. 42–45.

Chirkov, V.P. (1998). Theoretical basis of forecasting service life of reinforced concrete structures. Tutorial.– Moscow: MIIT, 1998.– 56 p.

Chirkov, V.P. (2000). et al. Service Life – the basis for designing of transport systems // Transport Construction – № 1.– 15 p.

Mamajanov, R. (1989). Practical method of calculation of reinforced concrete bridge spans // Transport construction.– № 3.– P. 19–20.

Nizamutdinova, R.Z.T. (1994). Resource of Reinforced Concrete Bridge spans on the railway lines of industrial enterprises / Tash IIT. Dissertation for the degree of Candidate of Technical Sciences 05.23.15.– Tashkent, 1994.

Shesterikov, V.I. (1991). Estimation of road bridges condition and forecasting of its changes by means of physical wear indicator.– P. 1–48. (Automobile Roads,– Vol. 4).
Recommendation on Evaluation and Reliability of Transport Structures.– Moscow: Central Research Institute of Railway Transport, 1989.– 71 p.
Kildeeva, O.I.T. (1998). Resource of Reinforced Concrete Bridge Spans by Armature Corrosion // Istedod.– № 7 (7).– P. 100–108.

submitted 14.12.2023;
accepted for publication 22.12.2023;
published 24.01.2024

Contact: general-Saatova-nsoatova@bk.ru

The Austrian Journal of Technical and Natural Sciences, No 11–12
ISSN 2310-5607

PREMIER Publishing
ppublishing.org

DOI:10.29013/AJT-23-11.12-63-68

QUALITATIVE CHARACTERISTICS OF A FUEL BRIQUETTE OBTAINED BASED ON LICORICE ROOT AND A BINDING MIXTURE

Tursunov Bakhodir Junaydullayevich [1], ***Adizov Bobirjon Zamirovich*** [2]

[1] Department of General Technical Sciences, Asian International University Uzbekistan

[2] Institute of General and Inorganic Chemistry of the Academy of Sciences of the Republic of Uzbekistan, Uzbekistan

Cite: *Tursunov, B. J., Adizov, B. Z. (2023). Qualitative Characteristics of a Fuel Briquette Obtained Based on Licorice Root and a Binding Mixture. Austrian Journal of Technical and Natural Sciences 2023, No 11-12.* https://doi.org/10.29013/AJT-23-11.12-63-68

Abstract

Based on dried spent licorice roots (length 10–15 mm and thickness 3–7 mm) and a ready-made binder mixture (gossypol resin 50%, oil sludge 70% and quicklime 1.5%), a fuel briquette was obtained in a ratio of 12:1. The qualitative characteristics of the fuel briquette were determined in the following order: water absorption of the fuel briquette, total moisture of the fuel briquette, ash content, mass fraction of total sulfur in the fuel briquette and the release of volatile substances. Based on the results obtained, the fuel briquette FB-4 turned out to be the best briquette.

Keywords: *Licorice root, binder mixture, fuel briquette, water absorption, sulfur, ash content, volatile substances*

Introduction

Currently, in Uzbekistan, most fuel briquettes are made from coal and wood, as they are very economical and environmentally friendly. Analyzing information, articles, patents, dissertations and other data on the production of fuel briquettes, we can conclude that raw materials have a very important aspect for the quality of the product.

In Uzbekistan, about 5 thousand tons of oil sludge are generated annually at refineries, and in oil and fat plants about 20 thousand tons of gossypol resin are used as a by-product.

In recent years, in Karakalpakstan, the production of medicines from licorice roots has increased many times and a huge amount of waste from spent licorice roots has accumulated, since in most cases they are not used and sometimes are not disposed of. The problem of recycling spent licorice roots in our country is one of the most pressing, since currently, with existing processing methods, almost half of the biomass of licorice roots is lost. This indicates a low level of woodworking technological processes. The most significant results in the use of spent licorice roots have been achieved by countries with a highly developed sawmill and woodworking industry, which is the main supplier of waste.

Today, after processing licorice, waste is generated in large quantities, that is, licorice

roots. Spent licorice roots are used as combustion wood or fertilizer for poorly enriched soil. Many scientists are working on how to rationally use waste licorice roots for the needs of humanity.

The binder mixture was prepared from gossypol resin, oil sludge and quicklime. During the experiments, the composition of the sample of the finished binder mixture was selected: gossypol resin 50%, oil sludge 70% and quicklime 1.5%. Then, in order to obtain a high-quality fuel briquette, you first need to dry the spent licorice roots to ensure adhesion to the binder mixture.

High-quality drying of spent licorice roots was carried out in an ABM-065 drum dryer. After conducting experiments, a fraction of licorice root with a length of 10–15 mm and a thickness of 3–7 mm was selected, which was dried at a temperature of 70 ºC. Based on dried spent licorice roots (length 10–15 mm and thickness 3–7 mm) and a ready-made binder mixture (gossypol resin 50%, oil sludge 70% and quicklime 1.5%), a fuel briquette was obtained in a ratio of 12:1.

Methods

The qualitative characteristics of the fuel briquette were determined in the following order: water absorption of the fuel briquette, total moisture of the fuel briquette, ash content, mass fraction of total sulfur in the fuel briquette and the release of volatile substances.

Determination of water absorption of fuel briquettes. The water absorption of fuel briquettes (GOST 21289–75) was determined by keeping them in water at room temperature for 2 hours. Seven whole briquettes were weighed and immersed on a metal mesh in water to a depth of 30 mm from the surface. After being under water, the grid with briquettes was taken out, the water was allowed to drain for 2 minutes, then the briquettes were weighed on technical scales.

The water absorption of the fuel briquette (W), in percent, was calculated using the formula

$$W = \frac{m_1 - m}{m}$$

where m -mass of briquettes before testing, g; m_1 – mass of briquettes after testing, g.

Determination of total moisture. The determination of total moisture was carried out according to GOST R 52911–2008 using a one-step method.

The initial fuel briquette sample was crushed to a maximum piece size of 11.2 mm and reduced to a minimum weight of 2.5 kg. The tray with the briquette was placed in a drying cabinet at 105–110 ºC in air. Air exchange rate – up to 5 times per hour. Drying was considered complete if the weight loss of the sample during the time between two dryings did not exceed 0.2% of the total weight loss.

The mass fraction of total moisture Wt, in percent, was determined by the formula

$$W_t = \frac{m_2 - m_3}{m_2 - m_1} \cdot 100$$

where m_2 -mass of the tray with the sample before drying, g; m_3 – mass of the tray with the sample after drying, g; m_1 – mass of an empty tray, g.

The arithmetic mean value of the results of two parallel determinations was taken as the result of determining the mass fraction of total moisture. Calculations were carried out with an accuracy of 0.01% and rounded to 0.1%.

Determination of ash content. To determine the ash content of a fuel briquette (GOST 11022–95) (Konyukhov, V.Yu., Kerban, N.V., 2015), an analytical sample was used, crushed to the size of particles passing through a sieve with a mesh size of 0.2 mm. Before starting the determination, the analytical sample was thoroughly mixed for 1 min mechanically.

The pre-heated crucible was weighed, 1–2 g of sample was evenly distributed and weighed again. Weighing error is no more than 0.1 mg. The crucible with the sample was placed in a muffle furnace at room temperature. Over 60 minutes, the oven temperature was increased to 500 ºC and this temperature was maintained for 30 minutes. Next, heating was continued to (815 ± 10) ºC in the same oven and maintained at this temperature for at least 60 minutes.

After calcination, the crucible was removed from the furnace and cooled on a thick metal plate for 10 min, and then placed in a desiccator without a drying agent. After cooling, the crucible with the ash residue was weighed.

Then control calcinations were carried out at (815 ± 10) ºC for several 15-minute periods until the subsequent mass change was no more than 1 mg.

The ash content of analytical sample A, %, by weight, was calculated using the formula

$$A = \frac{m_3 - m_1}{m_2 - m_1} \cdot 100$$

where is the m_1 -mass of the crucible, g; m_2– mass of crucible with sample, g; m_3– mass of crucible with ash, g.

The arithmetic mean of the two closest definitions was taken as the test result.

Determination of total sulfur. Determination of the mass fraction of total sulfur in the fuel briquette was carried out according to GOST 8606–93 using the gravimetric method. This method is based on the absorption of sulfur oxides formed during the combustion of a sample of fuel by an Eschka mixture consisting of magnesium oxide and anhydrous sodium carbonate with the formation of magnesium and sodium sulfates. The resulting salts were dissolved in hot water and precipitated with barium chloride in a solution acidified with hydrochloric acid. Based on the amount of barium sulfate, the mass fraction of total sulfur, %, was calculated using the formula

$$S = \frac{13{,}74\left(m_2 - m_3 + 0{,}03348\rho_{K_2SO_4}\right)}{m_1}$$

where is the m_1– mass of the sample, g; m_2– mass of barium sulfate obtained during determination, g; m_3– mass of barium sulfate obtained during control determination, g; $\rho_{K_2SO_4}$ – mass concentration of potassium sulfate solution, g/dm³.

The result was taken as the arithmetic mean of two parallel determinations with an accuracy of ± 0.1%.

Determination of the yield of volatile substances. The yield of volatile substances was determined according to GOST 6382–2001 (Rasskazova, A.V., Alexandrova, T.N., 2013) by heating a sample sample without access to air at a temperature of 900 ºC for 7 minutes and calculated by the weight loss of the sample minus the weight loss due to the humidity of the sample.

The yield of volatile substances from the analytical sample of the tested fuel V^a,%, was calculated using the formula

$$V^a = \frac{100(m_2 - m_3)}{m_2 - m_1} - W^a$$

where is the m_1 -mass of an empty crucible with a lid, g; m_2– mass of the crucible with lid and sample before testing, g; m_3– mass of the crucible with a lid and non-volatile residue after testing, g; W^a – mass fraction of moisture in the analytical sample, %.

The yield of non-volatile residue from the analytical sample of the tested fuel $(NV)^a$, %, was calculated using the formula

$$(NV)^a = \frac{100(m_3 - m_1)}{m_2 - m_1}$$

If the mass fraction of carbon dioxide from carbonates in the fuel sample is more than 2%, the yield of volatile substances corrected for carbon dioxide from carbonates $V^a_{CO_2}$, %, was calculated using the formula

$$V^a_{CO_2} = V^a - \left[(CO_2)^a - (CO_2)^a_{NV} \cdot \frac{(NV)^a}{100}\right]$$

where $(CO_2)^a$ is the mass fraction of carbon dioxide from carbonates in the analytical sample; $(CO_2)^a_{NV}$ – mass fraction of carbon dioxide from carbonates in the non-volatile residue.

The result was taken as the arithmetic mean of two determinations that were within the acceptable discrepancies.

Results and discussion

To conduct research on the water absorption of fuel briquettes, we obtained samples based on dried spent licorice root (fraction size 10–15 mm long and 3–7 mm thick) and a binder mixture (Table 1).

Table 1. – *Ratio of dried spent licorice root (DSLR) and binder mixture (BM) for obtaining fuel briquettes*

Samples FB	DSLR: BM
Fuel briquette –1	9:1
Fuel briquette –2	10:1
Fuel briquette –3	11:1
Fuel briquette –4	12:1
Fuel briquette –5	13:1
Fuel briquette –6	14:1
Fuel briquette –7	15:1

Note: FB – fuel briquette, DSLR – dried spent licorice root, BM – binder mixture.

The final results of water absorption of fuel briquettes can be seen in Figure1.

Figure 1. *Dependence of water absorption of a fuel briquette on its composition*

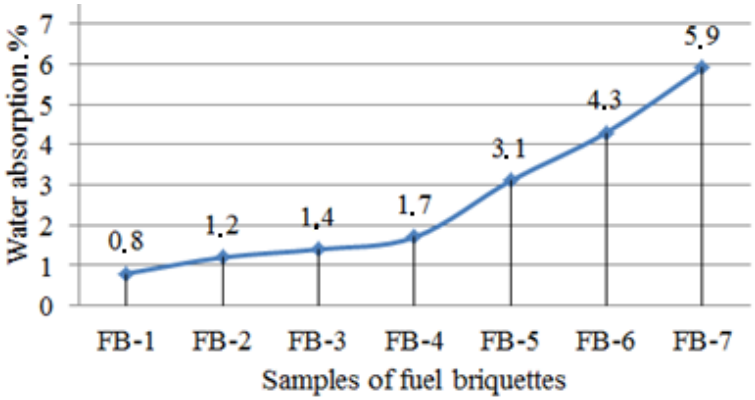

As can be seen from Figure 1, fuel briquettes FB-1, FB-2, FB-3 and FB-4 have the lowest water absorption rate than others, because this aspect is influenced by the adhesive strength of the composition of the fuel briquette.

Each sample of fuel briquette was examined to determine the mass fraction of total moisture, which is shown in Table 2.

Table 2. *Mass fraction of total moisture of the fuel briquette*

Index	Samples of fuel briquettes						
	FB-1	FB-2	FB-3	FB-4	FB-5	FB-6	FB-7
Mass fraction of total moisture. %	0.06	0.09	0.14	0.19	0.29	0.36	0.48

As can be seen from Table 2, the lower the mass fraction of total moisture in the briquette, the better its quality for use as a fuel briquette. But since not only quality, but also efficiency also plays an important role in the production of fuel briquettes. Based on the GOST requirements, the most acceptable sample turned out to be FB-4 for production.

Research to determine the ash content of a fuel briquette plays a very important role, since the formation of ash affects the environment. The formation of ash for each briquette sample with increasing temperature can be seen in Figure 2.

Figure 2. *Dependence of the ash content of a fuel briquette on the amount of binder mixture in the composition*

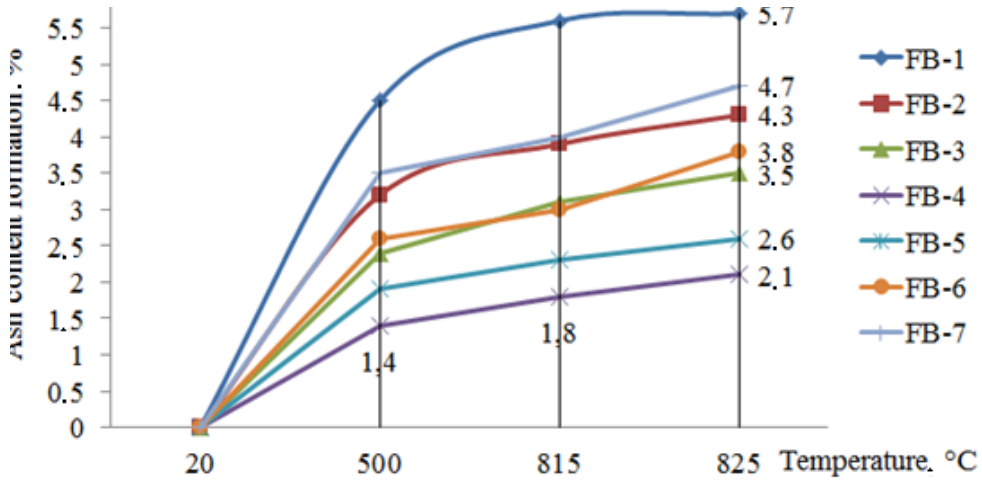

As can be seen from Figure 2, the formation of ash content of the FB-4 fuel briquette at a temperature of 500 °C is 1.4%, at a temperature of 815 °C it is 1.8%, and at a temperature of 825 °C the ash content of the analytical sample is 2.1%. The formation of ash content in other fuel briquette samples was higher than in the FB-4 fuel briquette.

The following study to determine the mass fraction of total sulfur in a fuel briquette was carried out according to the gravimetric method. Based on the amount of barium sulfate, the mass fraction of total sulfur in each sample of fuel briquette was calculated; the results obtained are shown in Table 3.

Table 3. *Mass fraction of total sulfur in the fuel briquette*

Index	Samples of fuel briquettes						
	FB-1	FB-2	FB-3	FB-4	FB-5	FB-6	FB-7
Mass fraction of total sulfur. %	0.49	0.38	0.23	0.16	0.12	0.09	0.07

The following study to determine the yield of volatile substances from a fuel briquette was carried out in accordance with GOST 6382–2001. The results of the data on the release of volatile substances from each sample of the fuel briquette can be seen in Figure 3.

Figure 3. *Dependence of the yield of volatile substances from a fuel briquette on its composition*

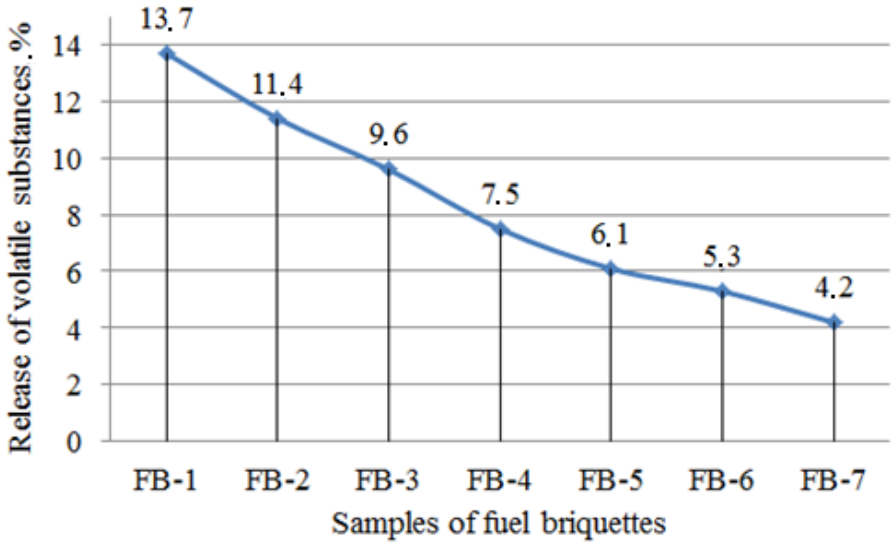

As can be seen from Figure 3, the yield of volatile substances from a fuel briquette will directly depend on the amount of binder mixture used. Since the ratio of licorice root and binder mixture in each briquette is different and the amount of binder mixture decreases, the yield of volatile substances in the samples also decreased from 13.7 to 4.2%.

Conclusion

In this work, samples of fuel briquettes were obtained based on dried spent licorice root (fraction size 10–15 mm long and 3–7 mm thick) and a binder mixture in a ratio of 12:1. After all tests have been carried out, namely, the water absorption of the TB-4 fuel briquette meets the requirements of the standard, the mass fraction of the total moisture of the TB-4 fuel briquette is less than 0.2%, the formation of ash when heating the TB-4 fuel briquette has the lowest indicator. The mass fraction of total sulfur in the TB-4 fuel briquette complies with GOST requirements, and the yield of volatile substances from the TB-4 fuel briquette directly depends on the amount of binder mixture used in the briquette.

References

GOST 21289–75. Coal briquettes. *Methods for determining mechanical strength*. Enter. 1975–28–11. – M.: Publishing house of standards, 1986. – 6 p.

GOST R 52911–08. *Solid mineral fuel. Methods for determining total moisture –Introduction*. 2008–26–03. – M.: Standartinform, 2008. – 12 p.

GOST 11022–95 *Solid mineral fuel. Methods for determining ash content – Intro*. 1997.01.01. – M.: Publishing house of standards, 1983. – 9 p.

GOST 8606–93 *Solid mineral fuel. Determination of total sulfur. Eshka method – Intro*. 1995.01.01. – M.: Publishing house of standards, 1983. – 10 p.

GOST 6382–01 *Solid mineral fuel. Methods for determining the yield of volatile substances – Introduction*. 2003.01.01. – M.: Publishing house of standards, 1983. – 6 p.

Konyukhov, V.Yu., Kerban, N. V. *Ways of fulfilling the ancient departure*. ISTU Youth Bulletin. – 2015. – No. 3. – P. 2.

Mokhirev A. P., Bezrukov Yu. A., Medvedev S. O. *Processing of wood waste from a timber industry enterprise as a factor in sustainable environmental management*. Engineering Bulletin of the Don. – 2015. – T. 36, No. 22. – P. 81.

Rasskazova, A.V., Alexandrova, T. N. *Technological and environmental aspects of the production of coal briquettes* // Mining Information and Analytical Bulletin (Scientific and Technical Journal). – 2013. – No. 4. – P. 209–215.

submitted 07.11.2023;
accepted for publication 27.11.2023;
published 24.01.2024

Contact: bahodirtursunov433@gmail.com

Contents